

**Testing A Theory  
On Turbulent Flow Near Smooth and Rough Walls**

DISSERTATION

Submitted in Partial Fulfillment  
of the Requirements for the  
Degree of

DOCTOR OF PHILOSOPHY (Aeronautics & Astronautics)

at the

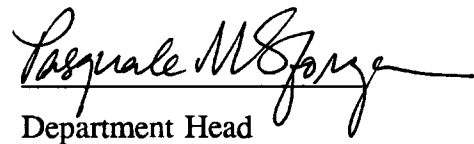
POLYTECHNIC UNIVERSITY

by

**Kyung-Soo Jang**

January 1994

Approved:

  
Department Head

Date: 25 Oct 1993

Copy No. 1

ProQuest Number:27605949

All rights reserved

INFORMATION TO ALL USERS

The quality of this reproduction is dependent upon the quality of the copy submitted.

In the unlikely event that the author did not send a complete manuscript and there are missing pages, these will be noted. Also, if material had to be removed, a note will indicate the deletion.



ProQuest 27605949

Published by ProQuest LLC (2019). Copyright of the Dissertation is held by the Author.

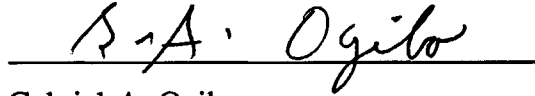
All rights reserved.

This work is protected against unauthorized copying under Title 17, United States Code  
Microform Edition © ProQuest LLC.

ProQuest LLC.  
789 East Eisenhower Parkway  
P.O. Box 1346  
Ann Arbor, MI 48106 – 1346

Approved by the Guidance Committee:

Major: Aeronautics & Astronautics



Gabriel A. Oyibo

Associate Professor of Aerospace Engineering

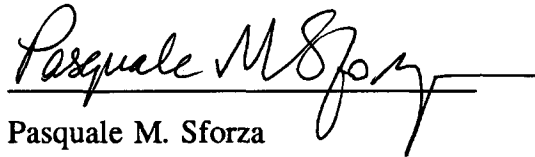
Minor: Mathematics



Clifford W. Marshall

Professor of Mathematics

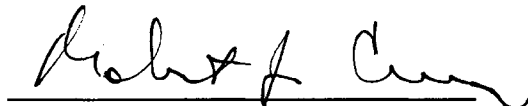
Additional Member:



Pasquale M. Sforza

Professor of Aerospace Engineering

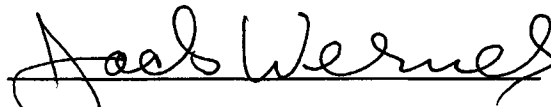
Additional Member:



Robert J. Cresci

Professor of Aerospace Engineering

Additional Member:



Jack Werner

Associate Professor of Aerospace Engineering

Microfilm or other copies of this  
dissertation are obtainable from

UNIVERSITY MICROFILMS

300 N. Zeeb Road

Ann Arbor, Michigan 48106

## VITA

Kyung-Soo, Jang was born in Dong-Myung, Korea on January 2, 1961 as a first son of Young-Gwan, Jang and Young-Ja, Lee. He entered the Department of Mechanical Engineering of the Korea University in Seoul, Korea in March 1979, from which he graduated with a Diploma of Bachelor of Science in January of 1983 and a Diploma of Master of Science in January of 1985. From August 1985 he had served in the Korean Army and was discharged as a Second Lieutenant in February of 1986.

In January 1988 he enrolled in the Department of Mechanical Engineering in Polytechnic University. He was awarded a Diploma of Engineering Degree in June of 1993 with the research published in the *International Journal of Heat and Mass Transfer*.

In September 1991 he transferred from the Department of Mechanical Engineering to the Department of Aerospace Engineering in the same University and met Professor Gabriel A. Oyibo who is the advisor of his Ph.D. Dissertation.

## DEDICATION

*If I close my eyes,  
the space disappears.*

- Kyung-Soo Jang -

Dedicated  
to my parents  
Young-Gwan Jang and Young-Ja Lee  
and to my wife  
Jung-Eun Lee.

## ACKNOWLEDGEMENTS

The author wish to appreciate his sincere gratitude to his advisor, Professor Gabriel A. Oyibo, for his continued advice and encouragement which made the completion of this work possible.

The author would like to thank his Guidance Committee: Professor P. Sforza, Professor R. Cresci, Professor J. Werner and Professor C. Marshall for their interest in reviewing this dissertation and for their constructive criticism.

Special thank you goes to Dr. David C. Wilcox, a reviewer in *AIAA Journal*, for reviewing part of this thesis and invaluable guidance.

The author is deeply indebted to his father, Young-Gwan Jang and mother, Young-Ja Lee for their endless caring, love, encouragement and life time support.

Finally the author also thanks his family: wife, Jung-Eun Lee, first son, Jae-Won Jang and new born second son Seung-Won Jang for their smiles and suffering from every pain and inconvenience caused by him.

**ABSTRACT****Testing A Theory  
On Turbulent Flow Near Smooth and Rough Walls**

by

**Kyung-Soo Jang**

Advisor

**Gabriel A. Oyibo**

Submitted in Partial Fulfillment of the Requirements for the  
Degree of Doctor of Philosophy (Aeronautics & Astronautics)

January 1994

A theoretical analysis and turbulence modelling for the flow near smooth and rough walls is presented.

In Chapter 2 of this thesis, a theoretical analysis which will yield a continuous velocity and shear distribution for turbulent flow near smooth, transitionally rough and fully rough walls is described. This analysis introduces a new roughness parameter  $C_j$  whose value determines velocity profiles and shear distributions which represent turbulent flow near smooth, transitionally rough and fully rough walls. The expressions developed for the velocity and shear stress are compared with those of van Driest and available experimental data.

In Chapter 3, the algebraic turbulence model obtained in Chapter 2 is implemented within a newly developed computational code which solves the fully elliptic time-averaged Reynolds transport equations. A developing turbulent flow in a pipe is selected for a test problem. The developing mean velocity and near-wall variations of turbulence



properties in the fully developed region are demonstrated and compared with van Driest's theory and available experimental data.

In Chapter 4, a computational code to solve fully elliptic Reynolds-averaged momentum equations are combined with a newly developed low-Reynolds number  $k$ - $\epsilon$  two equation turbulence model is developed and solved for the developing turbulent flow in a pipe. Two computational/roughness parameters  $C_j$  and  $A_C$  are introduced into the damping factor of the damping function in a low-Reynolds number  $k$ - $\epsilon$  turbulence model. This new low-Reynolds number turbulence model also predicts the variations of the turbulence properties for the flow near smooth, transitionally rough and fully rough walls. The computational results are compared with van Driest's theory and experimental data.

Using the theory described, an algebraic turbulence model and a low-Reynolds number  $k$ - $\epsilon$  two equation model a developing turbulent flow in a pipe is tested. The discretized governing equations are simultaneously solved for all flow variables ( $U, V, P$  for algebraic model and  $U, V, P, k$  and  $\epsilon$  for  $k$ - $\epsilon$  two equation model) using a line-by-line marching iterative solution technique for streamwise distances up to 100 pipe diameters for several bulk Reynolds numbers.

# List of Figures and Tables

## Chapter 2

- Figure 2.1 . Logarithmic velocity profiles for turbulent flow near smooth and rough walls: Comparison of theories of the present study and van Driest and experiment for smooth and rough surfaces.
- Figure 2.2 Logarithmic velocity profiles for turbulent flow near smooth and rough walls: Comparison of theories of the present study and van Driest and experiment for a smooth pipe
- Figure 2.3 Functional relationship between roughness Reynolds number  $k_*$  (van Driest's theory) and roughness parameter  $C_j$  (present theoretical approach)
- Figure 2.4 Near-wall distribution of Reynolds shear stress for flow near smooth and rough walls: Comparison of results of the present theory and experiment for a smooth pipe
- Figure 2.5 Near-wall distribution of Reynolds shear stress for flow near smooth and rough walls: Comparison of results of van Driest's theory and experiment for a smooth pipe
- Figure 2.6 Near-wall distribution of Reynolds shear stress for flow near smooth and rough walls: Comparison of results of the present theory and van Driest's theory

- Figure 2.7 Damped universal constant for turbulent flow near smooth and rough walls: Comparison of the present theory and van Driest's theory and experimental data
- Figure 2.8 Mixing length for turbulent flow near smooth and rough walls: Comparison of the present theory and van Driest's theory
- Figure 2.9 Turbulent viscosity for turbulent flow near smooth and rough walls: Comparison of the present theory and van Driest's theory
- Table 2.1 Comparison of roughness parameter  $C_j$  (present theory) and roughness Reynolds number  $k_*$  (van Driest's theory)

### Chapter 3

- Figure 3.1 Finite difference domain for discretized governing equations
- Figure 3.2 Computational geometry and boundary conditions
- Figure 3.3 Flow chart for computational procedure
- Figure 3.4 Variation of axial velocity with distance downstream of pipe inlet at  $C_j=1.0$  for  $r/R=0.0, 0.5, 0.75, 0.94$  for  $Re_D=10,000, 50,000$  and  $500,000$
- Figure 3.5 Variation of axial velocity with  $r/R$  for  $0.2 \leq C_j \leq 1.0$
- Figure 3.6 Logarithmic velocity profiles for turbulent flow near smooth and rough walls: Comparison of results of the present algebraic turbulence model ( $Re_D=10,000$ ) and experiment for a smooth pipe
- Figure 3.7 Logarithmic velocity profiles for turbulent flow near smooth and rough walls: Comparison of results of the present algebraic turbulence model ( $Re_D=50,000$ ) and experiment for a smooth pipe

- Figure 3.8 Logarithmic velocity profiles for turbulent flow near smooth and rough walls: Comparison of results of the present algebraic turbulence model ( $Re_D=500,000$ ) and experiment for smooth and rough surfaces
- Figure 3.9 Velocity profiles for turbulent flow near smooth and rough walls: Comparison of results of the present algebraic turbulence model ( $Re_D=10,000$ ) and experiment for a smooth pipe (Notations are the same as in Figure 3.6)
- Figure 3.10 Velocity profiles for turbulent flow near smooth and rough walls: Comparison of results of the present algebraic turbulence model ( $Re_D=50,000$ ) and experiment for a smooth pipe (Notations are the same as in Figure 3.6)
- Figure 3.11 Velocity profiles for turbulent flow near smooth and rough walls: Comparison of results of the present algebraic turbulence model ( $Re_D=500,000$ ) and experiment for a smooth pipe (Notations are the same as in Figure 3.6)
- Figure 3.12 Near-wall distribution of Reynolds shear stress for flow near smooth and rough walls: Comparison of results of the present algebraic turbulence model ( $Re_D=10,000$ ) and experiment for smooth surfaces
- Figure 3.13 Near-wall distribution of Reynolds shear stress for flow near smooth and rough walls: Comparison of results of the present algebraic turbulence model ( $Re_D=50,000$ ) and experiment for smooth surfaces
- Figure 3.14 Near-wall distribution of Reynolds shear stress for flow near smooth and rough walls: Comparison of results of the present algebraic turbulence model ( $Re_D=500,000$ ) and experiment for smooth surfaces
- Figure 3.15 Variation of Reynolds shear stress with  $r/R$  for  $0.0 \leq C_j \leq 1.0$ : Comparison of results of the present algebraic turbulence model ( $Re_D=10,000$ ) and experiment for a smooth pipe

- Figure 3.16 Variation of Reynolds shear stress with  $r/R$  for  $0.0 \leq C_j \leq 1.0$ : Comparison of results of the present algebraic turbulence model ( $Re_D = 50,000$ ) and experiment for a smooth pipe
- Figure 3.17 Variation of Reynolds shear stress with  $r/R$  for  $0.0 \leq C_j \leq 1.0$ : Comparison of results of the present algebraic turbulence model ( $Re_D = 500,000$ ) and experiment for a smooth pipe
- Figure 3.18 Functional relationship between roughness Reynolds number  $k_*$  (van Driest's theory) and roughness parameter  $C_j$  (algebraic turbulence model)
- Table 3.1 Comparison of roughness parameter  $C_j$  (algebraic turbulence model) and roughness Reynolds number  $k_*$  (van Driest's theory)

## Chapter 4

- Figure 4.1 Computational geometry and boundary conditions
- Figure 4.2 Finite difference domain for discretized governing equations
- Figure 4.3 Variation of damping function  $f_\mu$  vs  $y^+$ : Comparison of results of various turbulence models and the present result with  $C_j = 0.9$  and empirical data[20]
- Figure 4.4 Variation of damping function  $f_\mu$  vs  $y^+$ : Comparison of results of the present calculations, empirical data[20] ■, modified van Driest's model[109] ◆, and direct numerical simulation[110] Δ
- Figure 4.5 Variation of axial velocity with distance downstream of pipe inlet at  $C_j = 1.0$  for  $r/R = 0.0, 0.5, 0.75, 0.94$  for  $Re_D = 380,000$  (Notations for lines are the same as in Figure 4.6)
- Figure 4.6 Variation of axial velocity with  $r/R$  for different  $C_j$  at  $x/D = 80$  for  $Re_D = 10,000$

- Figure 4.7 Variation of axial velocity with  $r/R$  for different  $C_j$  at  $x/D=80$  for  $Re_D=380,000$
- Figure 4.8 Variation of turbulent kinetic energy with distance downstream of pipe inlet at  $r/R=0.0, 0.5, 0.75, 0.94$  for  $Re_D=380,000$ ,  $C_j = 0.9$  —,  $0.95$  — —,  $1.0$  - - - -
- Figure 4.9 Variation of turbulent viscosity with distance downstream of pipe inlet at  $r/R=0.0, 0.5, 0.75, 0.94$  for  $Re_D=380,000$ ,  $C_j = 0.9$  —,  $0.95$  - - -,  $1.0$  - - - -
- Figure 4.10 Effect of mean velocity on  $A_C$  and  $C_j$  for  $Re_D=500,000$
- Figure 4.11 Effect of turbulent kinetic energy on  $A_C$  and  $C_j$  for  $Re_D=500,000$
- Figure 4.12 Effect of dissipation rate of turbulent kinetic energy on  $A_C$  and  $C_j$  for  $Re_D=500,000$
- Figure 4.13 Near-wall variation of turbulent kinetic energy for different  $C_j$  for  $Re_D=50,000$
- Figure 4.14 Near-wall variation of turbulent kinetic energy for different  $C_j$  for  $Re_D=500,000$
- Figure 4.15 Near-wall variation of turbulent kinetic energy with  $y^+$  for  $C_j=1.0$  at  $x/D=80$  for  $Re_D=10,000, 38,000, 50,000, 380,000$  and  $500,000$
- Figure 4.16 Variation of turbulent kinetic energy with  $r/R$  for different  $C_j$  at  $x/D=80$  for  $Re_D=10,000$
- Figure 4.17 Variation of turbulent kinetic energy with  $r/R$  for different  $C_j$  at  $x/D=80$  for  $Re_D=380,000$
- Figure 4.18 Variation of turbulent kinetic energy with  $r/R$  for  $C_j=1.0$  at  $x/D=80$  for  $Re_D=10,000, 38,000, 50,000, 380,000$  and  $500,000$

- Figure 4.19 Variation of dissipation rate of turbulent kinetic energy with  $r/R$  for different  $C_j$  at  $x/D=80$  for  $Re_D=10,000$
- Figure 4.20 Variation of dissipation rate of turbulent kinetic energy with  $r/R$  for different  $C_j$  at  $x/D=80$  for  $Re_D=380,000$
- Figure 4.21 Variation of dissipation rate of turbulent kinetic energy with  $r/R$  for  $C_j=1.0$  at  $x/D=80$  for  $Re_D=10,000, 38,000, 50,000$  and  $380,000$
- Figure 4.22 Logarithmic velocity profiles for turbulent flow near smooth and rough walls: Comparison of results of the present  $k-\varepsilon$  turbulence model ( $Re_D=50,000$ ), van Driest's theory, and experimental data for smooth and rough surfaces
- Figure 4.23 Logarithmic velocity profiles for turbulent flow near smooth and rough walls: Comparison of results of the present  $k-\varepsilon$  turbulence model ( $Re_D=500,000$ ), van Driest's theory, and experimental data for smooth and rough surfaces
- Figure 4.24 Velocity profiles for turbulent flow near smooth and rough walls: Comparison of results of the present  $k-\varepsilon$  turbulence model ( $Re_D=50,000$ ) and experimental data for a smooth pipe
- Figure 4.25 Velocity profiles for turbulent flow near smooth and rough walls: Comparison of results of the present  $k-\varepsilon$  turbulence model ( $Re_D=500,000$ ) and experimental data for a smooth pipe
- Figure 4.26 Logarithmic velocity profiles for turbulent flow near smooth and rough walls: Comparison of results of the present  $k-\varepsilon$  turbulence model with  $C_j=1.0$  for  $Re_D=10,000, 38,000, 50,000, 380,000$  and  $500,000$  and experimental data for a smooth pipe
- Figure 4.27 Velocity profiles for turbulent flow near smooth and rough walls: Comparison of results of the present  $k-\varepsilon$  turbulence model with  $C_j=1.0$  for

$Re_D=10,000, 38,000, 50,000, 380,000$  and  $500,000$  and experimental data for a smooth pipe

- Figure 4.28 Distribution of wall shear-stresses with roughness parameter  $C_j$  for  $Re_D=10,000, 38,000, 50,000, 380,000$  and  $500,000$
- Figure 4.29 Effect of turbulent viscosity  $\nu_t$  on  $A_C$  and  $C_j$  for  $Re_D=500,000$
- Figure 4.30 Geometry of surface roughness
- Figure 4.31 Skin friction coefficient vs relative roughness
- Figure 4.32 Functional relationship between roughness Reynolds number  $k_*$  (van Driest's theory) and roughness parameter  $C_j$  ( $k$ - $\epsilon$  turbulence model)
- Figure 4.33 Near-wall distribution of Reynolds shear stress for flow near smooth and rough walls: Comparison of the present  $k$ - $\epsilon$  turbulence model for  $Re_D=50,000$ , van Driest's theory, and experimental data for smooth surfaces
- Figure 4.34 Near-wall distribution of Reynolds shear stress for flow near smooth and rough walls: Comparison of the present  $k$ - $\epsilon$  turbulent model for  $Re_D=500,000$ , van Driest's theory, and experimental data for smooth surfaces
- Figure 4.35 Near-wall distribution of Reynolds shear stress for flow near smooth and rough walls: Comparison of the present  $k$ - $\epsilon$  turbulent model with  $C_j=1.0$  at  $x/D=80$  for  $Re_D=10,000, 38,000, 50,000, 380,000$  and  $500,000$  and experimental data for smooth surfaces
- Figure 4.36 Variation of Reynolds shear stress with  $r/R$  for different  $C_j$  at  $x/D=80$  for  $Re_D=10,000$
- Figure 4.37 Variation of Reynolds shear stress with  $r/R$  for different  $C_j$  at  $x/D=80$  for  $Re_D=380,000$



- Figure 4.38 Variation of Reynolds shear stress with  $r/R$  for  $C_j=1.0$  at  $x/D=80$  for  $Re_D = 10,000, 38,000, 50,000, 380,000$  and  $500,000$
- Figure 4.39 Near-wall variation of  $P_k/\epsilon$  for different  $C_j$  at  $x/D=80$  for  $Re_D=50,000$
- Figure 4.40 Near-wall variation of  $P_k/\epsilon$  for different  $C_j$  at  $x/D=80$  for  $Re_D=500,000$
- Table 4.1 Comparison of roughness parameter  $C_j$  ( $k$ - $\epsilon$  turbulence model) and roughness Reynolds number  $k_*$  (van Driest's theory)

## Chapter 5

- Figure 5.1 Functional relationship between roughness Reynolds number  $k_*$  (van Driest's theory) and present roughness parameter  $C_j$  for different turbulence model

## List of Symbols

$A_*$	van Driest's constant = 26
$A_\mu, A_{cl}, A_t$	turbulence model constants
$A_C$	new turbulence model constant
$C_1, C_2, C_\mu$	turbulence model constants
$C_j$	new computational/roughness parameter
$D$	pipe diameter
$f_1, f_2, f_\mu$	turbulence model functions
$K$	turbulent kinetic energy
$k$	normalized turbulent kinetic energy, $K/u_0^2$
$k_s$	equivalent sandgrain roughness scale
$k_*$	roughness Reynolds number, $u_\tau k_s/\nu$
$k_0$	initial value of turbulent kinetic energy
$k^+$	normalized turbulent kinetic energy, $K/u_\tau^2$
$l$	mixing length
$l^+$	normalized mixing length
$E$	rate of dissipation of turbulent kinetic energy

$\varepsilon$	normalized rate of dissipation of turbulent kinetic energy, $ED/u_0^3$
$\varepsilon_0$	initial value of dissipation rate of turbulent kinetic energy
$\varepsilon^+$	normalized dissipation rate of turbulent kinetic energy, $E\nu/u_\tau^4$
$\bar{p}$	time-averaged static pressure
$P$	normalized static pressure, $\bar{p}/\rho u_0^2$
$P_k$	production of turbulent kinetic energy
$Re_D$	Reynolds number, $\rho u_0 D/\mu$
$R_k$	turbulence Reynolds number, $K^{1/2}y_n/\nu$
$R_t$	turbulence Reynolds number, $K^2/E\nu$
$(\bar{u}, \bar{v})$	horizontal and radial time-averaged mean velocity components
$(u', v')$	fluctuating horizontal and radial velocity components
$u_\tau$	friction velocity, $\sqrt{\tau_w/\rho}$
$(U, V)$	normalized horizontal and radial mean velocity components, $(\bar{u}, \bar{v})/u_0$
$u_0$	horizontal inlet velocity
$u^+$	normalized axial mean velocity, $\bar{u}/u_\tau$
$\overline{UV}^+$	normalized mean Reynolds shear stress, $\overline{u'v'}/u_\tau^2$
$(x, y)$	horizontal and radial coordinates
$(X, r)$	normalized horizontal and radial coordinates, $(x, y)/D$
$y_n$	distance normal to wall
$y^+$	wall distance parameter, $u_\tau y_n/\nu$
$\rho$	density of fluid
$\mu$	viscosity of fluid

$\nu$	kinematic viscosity of fluid, $\mu/\rho$
$\mu_t$	turbulent(eddy) viscosity
$\nu_t$	normalized turbulent(eddy) viscosity, $\mu_t/\mu$
$\sigma_k$	diffusion Prandtl number for turbulent kinetic energy
$\sigma_\epsilon$	diffusion Prandtl number for the dissipation rate of turbulent kinetic energy

## Subscript

$i$	$i^{th}$ node
$j$	$j^{th}$ node
$l$	laminar
$t$	turbulent
$w$	at wall
$0$	pipe inlet condition

# Contents

ACKNOWLEDGEMENTS .....	vi
ABSTRACT .....	vii
LIST OF FIGURES AND TABLES .....	ix
LIST OF SYMBOLS .....	xvii

## CHAPTER 1 INTRODUCTION

1. INTRODUCTION .....	1
1.1 EDDY VISCOSITY MODEL .....	2
1.1.1 Zero Equation Model .....	2
1.1.2 One Equation Model .....	3
1.1.3 Two Equation Model .....	4
1.2 REYNOLDS STRESS MODEL .....	4
1.3 NEAR-WALL TURBULENCE MODELLING .....	5
1.3.1 Turbulence Modelling Near Smooth Walls .....	5
1.3.2 Turbulence Modelling Near Rough Walls .....	6

1.4 COMPUTATIONAL TECHNIQUES .....	9
2. OBJECTIVES .....	11
3. TOPICS OF THE PRESENT WORK .....	13

## CHAPTER 2 THEORETICAL APPROACH

1. INTRODUCTION .....	14
2. THEORETICAL APPROACH .....	15
2.1 Van Driest's Analysis .....	15
2.2 Present Analysis .....	21
3. RESULTS AND DISCUSSIONS .....	22
4. CONCLUSIONS .....	24

## CHAPTER 3 COMPUTATION 1

### ALGEBRAIC TURBULENCE MODEL

1. INTRODUCTION .....	36
2. PROBLEM FORMULATION .....	37
2.1 Governing Equations and Algebraic Turbulence Model .....	37
2.2 Finite Difference Equations and Computational Grid .....	39
2.3 Boundary Conditions .....	40
3. SOLUTION METHOD .....	41
4. RESULTS AND DISCUSSIONS .....	41

5. CONCLUSIONS .....	44
----------------------	----

## CHAPTER 4 COMPUTATION 2

### *k*- $\epsilon$ LOW-REYNOLDS NUMBER TURBULENCE MODEL

1. INTRODUCTION .....	65
2. PROBLEM FORMULATION .....	67
2.1 Governing Equations .....	67
2.2 Low-Reynolds Number Turbulence Model .....	69
2.3 New Computational Parameter $C_j$ and Modelling Constant $A_C$ .....	72
2.4 Computational Grid and Boundary Conditions .....	73
3. SOLUTION METHOD .....	75
4. RESULTS AND DISCUSSIONS .....	76
4.1 Sensitivity Test of $C_j$ and $A_C$ .....	76
4.2 Physical Meaning of $C_j$ as a Roughness Function .....	80
5. CONCLUSIONS .....	84

## CHAPTER 5 SUMMARY AND CONCLUSIONS

1. SUMMARY .....	127
2. CONCLUSIONS .....	129

BIBLIOGRAPHY .....	133
--------------------	-----

**APPENDIX**

Discretized Equations ..... 146



# Chapter 1

## INTRODUCTION

### 1. INTRODUCTION

The fluid flow passing through many engineering systems of practical interest is turbulent. Turbulence in fluid flow has some statistical or non-deterministic characteristics. Such statistical characteristics of turbulent flow variables may be represented by two components, namely the mean quantity and the fluctuating quantity. When the time-averaged Reynolds transport equations are used to describe turbulent flows some of the important information about the dynamics of turbulence is lost and the number of unknown variables exceeds the number of equations to be solved. In order to provide the necessary closure to the governing equations, relations between the Reynolds-stresses and the mean velocity components have to be prescribed. The type of turbulence modelling depends on the assumption made to describe the Reynolds-stress tensor. In general it can be divided into two categories. The first one follows the turbulent or eddy viscosity concept proposed by Boussinesq in order to mimic the laminar flow analysis. The second one uses additional transport equations

with the Reynolds-stresses themselves as dependent variables. The applications and limitations for the representative models in each category are briefly described below.

## 1.1 Eddy Viscosity Model

Since Boussinesq<sup>1</sup> described the gradient transport idea many engineers have used it. It assumes that the Reynolds-stresses can be related to the mean velocity gradient via a turbulent or eddy viscosity:

$$-\rho \overline{u'v'} = \mu_t \left[ \frac{\partial \bar{u}}{\partial y} + \frac{\partial \bar{v}}{\partial x} \right] \quad (1.1)$$

Therefore this type of turbulence model relates the turbulent stress to the mean rate of strain in a manner similar to the relationship between the stress and the rate of strain in laminar flow.

### 1.1.1 Zero Equation Model

One of the simplest and most successful models of the zero equation models is the one based on the Prandtl's mixing length theory<sup>2</sup>, which relates the turbulent viscosity to a mixing length multiplied by the mean velocity gradient.

$$\mu_t = \rho l^2 \left| \frac{\partial \bar{u}}{\partial y} \right| \quad (1.2)$$

where a mixing length,  $l$ , is a characteristic length scale of turbulence and is specified as an algebraic function of local flow properties. Prandtl's development led to the result that the mixing length is proportional to the distance in the transverse direction,  $y$

$$l = K y, \quad K = 0.41 \quad (1.3)$$

Its applications are confined to simple flows where the turbulence is influenced by the local properties of the velocity field. This model implies that turbulence is in local equilibrium throughout the flow field which means that the dissipation and production of turbulent energy are the same at each point in the flow. It also requires the turbulent viscosity  $\mu_t$  to be zero whenever the mean velocity gradient is zero, which is not true under all circumstances. Therefore the mixing length hypothesis cannot account for all the transport and history effects of turbulence. The mixing length is obtained through empirical correlations only.

### 1.1.2 One Equation Model

The deficiency of the mixing length model can be corrected by introducing a transport process partial differential equation. These "one equation" models are the simplest ones accounting for the transport and history effects of turbulence. An additional partial differential equation is provided which relates the transport of turbulent kinetic energy to the turbulent velocity scale. The model uses the eddy viscosity concept, together with dimensional analysis to obtain the so-called Kolmogorov<sup>3</sup>-Prandtl<sup>2</sup> expression.

$$\mu_t = \rho k^{1/2} l \quad (1.4)$$

where the turbulent kinetic energy  $k$  is defined by:

$$k = \frac{1}{2} (\overline{u'^2} + \overline{v'^2} + \overline{w'^2}) \quad (1.5)$$

and  $\overline{u'^2}$ ,  $\overline{v'^2}$  and  $\overline{w'^2}$  are the components of normal intensities in each direction. The turbulent viscosity no longer becomes zero when the mean velocity gradient is zero. In this model, as in the zero equation model, the mixing length is evaluated by an algebraic expression which depends only on the local flow parameters. In general the

application of the one equation model is limited to simple shear layer flows and the result often does not show an improvement over a zero equation model.

### 1.1.3 Two Equation Model

Two equation models involve an additional transport equation which provides the turbulence mixing length. Among two equation models, the  $k$ - $\varepsilon$  two equation model using a transport equation for the turbulent kinetic energy and one for the dissipation rate of the turbulent kinetic energy has become the most popular because the dissipation rate equation requires no extra terms near the wall. The dissipation rate of turbulent kinetic energy  $\varepsilon$  is defined as:

$$\varepsilon = \frac{k^{3/2}}{l} \quad (1.6)$$

And the dimensional analysis of Prandtl and Kolmogorov defines the turbulent viscosity as:

$$\mu_t = C_\mu \rho \frac{k^2}{\varepsilon} \quad (1.7)$$

where  $C_\mu$  is an empirical constant usually given by 0.09. Many engineers and scientists have made computations using these turbulence models for solving complex turbulent flows and in many instances obtained good comparisons with experimental data.

## 1.2 Reynolds-Stress Model

Even though the  $k$ - $\varepsilon$  two equation model is still used for solving complex turbulent flows in many engineering applications higher order closure models are necessary to get more realistic results. Experimental evidence shows that the linear relation between the Reynolds-stress and the mean rate of strain is inaccurate and that the assumption of a scalar turbulent viscosity cannot be expected to be universally valid. Analysis of such cases requires the solution of the Reynolds-stress equations where the

Reynolds-stresses themselves are dependent variables of partial differential equations. Such modelling requires the solution of three or more transport equations in addition to the time-averaged momentum and continuity equations. Although complicated and tedious they can be potentially more useful and less problem dependent. To date these models have been used as turbulence research tools and are still under development.

For the calculation of turbulent stresses and heat fluxes in incompressible flow Rodi<sup>4</sup> described some of the available models and presented typical examples of calculations relevant to aerospace problems. Marvin<sup>5</sup> broadly reviewed the status of turbulence modelling for computational aerodynamics and discussed the performance of different models in various compressible flow problems. The two equation models seem to perform better for separated flows especially in the recovering regions downstream.

## 1.3 Near-Wall Turbulence Modelling

### 1.3.1 Turbulence Modelling Near Smooth Walls

In the region very close to the wall the magnitude of turbulent viscosity diminishes and becomes comparable with the laminar viscosity. Thus, a more detailed hypothesis for  $\mu_t$  is needed to account for the region near the wall. The hypothesis for this region is especially important, because very steep gradients of mean velocity and other turbulent variables exist near a wall, and also because the shear stress and fluxes at the wall are of great practical interest. There are many versions of models for the turbulent viscosity near a smooth wall. Most of them come from the universal logarithmic velocity distribution law of the wall and an assumption of uniform shear stress. All such expressions have been designed in accordance with the experimental data in the absence of pressure gradient, non-uniform fluid properties and mass transfer

at the wall. Several authors(Reichardt<sup>6</sup>, van Driest<sup>7</sup> and Deissler<sup>8</sup>) have suggested velocity profiles which vary smoothly and fit better to experiments in such cases.

For higher order near-wall turbulence models the Reynolds-stress transport equations<sup>9-14</sup>, which are closed by either using wall functions or introducing a wall effect into the pressure-strain terms, have more flexible applications than others. However their ability to predict near-wall Reynolds-stresses are not quite as good as those of two equation models<sup>15-18</sup>. These higher order models require more transport equations to be solved, which are either very expensive to calculate or often exceed the limits of computers. The  $k$ - $\epsilon$  two equation model<sup>15,19</sup> is one of the most popular among those in the two equation model family but its usage is limited only to the fully turbulent region in which the Reynolds number is sufficiently high, so that the eddy viscosity can be assumed to be isotropic. This requires an empirical wall function<sup>19</sup> to bridge the region between the wall and the fully turbulent region away from the wall, in which the most significant variations of turbulence properties occur. Low-Reynolds number  $k$ - $\epsilon$  two equation models eliminate the need for wall functions and model the turbulent viscosity directly to account the existence of the wall.

Patel, Rodi and Scheuerer<sup>20</sup> extensively tested eight different two equation, low-Reynolds number turbulence models to compare their ability to predict the near-wall behavior of turbulence properties. It was concluded in their studies that the models of Launder and Sharma<sup>21</sup>, Chien<sup>22</sup> and Lam and Bremhorst<sup>23</sup>, which are based on  $k$ - $\epsilon$  model, and that of Wilcox and Rubesin<sup>24</sup>, which is based on  $k$ - $w$  model yield comparable results and perform considerably better than the others.

### 1.3.2 Turbulence Modelling Near Rough Walls

Many practical engineering structures cannot be regarded as being hydraulically or aerodynamically smooth. The resistance to flow caused by the existence of rough surfaces is generally larger than that obtained by the smooth wall approximation.

Therefore experiments of such flows began very early<sup>25-30</sup>. A comprehensive review of the numerous earlier experimental results is made by Hopf<sup>26</sup>. Systematic and extensive measurements on rough pipes have been performed by Nikuradse<sup>30</sup>, who focused on the behavior of turbulent flow on the rough walls by measuring pressure drop and velocity profiles in pipes roughened with tightly glued sandgrains. In experiments using a rectangular channel with the upper surface roughened and the other sides smooth, Schlichting<sup>31</sup> first proposed the equivalent sandgrain roughness  $k_s$  concept, which is related to the size of the sandgrain in Nikuradse's experiment. The equivalent sandgrain roughness of Schlichting was used to relate his skin friction results to the results obtained by Nikuradse for the sand roughened pipes. Schlichting divided the wall roughness into three regimes, *i.e.* the hydraulically smooth, the transitionally rough and the completely rough regimes:

$$\begin{array}{ll}
 0 < k_* < 5 & \text{hydraulically smooth} \\
 5 < k_* < 70 & \text{transitionally rough} \\
 k_* > 70 & \text{completely rough}
 \end{array} \quad (1.8)$$

where the roughness Reynolds number  $k_*$  is defined by the friction velocity  $u_\tau$ , equivalent sandgrain size  $k_s$  and kinematic viscosity of fluid  $\nu$ .

Using experimental data the relation between the resistance formula and the velocity distribution, which was found earlier in the case of smooth pipes, could be extended to the case of rough pipes. But the theoretical approach to the laws of friction for rough pipes is frustrated by the large number of parameters describing roughness due to the diversity of geometric forms.

In general there are two approaches which have been used in formulating the required roughness models: the classic equivalent sandgrain roughness approach and the discrete element approach. The problem using the equivalent sandgrain roughness approach is determining the roughness Reynolds number  $k_*$  for a specific surface of interest so that Nikuradse's experimental data can be used. Bettermann<sup>32</sup>, Dvorak<sup>33</sup>,

Simpson<sup>34</sup>, Dirling<sup>35</sup>, Dalle Donne and Meyer<sup>36</sup> used the equivalent sandgrain concept to correlate the roughness on the wall. Later, Schlichting's roughness experiment was re-evaluated by Coleman, Hodge and Taylor<sup>37</sup>. They showed that the original skin friction coefficients are higher than their corrected values by amounts ranging from 0.5 to 73 percent, while the original equivalent sand roughness values are higher than their corrected ones by 26 to 555 percent. Sigal and Danberg<sup>38</sup> used the corrected data to correlate the roughness density effect on the turbulent boundary layer flow. The equivalent sandgrain roughness concept has been used in predicting turbulence through modeling methods such as integral methods and differential (finite difference) methods. The integral methods generally account for roughness through modified velocity profiles, together with skin-friction and Stanton number correlations based on the sandgrain roughness Reynolds number (Bettermann<sup>32</sup>, Dvorak<sup>33</sup>, Simpson<sup>34</sup>, Dirling<sup>35</sup>, Dalle Donne and Meyer<sup>36</sup>, Koh<sup>39</sup>). Differential methods use modified eddy viscosity formulations to account for surface roughness, based on the equivalent sandgrain roughness (Healzer<sup>40</sup>, Cebeci and Chang<sup>41</sup>, Ligrani<sup>42</sup>).

Another approach to the modelling problem to account the roughness effects is the discrete element method, in which the effects of a collection of individual roughness elements on the flow are generally considered by including a form drag in the momentum equation and accounting for the blockage effect of roughness elements on the flow. In the same paper in which Schlichting introduced the equivalent sandgrain roughness concept, he proposed that the flow resistance of a rough surface be divided into two components: that due to the form drag on the roughness elements and that due to the viscous shear on the smooth surface area between the roughness elements. Some investigators have used this method coupled with  $k_\epsilon$  influences on the turbulence model (Hodge and Adams<sup>43</sup>, Lin and Bywater<sup>44</sup>, Christoph and Pletcher<sup>45</sup>). Others (Finson and Wu<sup>46</sup>, Finson and Clark<sup>47</sup>, Finson<sup>48</sup>, Taylor, Coleman and Hodge<sup>49,50</sup>, Hosni, Colemann and Taylor<sup>51</sup>, Scaggs, Taylor and Coleman<sup>52</sup>) have used the discrete element approach in a manner in which there is no dependence on the equivalent sandgrain



roughness concept.

In the present study the effects of wall roughness are considered by introducing a roughness parameter into the damping function originated by van Driest<sup>7</sup>.

## 1.4 Computational Techniques

One representative numerical method for solving steady state transport equations is the SIMPLE(Semi-Implicit Method for Pressure-Linked Equations) algorithm<sup>53</sup>. It uses a form of the relaxation method and a segregated solution technique in which the pressure and velocity fields are solved separately. Since Patankar and Spalding first described the SIMPLE algorithm to solve the parabolized Navier-Stokes equations it has been continually developed for over a decade, yielding many versions: i)SIMPLER<sup>54</sup>, FIMOSE<sup>55</sup> *etc.*, depending on the method of updating the pressure ii)QUICK<sup>56</sup>, QUICKER<sup>57</sup>, *etc.*, depending on the difference scheme used to discretize the convective terms iii)SIMPLEC<sup>58</sup>, CTS-SIMPLE<sup>59</sup>, *etc.*, depending on the application of turbulence models. Even though the SIMPLE algorithm produces very stable computational solutions its convergence rate is not satisfactory. A significant number of numerical studies have been successfully carried out using one of the family of SIMPLE algorithm for complex geometries and turbulent flow problems including one<sup>60</sup> of the present author's works.

A kind of SIMPLE algorithm<sup>53-55</sup> has been used by Martinuzzi<sup>61</sup>, Martinuzzi and Pollard<sup>62</sup>, Pollard and Martinuzzi<sup>63</sup> to test a total of 11 turbulence models, including a standard  $k$ - $\epsilon$  model with a wall function<sup>19</sup>, a low-Reynolds number model of Lam and Bremhorst<sup>23</sup>, four algebraic stress models and five Reynolds stress models with and without wall terms for a developing turbulent pipe flow. Among them the results of the low-Reynolds number turbulence model of Lam and Bremhorst are in better agreement with experimental data than the results obtained from other turbulence models.

Other approaches for solving the resulting set of equations include a simultaneous solution technique like the method used in the present study. It simultaneously solves for all flow properties along lines perpendicular to the streamwise direction, line-by-line marching to the downstream direction. The applications of simultaneous solution techniques are shown in Jang and Vradis<sup>64</sup>, Benston and Vradis<sup>65</sup>, Vanka<sup>66</sup>, Rubin and Reddy<sup>67</sup>, Zedan and Schneider<sup>68</sup>. The efficiency and accuracy of the simultaneous solution method is well verified. But most of above applications of the simultaneous solution technique were for laminar problems except for Jang and Vradis<sup>64</sup> who solved for the flow in a developing turbulent planar jet with various turbulence models<sup>69</sup> implemented in the parabolic governing equations. Vanka<sup>70</sup> also demonstrated the simultaneous solution method with a multi-grid technique for various practical and complex flows including a turbulent flow in an axisymmetric pipe with a sudden expansion. But the attempt to solve for all flow properties in a coupled form was not successful because the multi-grid system combined with a wall function in the  $k$ - $\epsilon$  turbulence model failed to achieve a convergent solution. Consequently the solution of the  $k$  and  $\epsilon$  equations must be decoupled from the momentum and continuity equations. The strongly coupled source forms for the turbulent flow equations tend to cause divergence and instability of the numerical scheme<sup>70-72</sup>. Using the simultaneous solution technique the present author recently succeeded in solving for all the flow properties in a low-Reynolds number  $k$ - $\epsilon$  two equation turbulent model describing the developing turbulent flows in a pipe<sup>73,75</sup> and in a channel<sup>74</sup>. The near-wall variations and the developing processes of the turbulent properties such as the time-averaged mean velocities, turbulent kinetic energy, its dissipation rate and Reynolds-stresses were demonstrated in detail and compared well with available experimental data.

To analyze a fluid flow in which the pressure gradient is not constant, fully elliptic transport equations are essential<sup>76</sup>. The transport equations governing a developing turbulent flow are inherently fully elliptic and characterized by strongly coupled forms and nonlinearities. Solving simultaneously for all flow properties in such strongly

coupled partial differential equations is physically more appropriate than using a segregated or decoupled solution method.

## 2. OBJECTIVES

This study is concerned with i) an analytical approach to develop mathematical forms for an algebraic turbulence model and a low-Reynolds number  $k$ - $\epsilon$  two equation model, which account for the flow near smooth and rough walls and ii) the development of computational codes for an algebraic turbulence model and a low-Reynolds number  $k$ - $\epsilon$  two equation turbulence model which simultaneously solve all flow properties in a developing turbulent pipe flow using a line-by-line marching iterative solution technique.

The main objective of this thesis is to develop turbulence models capable of accurately describing the behavior of turbulence properties for the flow near smooth, transitionally rough and fully rough walls. Two turbulence models are developed; one an algebraic model based on theoretical analysis and the other a  $k$ - $\epsilon$  low-Reynolds number turbulence model based on numerical simulations combined with a new wall damping function. Both of these models are supposed to handle the entire range of turbulent flow from the wall with various kinds of roughness to the fully turbulent region. The models introduce new roughness parameters, which are related to the roughness Reynolds numbers. The specific objectives are:

- i) To develop analytical expressions for a continuous, smooth velocity profile, a turbulent or eddy viscosity, and the Reynolds-shear stresses for turbulent flow near smooth, transitionally rough and fully rough walls.
- ii) To verify the accuracy of these analytic expressions by comparing with those of van Driest's, since it is a similar formulation for flow over rough surfaces, and

available experimental data.

- iii) To verify the accuracy of the developed algebraic turbulence model by incorporating it into a newly developed elliptic code and solving simultaneously for all flow properties in the time-averaged Reynolds transport equations for developing turbulent flow in a pipe.
- iv) To develop a low-Reynolds number  $k$ - $\epsilon$  turbulence model based on the idea of the theoretical analysis for the algebraic turbulence model.
- v) To develop a new fully elliptic code to solve the time-averaged Reynolds transport equations and  $k$ - $\epsilon$  two equations in which the new low-Reynolds number turbulence model is implemented.
- vi) To develop a simultaneous solution technique for a developing turbulent flow in a pipe using a line-by-line marching iterative solution method.

In the beginning of the study the author did not have any idea of the turbulent flow over rough surfaces. He had studied carefully the original  $k$ - $\epsilon$  low-Reynolds number turbulence model of Lam and Bremhorst. Initially a quantity  $C_j$  was introduced into the damping function  $f_\mu$  as a purely computational parameter to help the convergence of the  $k$ - $\epsilon$  model equations. The results showed that with a given set of boundary conditions computations agree well with other numerical and experimental results for certain range of  $C_j$ . Further investigations revealed that  $C_j$  has some physical meaning. It was found that it can serve as a measure of the wall roughness for a given turbulent flow. This encouraged the comparison with van Driest's theory, in which continuous velocity and shear distributions for turbulent flow near smooth and rough walls were studied. An empirical relationship was eventually developed to relate  $C_j$  with the roughness Reynolds number  $k_*$  based on the friction velocity,  $u_\tau$ , equivalent sandgrain roughness scale  $k_s$  and kinematic viscosity of fluid  $\nu$ .

### 3. TOPICS OF THE PRESENT WORK

In Chapter 2, "Theoretical Approach", a theoretical analysis which will yield a continuous velocity and shear distribution for turbulent flow near smooth, transitionally rough and fully rough walls is developed. The results for the mean velocity and shear stresses are compared with those of van Driest's analysis and available experimental data.

In Chapter 3, "Computation 1: Algebraic Turbulence Model", the algebraic turbulence model is tested for developing turbulent flow in a pipe. Comparisons are carried out with the results of theoretical analysis and experiments.

In Chapter 4, "Computation 2:  $k$ - $\epsilon$  Low-Reynolds Number Turbulence Model", a numerical code using a simultaneous solution method to solve the Reynolds transport equations, combined with a newly developed low-Reynolds number  $k$ - $\epsilon$  two equation turbulence model is developed. The developing turbulent flow in a pipe is used to test this model and the results are compared with the results of theory and experimental data.

The "Summary and Conclusions" are presented in Chapter 5.

# Chapter 2

## Theoretical Approach

### 1. INTRODUCTION

Parts of many practical engineering systems, such as re-entry vehicles, missiles, air craft, ships, turbines, heat exchangers, piping networks and atmospheric flows, cannot be regarded as having aerodynamically or hydraulically smooth surfaces. The resistance to flow caused by turbulent flow on rough walls is larger than that for turbulent flow on smooth walls. Therefore accurate predictive models for turbulent flow over rough surfaces are of significant interest.

In the present study a theory which yields a continuous velocity and shear distribution for turbulent flow near smooth and rough walls is developed. This analysis introduces a roughness parameter  $C_j$  into van Driest's damping factor<sup>7</sup> for a smooth wall. The parameter is related to the roughness Reynolds number  $k_*$  and permits the van Driest model for turbulent flow near a smooth wall to be modified to account for the effect of wall roughness. The expressions developed here for the mean velocity and shear stresses are compared with those of van Driest's theory and available

experimental data. Comparisons of mean velocity profiles in the logarithmic law region between the present theory and van Driest's show that the roughness parameter  $C_j$  is inversely proportional to the roughness Reynolds number  $k_*$ . In the fully turbulent region the shear stresses determined by the present theory agree well with those from van Driest's theory and experimental data.

## 2. THEORETICAL APPROACH

### 2.1 Van Driest's Analysis

For the flow near an oscillating flat plate Stokes<sup>77</sup> showed that the velocity profile has the form of a damped harmonic oscillation of the plate, the amplitude factor of which is  $\exp(-y/A)$ , in which  $A$  is a constant that depends upon the frequency of oscillation of the plate and the kinematic viscosity  $\nu$  of the fluid. When the plate is fixed and the external fluid oscillates relative to the plate<sup>78,79</sup>, the factor  $[1 - \exp(-y/A)]$  must be applied to the fluid oscillation to obtain the damping effect on the smooth wall. Van Driest<sup>7</sup> first introduced this damping factor into expressions of the universal constant and mixing length of turbulence modelling to take into account the existence of a smooth wall. The total mean shear stress  $\tau$  for turbulent flow is identified as

$$\tau = \mu \left( \frac{\partial \bar{u}}{\partial y} \right) - \rho \bar{u}' v' \quad (2.1)$$

where  $\bar{u}$  is the mean velocity parallel to the wall,  $u'$  the instantaneous fluctuation of velocity in the direction of stream,  $v'$  that in the direction normal to the wall,  $y$  the length scale normal to the wall and measured positive from the wall,  $\rho$  the density of the fluid, and  $\mu$  the viscosity of the fluid. The first term on the right-hand side of equation(2.1) represents the effect of molecular viscosity on the mean flow whereas the

second term is a Reynolds-stress. According to Prandtl's mixing length hypothesis<sup>2,80</sup> it is written as

$$\tau = \mu \left( \frac{\partial \bar{u}}{\partial y} \right) + \rho K^2 y^2 \left( \frac{\partial \bar{u}}{\partial y} \right)^2 \quad (2.2)$$

where  $K$  represents a universal constant. Therefore the expression due to van Driest becomes:

$$\tau = \mu \left( \frac{\partial \bar{u}}{\partial y} \right) + \rho K^2 y^2 [1 - \exp(-y/A)]^2 \left( \frac{\partial \bar{u}}{\partial y} \right)^2 \quad (2.3)$$

where the presence of wall modifies the universal constant:

$$k = K [1 - \exp(-y/A)] \quad (2.4)$$

and the mixing length must be changed to

$$l = Ky [1 - \exp(-y/A)] \quad (2.5)$$

It is convenient to write equation(2.3) in dimensionless form as follows:

$$u^+ = \frac{u}{\sqrt{\tau_w/\rho}}, \quad y^+ = \frac{\sqrt{\tau_w/\rho} y}{\nu} \quad (2.6)$$

where  $\tau_w$  is the shear stress at the wall. Equation(2.3) becomes

$$\frac{\tau}{\tau_w} = \left( \frac{\partial u^+}{\partial y^+} \right) + K^2 y^{+2} [1 - \exp(-y^+/A_*)]^2 \left( \frac{\partial u^+}{\partial y^+} \right)^2 \quad (2.7)$$

in which  $A_*$  is van Driest's constant of turbulence and is equal to 26. Furthermore,

$$k = K [1 - \exp(-y^+/A_*)] \quad (2.8)$$

and



$$l^+ = Ky^+[1 - \exp(-y^+/A_*)] \quad (2.9)$$

where  $l^+ = \sqrt{\tau_w/\rho} l/v$ . According to equation(2.1) the Reynolds-stress  $\tau_r$  is obtained from

$$\tau = \mu\left(\frac{\partial \bar{u}}{\partial y}\right) + \tau_r \quad (2.10)$$

in which  $\tau_r = -\rho \bar{u}'v'$ . Hence, with equation(2.6),

$$\tau_r = \tau - \tau_w \left(\frac{\partial u^+}{\partial y^+}\right) \quad (2.11)$$

or

$$\frac{\tau_r}{\tau_w} = \left(\frac{\tau}{\tau_w}\right) - \left(\frac{\partial u^+}{\partial y^+}\right) \quad (2.12)$$

The eddy viscosity  $\mu_t$  is obtained from

$$\tau = \mu\left(\frac{\partial \bar{u}}{\partial y}\right) + \mu_t\left(\frac{\partial \bar{u}}{\partial y}\right) = (\mu + \mu_t)\left(\frac{\tau_w}{\mu}\right)\left(\frac{\partial u^+}{\partial y^+}\right) \quad (2.13)$$

so that

$$\frac{\mu_t}{\mu} = \left[\left(\frac{\tau}{\tau_w}\right)/\left(\frac{\partial u^+}{\partial y^+}\right)\right] - 1 \quad (2.14)$$

For boundary layer flow with zero pressure gradient condition,  $\partial\tau/\partial y = 0$  at the wall and therefore  $\tau = \tau_w$  near the wall. Hence equation(2.7) yields the mean velocity gradient near the wall in the form

$$\frac{\partial u^+}{\partial y^+} = \frac{2}{1 + \sqrt{1 + 4K^2 y^{+2} [1 - \exp(-y^+/A_*)]^2}} \quad (2.15)$$

From this the well-known van Driest velocity profile for the turbulent flow near a smooth wall is obtained as

$$u^+ = \int_0^{y^+} \frac{2dy^+}{1 + \sqrt{1 + 4K^2 y^{+2} [1 - \exp(-y^+/A_*)]^2}} \quad (2.16)$$

where  $K$  is the von Karman constant which is equal to 0.4. The Reynolds shear stress and eddy viscosity become, from equations (2.12) and (2.14), respectively,

$$\frac{\tau_r}{\tau_w} = 1 - \left[ \frac{\partial u^+}{\partial y^+} \right] \quad (2.17)$$

$$\frac{\mu_r}{\mu} = \frac{1}{\left[ \frac{\partial u^+}{\partial y^+} \right]} - 1 \quad (2.18)$$

Van Driest also proposed analytic expressions for the flow near a transitionally rough wall and the beginning of a fully rough wall. For the flow near a beginning of fully rough wall the wall damping effects in equations (2.8), (2.9), (2.15) and (2.16) disappear, therefore the universal constant, mixing length, mean velocity gradient and profile become

$$k = K \quad (2.19)$$

$$l^+ = Ky^+ \quad (2.20)$$

$$\frac{\partial u^+}{\partial y^+} = \frac{2}{1 + \sqrt{1 + (2Ky^+)^2}} \quad (2.21)$$

which integrates to

$$u^+ = \frac{1}{K} \left\{ \frac{1 - \sqrt{1 + (2Ky^+)^2}}{2Ky^+} + \ln \left[ 2Ky^+ + \sqrt{1 + (2Ky^+)^2} \right] \right\} \quad (2.22)$$

For the flow region under the viscous influence of the wall, where the roughness Reynolds number  $k_*$  ( $=\sqrt{\tau_w/\rho}k_s/\nu$ ) is less than 60, and  $k_s$  is the average roughness size, the nearness of the wall still shows some effect through viscous damping. In this regime of wall roughness van Driest introduced a disturbance factor which will offsets the damping factor owing to the roughness. The proposed universal constant and mixing length are

$$k = K[1 - \exp(-y^+/26) + \exp(-60y^+/26k_*)] \quad (2.23)$$

$$l^+ = Ky^+[1 - \exp(-y^+/26) + \exp(-60y^+/26k_*)] \quad (2.24)$$

And the mean velocity gradient and profile are

$$\frac{\partial u^+}{\partial y^+} = \frac{2}{1 + \sqrt{1 + 4K^2 y^{+2} [1 - \exp(-y^+/26) + \exp(-60y^+/26k_*)]^2}} \quad (2.25)$$

$$u^+ = \int_0^{y^+} \frac{2dy^+}{1 + \sqrt{1 + 4K^2 y^{+2} [1 - \exp(-y^+/26) + \exp(-60y^+/26k_*)]^2}} \quad (2.26)$$

Equation(2.25) and (2.26) give expressions for a smooth wall and the beginning of a fully rough wall if  $k_*$  is 0 or 60, respectively.

The results shown in the above analysis follow the experimental data quite well for the entire region including the viscous sublayer region ( $0 < y^+ < 5$ ), and the

transitionally

( $5 < y^+ < 60$ ) and fully turbulent regions ( $y^+ > 60$ ). The results of the above analysis are approximately valid with a streamwise pressure gradient because the shear stress near the wall is approximately equal to the wall stress. For a smooth wall, the asymptotic curves in the laminar sublayer region and in the fully turbulent flow region are, respectively,

$$u^+ = y^+ \quad (2.27)$$

$$u^+ = 5.24 + 2.5 \ln y^+ \quad (2.28a)$$

or the more generally accepted expression shown by Schlichting<sup>79</sup>

$$u^+ = 5.5 + 2.5 \ln y^+ \quad (2.28b)$$

It is evident from the smooth-wall curve that the viscous damping effect of the wall extends out to about  $y^+ = 60$ . Therefore it is expected that any roughness elements should also extend to about  $y^+ = 60$  before they completely nullify the viscous influence of the wall. The mean velocity profile for the beginning of fully rough wall, *i.e.*  $k_* = 60$ , gives an asymptote:

$$u^+ = -1.325 + 2.5 \ln y^+ \quad (2.29)$$

Thus, if there are no viscosity effects for roughness greater than  $k_* = 60$ , then the general velocity profile beyond the roughness protuberances would be, from dimensional analysis,

$$\begin{aligned} u^+ &= \text{const.} + \frac{1}{K} \ln\left(\frac{y}{k}\right) \\ &= \text{const.} - \frac{1}{K} \ln k_* + \frac{1}{K} \ln y^+ \end{aligned} \quad (2.30)$$

so that, from equation(2.29) when  $K=0.4$  and  $k_* = 60$ , the velocity profile beyond  $k_* > 60$  becomes

$$u^+ = 8.95 - 2.5 \ln k_* + 2.5 \ln y^+ \quad (2.31a)$$

or, if we consider  $k_* = 70$  to be the beginning of fully rough regime, following Schlichting<sup>79</sup> we find

$$u^+ = 8.5 - 2.5 \ln k_* + 2.5 \ln y^+ \quad (2.31b)$$

which is simply a parallel shift of the logarithmic velocity profile for a smooth wall.

## 2.2 Present Analysis

According to van Driest's analysis, for a smooth wall the wall effect damps out exponentially and for a fully rough wall the exponential damping effect of the wall disappears. To contend with these two limiting cases as well as the transitionally rough wall case a new roughness parameter  $C_j$  is introduced into the damping factor for a smooth wall. The new damping factor is:

$$1 - C_j \exp(-y^+/26) \quad (2.32)$$

where  $C_j$  is a function of the roughness Reynolds number  $k_*$ . The proposed universal constant, mixing length, mean velocity gradient and profile are as follows:

$$k = K [1 - C_j \exp(-y^+/26)] \quad (2.33)$$

$$l^+ = K y^+ [1 - C_j \exp(-y^+/26)] \quad (2.34)$$

$$\frac{\partial u^+}{\partial y^+} = \frac{2}{1 + \sqrt{1 + 4K^2 y^{+2} [1 - C_j \exp(-y^+/26)]^2}} \quad (2.35)$$

$$u^+ = \int_0^{y^+} \frac{2dy^+}{1 + \sqrt{1 + 4K^2 y^{+2} [1 - C_j \exp(-y^+/26)]^2}} \quad (2.36)$$

Equation(2.36) for  $C_j=1.0$  gives van Driest's equation(2.16) for the smooth wall and while for  $C_j=0.0$  van Driest's equation(2.22) for the beginning of a fully rough wall is recovered. Otherwise  $C_j$  is related to the roughness Reynolds number and predicts the turbulence properties for the flow near transitionally rough walls, and is similar to the van Driest equation(2.26). Consequently the introduction of  $C_j$  constitutes a new near-wall turbulence model for the flow over smooth, transitionally rough and the beginning of fully rough walls. For large  $y^+$  the van Driest velocity profiles for both smooth and rough walls and the present expression all become

$$u^+ = constant + \frac{1}{K} \ln y^+ \quad (2.37)$$

which is von Karman's logarithmic velocity distribution law for fully turbulent flow.

### 3. RESULTS AND DISCUSSIONS

The calculated results of van Driest's equations for the mean velocity and Reynolds shear stress are compared with the present results and available experimental data. The integral equations for the mean velocities are numerically calculated by using a Gaussian Quadrature Integration Method<sup>81,82</sup> with 36 points. The functional relationship between roughness Reynolds number and new roughness parameter  $C_j$  is obtained.

Figures 2.1 and Figure 2.2 show semi-logarithmic plots for the mean velocities with experimental data of Laufer<sup>83</sup> for a smooth pipe measured in the fully developed

turbulent flow regime for two Reynolds numbers (50,000 and 500,000) and rough wall data of Ligriani and Moffat<sup>84</sup> for boundary layer flow on a rough surface. Also shown are the mean velocity profiles for the smooth, transitionally rough and fully rough walls from van Driest's analysis and from the present equation(2.36) with  $K=0.4$ . The results of the present theory with  $C_j=1.0$  predicts the solution of a smooth wall equation (2.16) and that with  $C_j=0.0$  predicts that of the beginning of a fully rough wall, equation(2.22) of van Driest's theory. For the transitionally rough wall regime the present results are obtained by comparing  $C_j$  with the corresponding roughness Reynolds number  $k_*$  in equation(2.26) which will yield the same logarithmic law velocity profiles within a 2 % error. As expected, for the two theories the mean velocities in the logarithmic law region far away from the wall are well matched with each other.

Direct comparison of mean velocity profiles in the logarithmic law region obtained from the present equation(2.36) with those of van Driest's equation(2.26) gives the functional relationship between the new roughness parameter  $C_j$  and roughness Reynolds number  $k_*$  as shown in Figure2.3(also Table 2.1). This clearly shows an inverse relationship given by

$$k_* = 60 ( 1 - C_j^{0.8} ) \quad (2.38)$$

Figures 2.4, 2.5 and the 2.6 show the near-wall distributions of the Reynolds shear stresses calculated from van Driest's theory and the present theory. Also plotted in the figures are the experimental data of Schubauer<sup>85</sup> for smooth pipe and boundary layer flows. In the fully turbulent region beyond  $y^+ \geq 60$  the Reynolds shear stresses calculated from both theories match with experiment for smooth walls. But very close to the wall the distribution of the shear stresses from van Driest's analysis (Figure 2.5) are steeper than those of the present analysis (Figure 2.4). The results of

$C_j=1.0$  and  $0.0$  correspond to those of  $k_* = 0.0$  and  $60$ , respectively.

Figure 2.7 shows the near-wall distributions of the damped universal constant,  $k$  according to van Driest's analysis, equation(2.23), and the present analysis, equation(2.33), respectively, for  $K=0.4$ . Also shown in the figure is the experimental data of Ligrani and Moffat<sup>84</sup> for boundary layer flow. The introduction of  $C_j$ , which corresponds to the roughness Reynolds number  $k_*$  in the logarithmic law velocity profile, makes the  $k$  near the wall differ from that of van Driest. Near the wall the present theory overpredicts the experimental data; however, overall trends are the same since in both cases  $k$  decreases near the wall as  $k_*$  decreases. Away from the wall all of the theoretical results and experimental data for  $k$  approach  $0.4$ .

In Figures 2.8 and 2.9 the corresponding mixing length from equations(2.24), (2.34) and turbulent viscosities calculated from equation(2.14) using mean velocity gradients are compared, respectively. Figure 2.8 shows that in the transitionally rough surfaces, except very close to the wall, the present model produces a little higher mixing length. The same explanation applies to the eddy viscosity shown in the Figure 2.9.

## 4. CONCLUSIONS

A new damping factor is suggested to predict turbulent flow near transitionally rough walls. A functional relationship between roughness Reynolds number  $k_*$  and a new roughness parameter  $C_j$  is obtained. In the logarithmic velocity distribution law region the modified mean velocity profiles and Reynolds shear stress are consistent with those of van Driest's formula.

In the present analysis the roughness parameter  $C_j$  is shown to be related only to roughness Reynolds number  $k_*$ . But the number of parameters describing roughness is extraordinarily large owing to the great diversity of geometric forms. By adjusting  $C_j$



to the logarithmic mean velocity profile via the empirical relationship similar to the equation(2.38) of any type of surface conditions the new model should permit better prediction of the mean velocity and the Reynolds-shear stress for the flow near roughened surfaces.

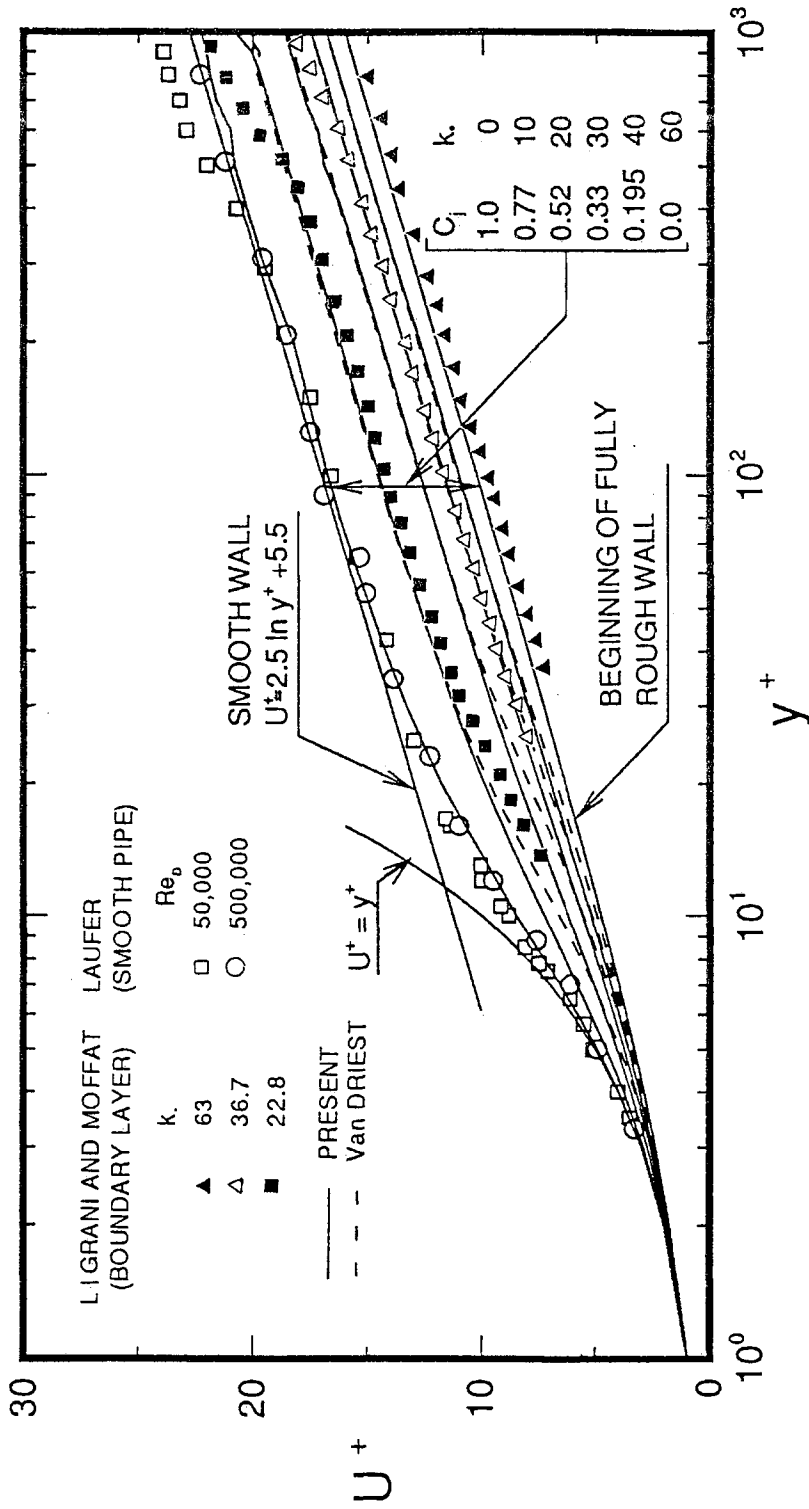


Figure 2.1 Logarithmic velocity profiles for turbulent flow near smooth and rough walls: Comparison of theories of the present study and van Driest and experiment for smooth and rough surfaces.

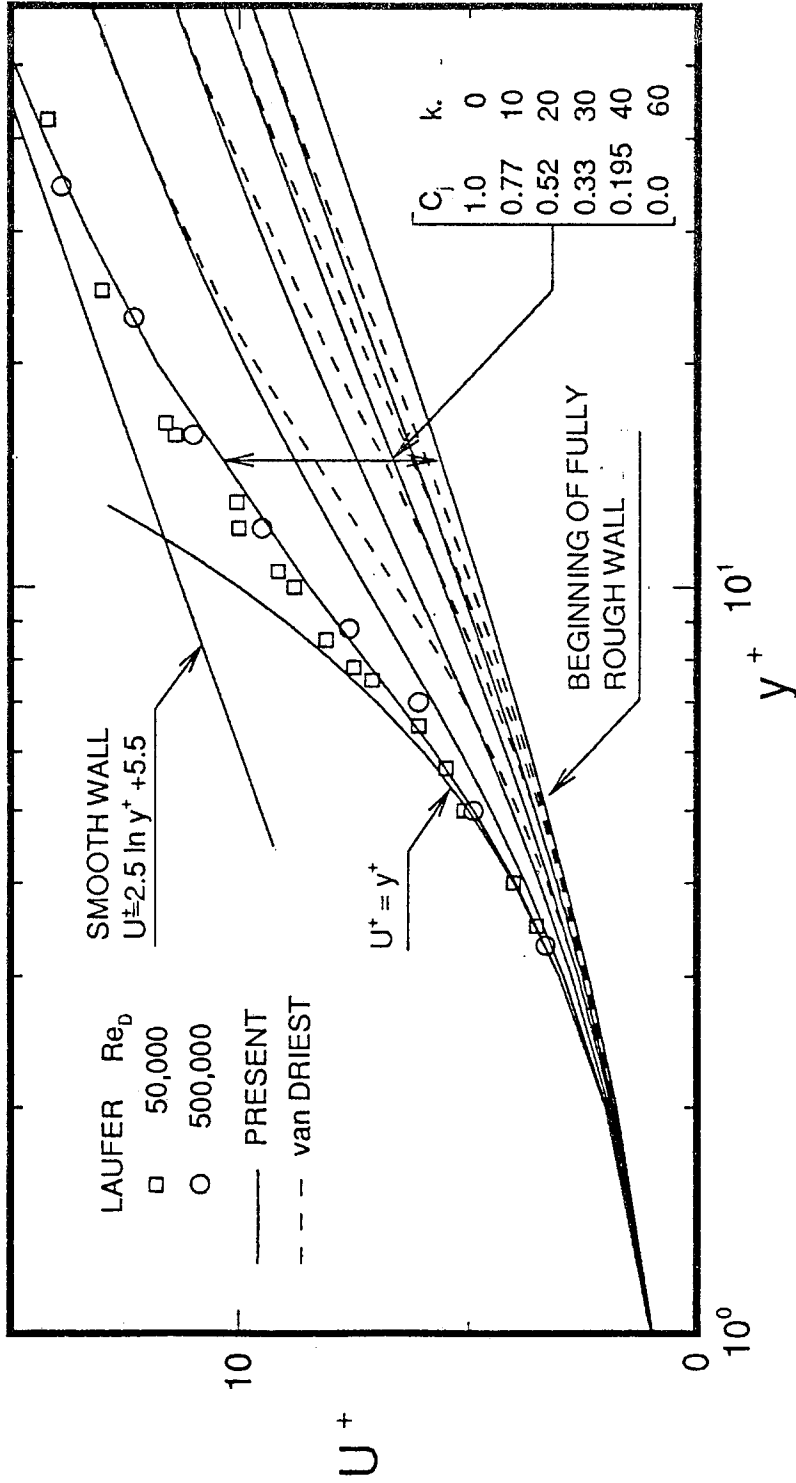


Figure 2.2 Logarithmic velocity profiles for turbulent flow near smooth and rough walls: Comparison of theories of the present study and van Driest and experiment for a smooth pipe

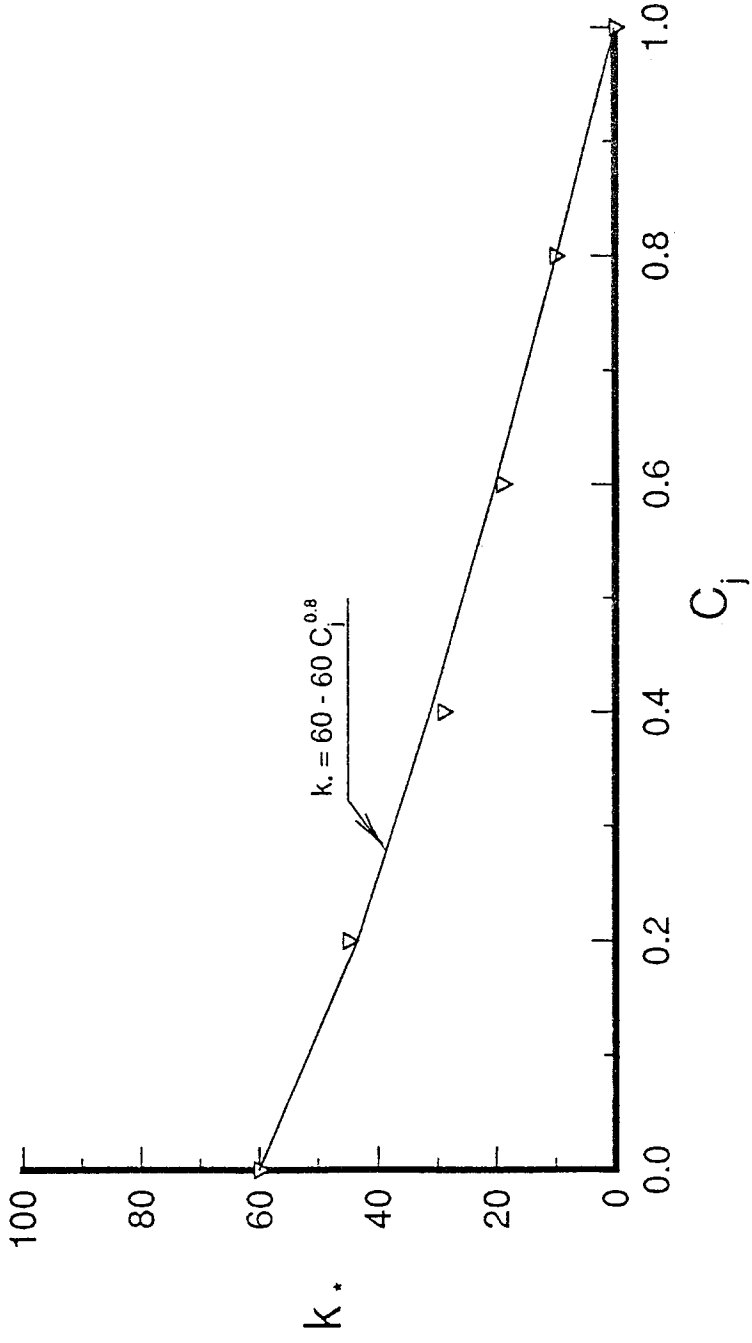


Figure 2.3 Functional relationship between roughness Reynolds number  $k_*$  (van Driest's theory) and roughness parameter  $C_j$  (present theoretical approach)

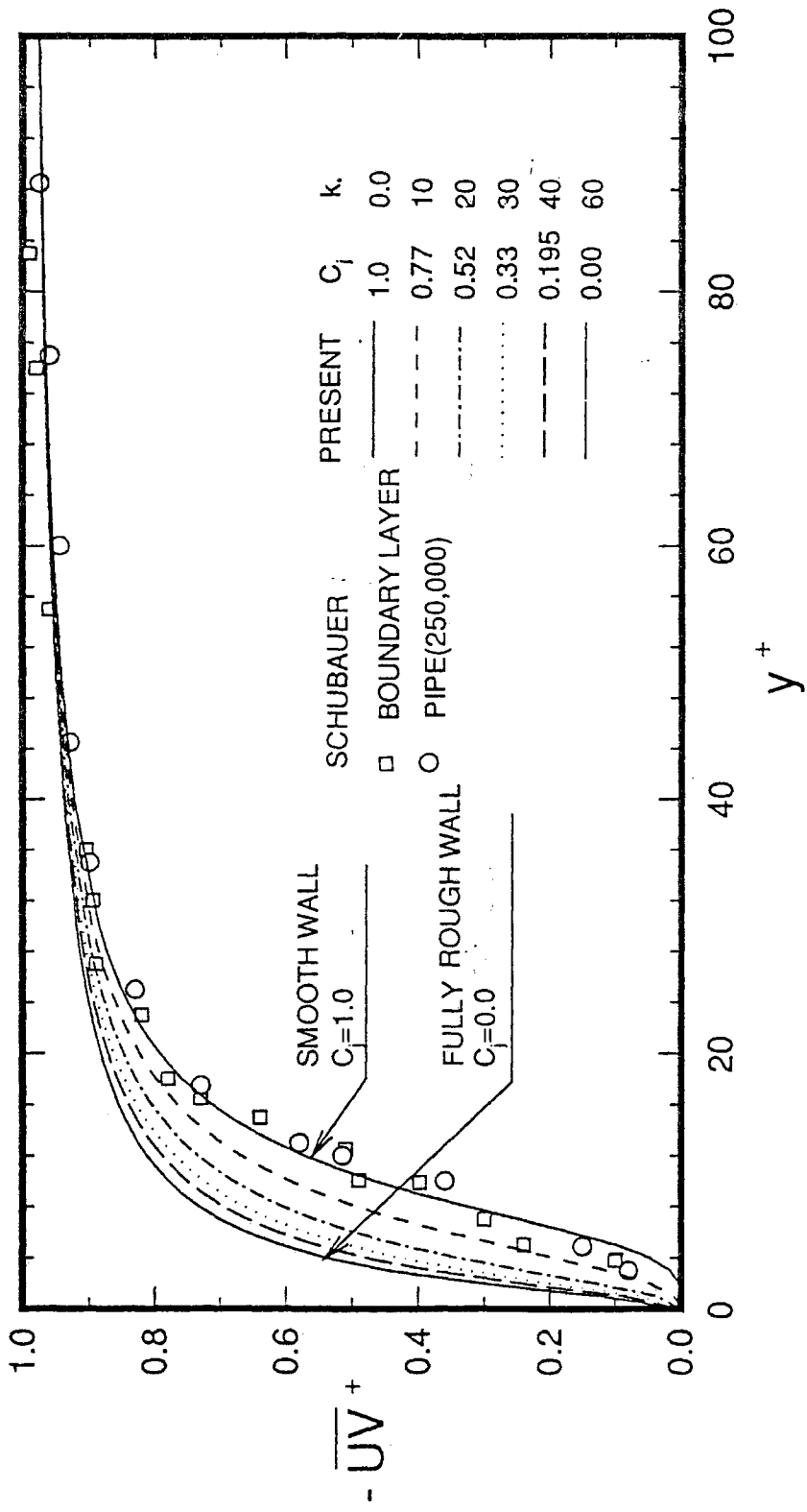


Figure 2.4 Near-wall distribution of Reynolds shear stress for flow near smooth and rough walls: Comparison of results of the present theory and experiment for a smooth pipe

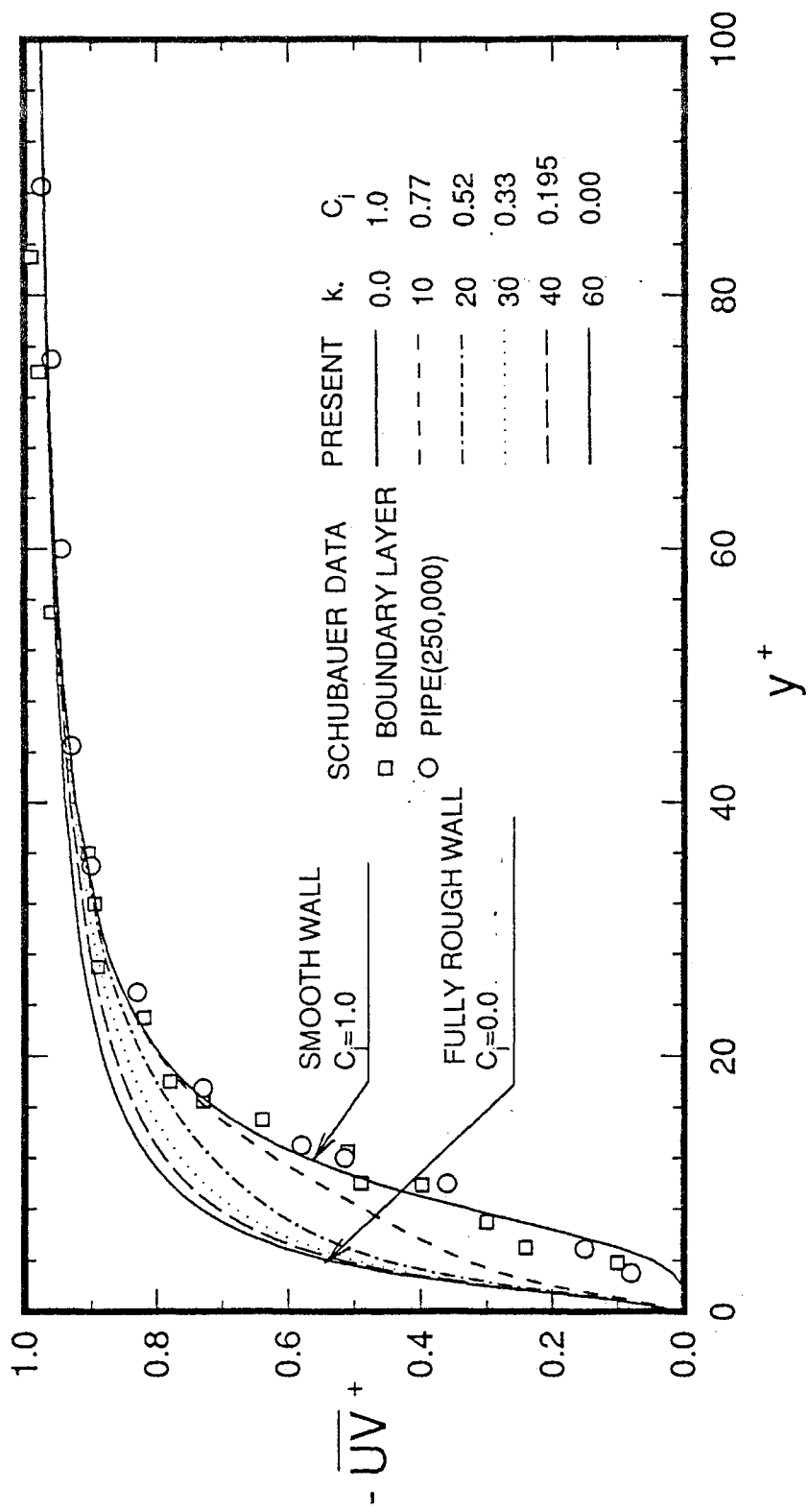


Figure 2.5 Near-wall distribution of Reynolds shear stress for flow near smooth and rough walls: Comparison of results of van Driest's theory and experiment for a smooth pipe

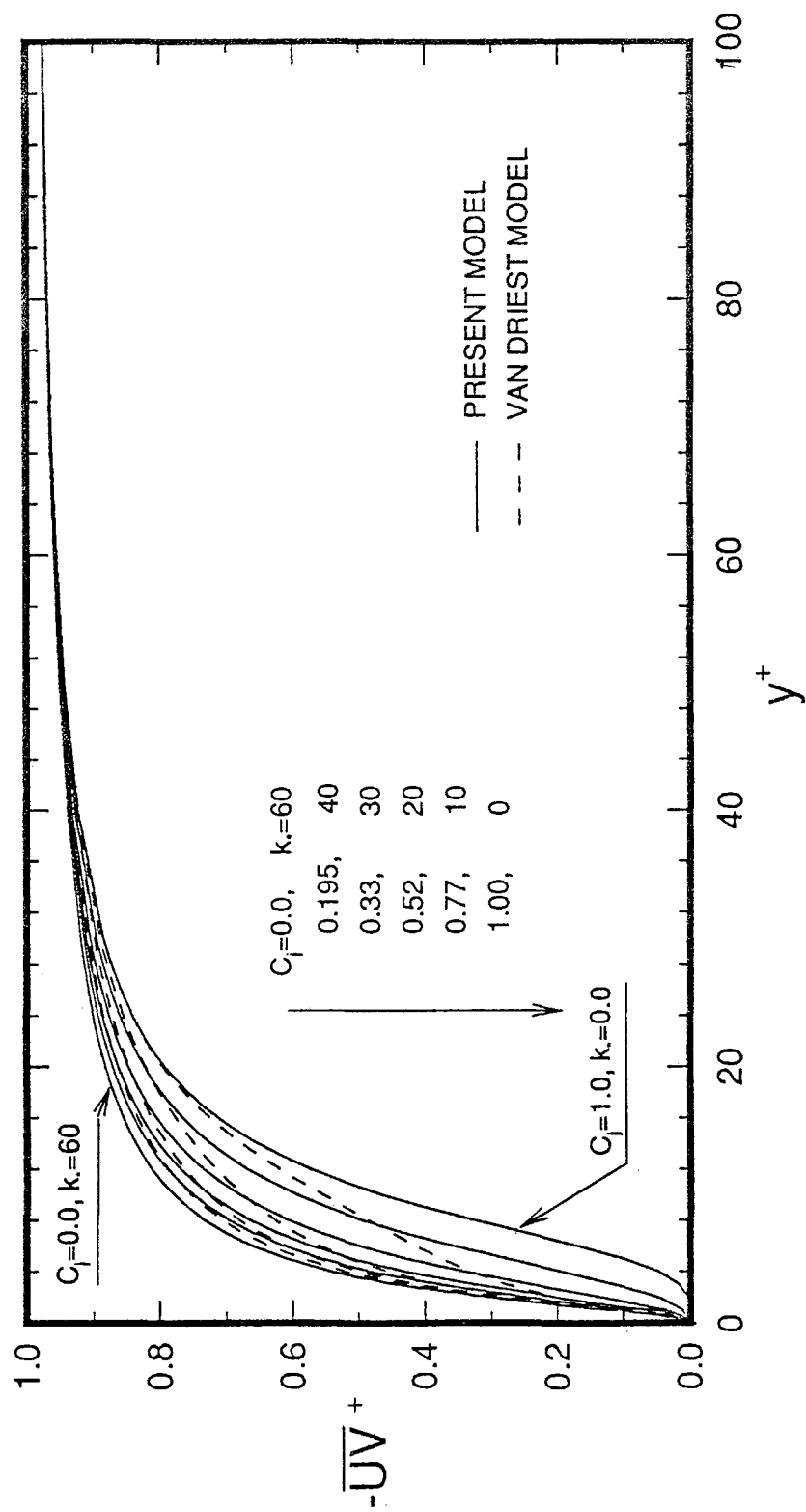


Figure 2.6 Near-wall distribution of Reynolds shear stress for flow near smooth and rough walls: Comparison of results of the present theory and van Driest's theory

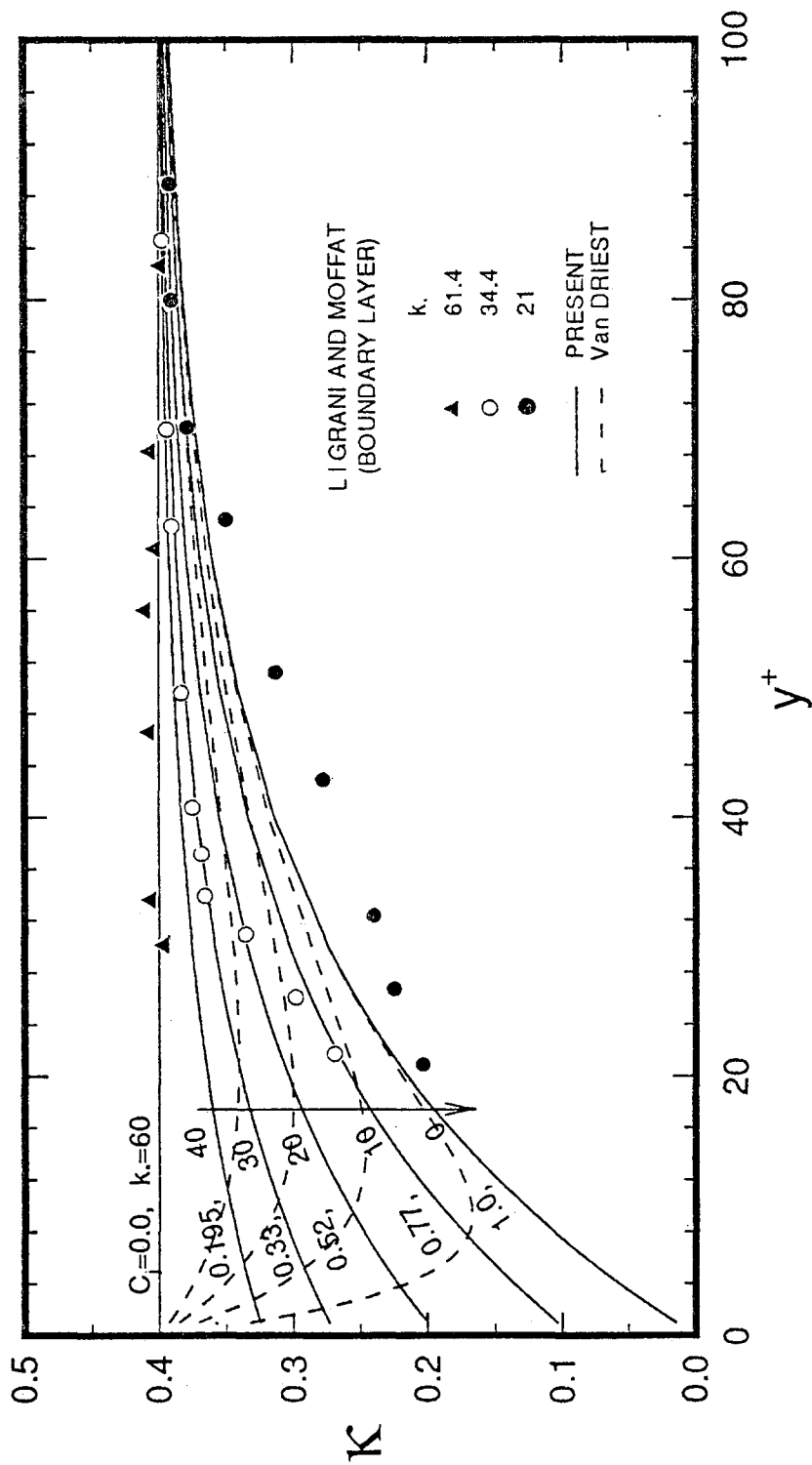


Figure 2.7 Damped universal constant for turbulent flow near smooth and rough walls: Comparison of the present theory and van Driest's theory and experimental data



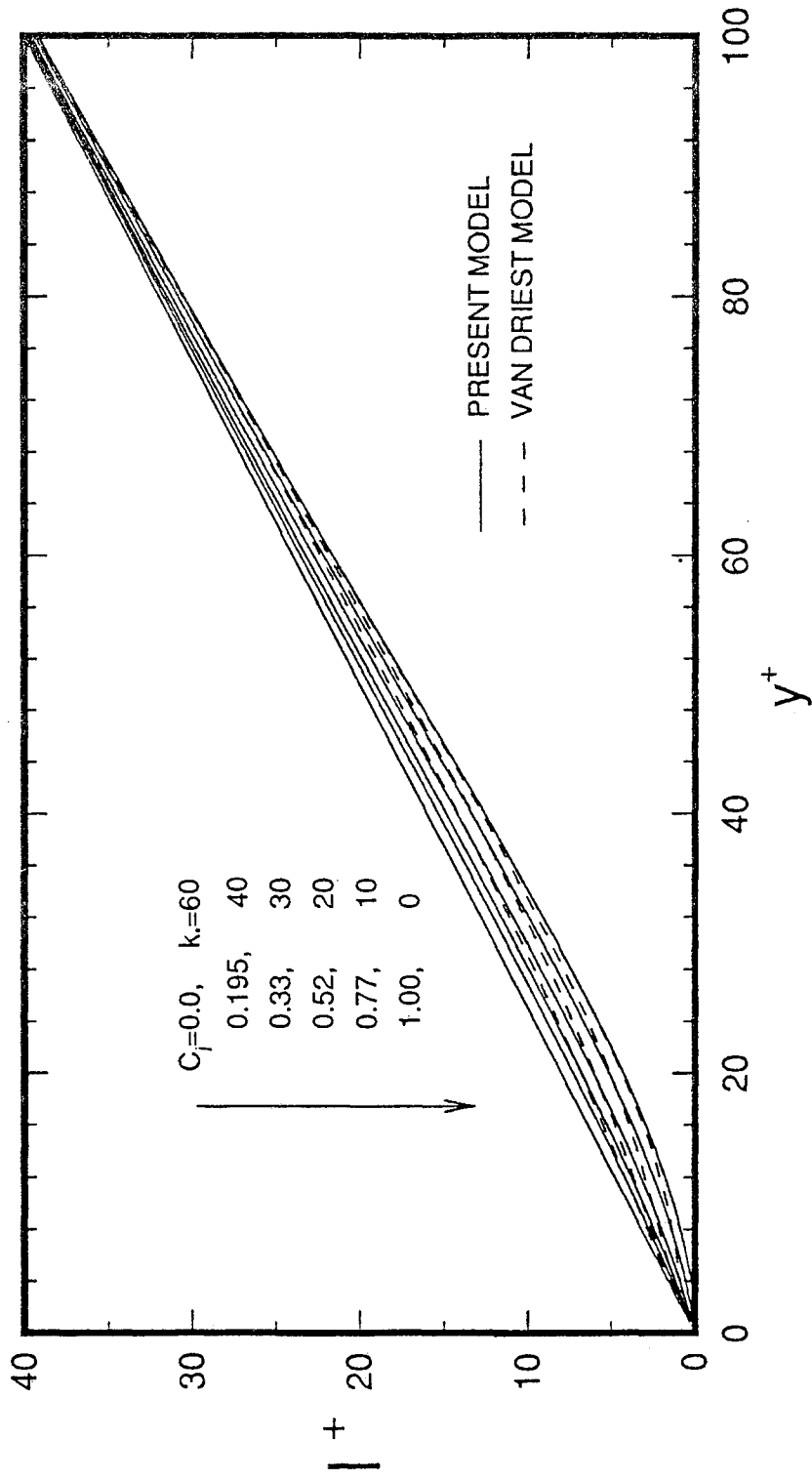


Figure 2.8 Mixing length for turbulent flow near smooth and rough walls: Comparison of the present theory and van Driest's theory

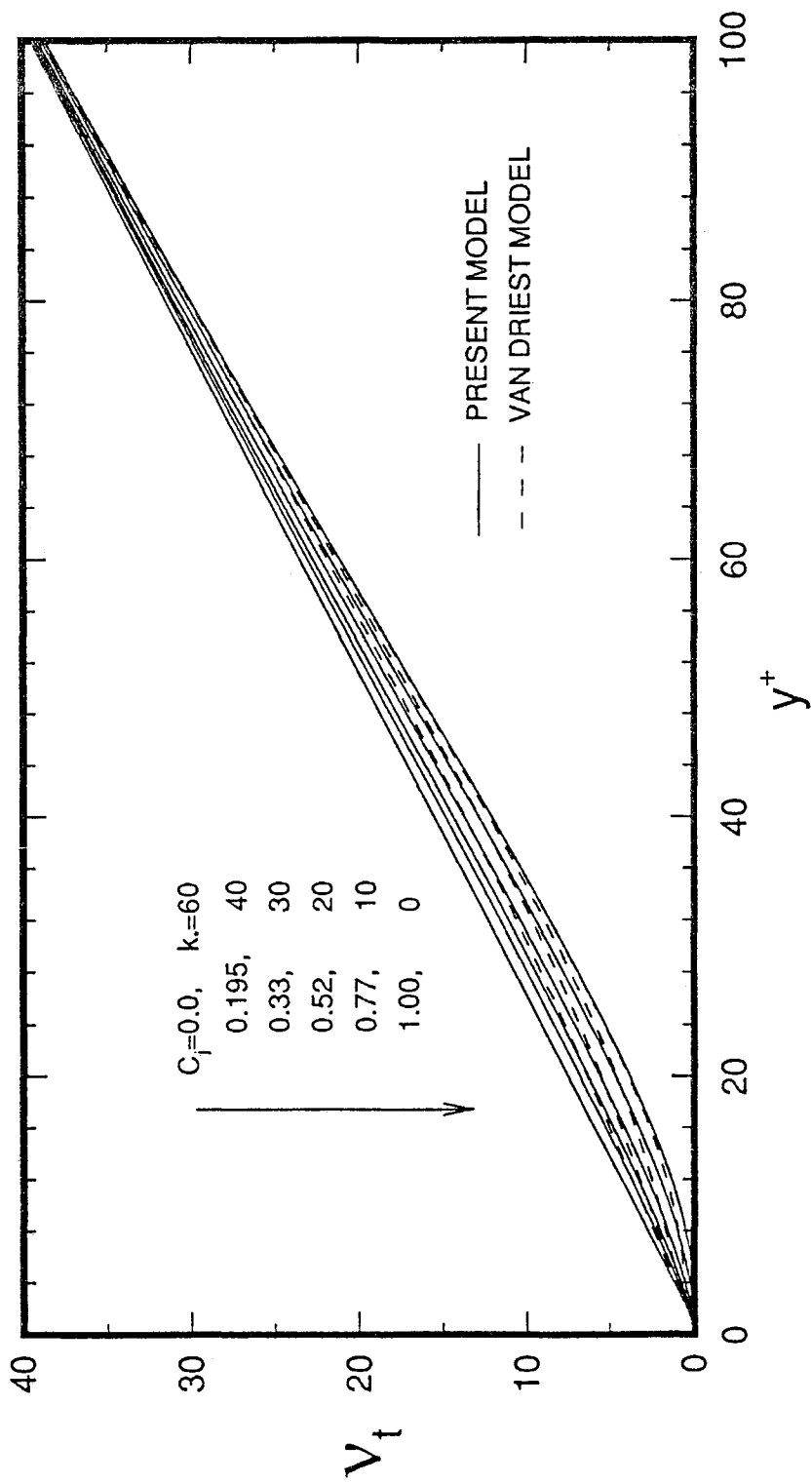


Figure 2.9 Turbulent viscosity for turbulent flow near smooth and rough walls: Comparison of the present theory and van Driest's theory

Table 2.1 Comparison of roughness parameter  $C_j$  (present theory) and roughness Reynolds number  $k_*$  (van Driest's theory)

Theoretical Approach	
$C_j$	$k_*$
1.0	0
0.77	10
0.52	20
0.33	30
0.195	40
0.0	60

# Chapter 3

## Computation 1

### Algebraic Turbulence Model

#### 1. INTRODUCTION

In the present study a steady state, incompressible, developing turbulent flow in a circular pipe is selected to evaluate the newly developed algebraic turbulence viscosity model in Chapter 2. A new roughness/computational parameter  $C_j$  is introduced into the damping factor in the algebraic turbulent viscosity  $\nu_t$  for the flow near smooth wall as originated by van Driest<sup>7</sup>. The new algebraic model is designed to predict the behavior of the turbulence properties for the flow near smooth, transitionally rough and fully rough walls. A fully elliptic computational code for the time-averaged Reynolds momentum equations combined with an algebraic turbulence model is developed.

The discretized governing equations are simultaneously solved for all flow variables ( $U, V, P$ ), using a line-by-line marching iterative solution technique, up to 100 pipe diameters downstream for bulk Reynolds numbers 10,000, 50,000 and 500,000.

The near-wall variations of turbulence properties and their distributions in the fully turbulent region are obtained and compared with available experimental and the calculated results of the van Driest's theory.

It is shown that the roughness parameter is inversely proportional to the roughness Reynolds number within a moderate range of the wall roughness. In the near-wall region the mean velocity and Reynolds shear stress over rough walls are increased compared with those over smooth walls. In the fully turbulent region the roughness effect of the wall disappears, so that the roughness on the wall does not affect the distributions of the Reynolds shear stress.

## 2. PROBLEM FORMULATION

### 2.1 Governing Equations and Algebraic Turbulence Model

The fully elliptic time-averaged Reynolds transport equations are written in cylindrical, axisymmetric coordinates. The following equations are written in nondimensionalized form for a steady, incompressible, two-dimensional turbulent flow. The flow properties are normalized as follows:

$$\begin{aligned} X &= \frac{x}{D}, \quad r = \frac{y}{D}, \quad U = \frac{\bar{u}}{u_0}, \\ V &= \frac{\bar{v}}{u_0}, \quad P = \frac{\bar{p}}{\rho u_0^2}, \end{aligned} \quad (3.1)$$

where  $x$  and  $y$  are the horizontal and radial coordinates,  $\bar{u}$  is the mean velocity parallel to the  $x$  direction,  $\bar{v}$  the cross mean velocity in the  $y$  direction,  $\bar{p}$  the mean static pressure,  $\rho$  the density of fluid.

Continuity Equation;

$$\frac{\partial U}{\partial X} + \frac{1}{r} \frac{\partial rV}{\partial r} = 0 \quad (3.2)$$

X-Momentum Equation;

$$\begin{aligned} U \frac{\partial U}{\partial X} + V \frac{\partial U}{\partial r} = & - \frac{\partial P}{\partial X} + \frac{1}{\text{Re}_D} \frac{\partial}{\partial X} \left[ (1+2v_t) \frac{\partial U}{\partial X} \right] \\ & + \frac{1}{\text{Re}_D} \left[ \frac{1}{r} \frac{\partial}{\partial r} r \left[ \frac{\partial V}{\partial r} + v_t \left( \frac{\partial U}{\partial r} + \frac{\partial V}{\partial X} \right) \right] \right] \end{aligned} \quad (3.3)$$

r-Momentum Equation;

$$\begin{aligned} U \frac{\partial V}{\partial X} + V \frac{\partial V}{\partial r} = & - \frac{\partial P}{\partial r} + \frac{1}{\text{Re}_D} \frac{\partial}{\partial X} \left[ (1+v_t) \frac{\partial V}{\partial X} + v_t \frac{\partial U}{\partial r} \right] \\ & + \frac{1}{\text{Re}_D} \left[ \frac{1}{r} \frac{\partial}{\partial r} \left[ (1+2v_t) r \frac{\partial V}{\partial r} \right] \right] \end{aligned} \quad (3.4)$$

where the Reynolds number is defined by mean velocity at the pipe inlet  $u_0$ , pipe diameter  $D$  and kinematic viscosity of fluid  $\nu$ . The turbulent or eddy viscosity is defined as

$$v_t = \frac{1}{\left[ \frac{\partial u^+}{\partial y^+} \right]} - 1, \quad (3.5)$$

with the modified mean velocity gradient

$$\frac{\partial u^+}{\partial y^+} = \frac{2}{1 + \sqrt{1 + 4K^2 y^{+2} [1 - C_j \exp(-y^+/26)]^2}} \quad (3.6)$$

where

$$u^+ = \frac{u}{\sqrt{\tau_w/\rho}}, \quad y^+ = \frac{\sqrt{\tau_w/\rho} y_n}{\nu} \quad (3.7)$$

and  $K$  is the von Karman constant, 0.4,  $y_n$  normal distance to wall and  $C_j$  is a roughness parameter related to the roughness Reynolds number  $k_*$  which is defined by  $\sqrt{\tau_w/\rho} k_s/\nu$ , and  $k_s$  is average roughness size.

## 2.2 Finite Difference Equations and Computational Grid

The fully elliptic governing partial differential equations (3.2)-(3.4) are discretized using the finite difference approximation with a first order upwind difference scheme for convective terms and a second order centered difference scheme for diffusion terms. In the future the fully second order computations for the convective terms will be carried out. The staggered grid of the Marker and Cell(MAC) method proposed by Welch *et al.*<sup>86</sup> is used for the calculation of  $U, V$  and  $P$ . The discretized grid positions based on the staggered grid system for the calculation of each flow property are shown in Figure 3.1. Based on this staggered grid system the continuity equation can be written using a second order accurate centered difference scheme without interpolation and the pressure can be calculated in the same grid point where the continuity equation is evaluated. Patankar<sup>54</sup> discussed the merits of the staggered grid in detail. The resulting finite difference equations in the nonuniform grid system are written in Appendix.

To resolve the large gradient of mean velocities and turbulence properties in the near-wall region, a nonuniform grid system is used. The positions of the grid system are carefully determined by modifying an exponentially stretching transformation used in ARC2D code<sup>87</sup> to generate a finer grid near the wall and the inlet region. In the fully turbulent region a uniform grid system connected smoothly to the nonuniform grid system is used. Depending on Reynolds number, the distance to the first grid point from the wall should be adjusted to get a reliable convergent solution. For Reynolds numbers 50,000 and 500,000 and  $C_j = 0.9$  in a  $120 \times 50$  grid system to get the grid independent results the typical positions used for the first grid are 0.00004 and 0.0000015 times of pipe radius, respectively. This is sufficient to put 14 grid points within laminar sublayer region ( $y^+ < 5$ ) and 24 grid points within the buffer region ( $y^+ < 40$ ).

## 2.3 Boundary Conditions

The set of the discretized linear equations are solved numerically for a steady state, incompressible, two dimensional, developing turbulent pipe flow with uniform inlet conditions for the mean velocities.

Since an iterative solution technique has been adopted to solve the set of elliptic governing equations, two boundary conditions, an inlet condition, and an exit condition are required. The pipe centreline is assumed to be an axis of symmetry. Along the wall no-slip conditions are enforced for mean velocity components. At the inlet, uniform values for the mean velocity are specified, *i.e.*  $U_0 = 1$ ,  $V_0 = 0$  are given along the radial direction at two axial stations. At the exit, for all flow variables except mean pressure the axial gradients are to be zero. For mean pressure an arbitrary value is specified, *i.e.*  $P = 1$ . Due to the staggered grid system and finite difference scheme used, the inlet and wall conditions are not necessary for the mean pressure. The details of computational geometry, boundary conditions, inlet conditions and exit conditions



are shown in Figure 3.2.

### 3. SOLUTION METHOD

At each grid point the coefficient element sets a  $3 \times 3$  matrix. The discretized equation set is solved numerically from the pipe inlet up to 100 pipe diameters downstream. After initializing the whole computational domain with the inlet conditions a block-tridiagonal-coefficient-matrix with  $3 \times 3$  matrix elements is solved along the radial coordinate direction from centreline to the wall, line-by-line marching to the downstream direction. To invert the block-tridiagonal-matrix an algorithm suggested by Issacson and Keller<sup>88</sup> is used.

The turbulent viscosity is evaluated at the same position as  $P$  at the end of each global iteration process for the whole computational domain using the newly obtained mean velocities. A fully explicit method is used for  $U, V$  and  $P$ .

Due to the staggered grid and the finite difference scheme used for the continuity equation the residual of a discretized continuity equation always becomes machine accuracy  $10^{-15}$  at any stage of the solution procedure thus the convergence is checked for the Reynolds-averaged momentum equations. In general for a  $120 \times 50$  grid size 130 iterations are sufficient to give a convergent solution. When the total residual of the discretized equations becomes less than  $10^{-6}$  the iteration process is stopped. The computational procedure is shown in Figure 3.3.

### 4. RESULTS AND DISCUSSIONS

In Figure 3.4 the developing axial mean velocity vs  $x/D$  for  $Re_D = 10,000, 50,000$  and  $500,000$  at  $r/R = 0.0, 0.5, 0.75, 0.94$  from the inlet to 100 pipe diameters

downstream is shown for  $C_j=1.0$ . Figure 3.4 shows, as expected, that at higher Reynolds numbers the mean velocity distribution across the sectional area are flatter than for the lower Reynolds numbers. For the same initial conditions the mean velocity of the lower Reynolds number turbulent flow reaches fully developed conditions faster than that of the higher Reynolds number turbulent flow. But experimental data for the axial mean velocity show that fully developed mean velocity profiles do not occur until more than 40 pipe diameters downstream. Therefore, the algebraic turbulence model predicts achievement of fully developed flow too fast because the algebraic turbulence model accounts neither for transport and history effects of turbulence nor for laminar and transition regions. The results of early development of the mean velocity lead to the increased flatness of the radial distribution of the fully developed mean velocity as shown in Figure 3.5. In Figure 3.5 the mean velocity profiles in the fully developed region,  $x/D=80$ , for  $Re_D=500,000$  and several  $C_j$  are compared with the smooth wall experimental data of Nikuradse<sup>89</sup> for  $Re_D=380,000$ . As  $C_j$  decreases the mean velocity in the fully turbulent region, *i.e.* near centreline region increases while in the near-wall region it decreases. It shows that the effect of wall roughness reaches the whole mean velocity field.

From Figure 3.6 to Figure 3.8 for  $Re_D=10,000$ , 50,000 and 500,000 the logarithmic velocities are demonstrated and from Figure 3.9 to Figure 3.11 the same results are plotted on linear coordinates. To show the effect of rough walls on the mean velocity the results of  $0.0 \leq C_j \leq 1.0$  are shown. The present result with  $C_j=1.0$  is corresponding to that of van Driest's theory for a smooth wall, *i.e.* equation(2.16) and that with  $C_j=0.0$  is the beginning of a fully rough wall, *i.e.* equation(2.22). Other values of  $C_j$  are for transitionally rough walls. Except for the wake regions the results of  $C_j=1.0$  compare well with the experimental data of Laufer<sup>83</sup> for smooth walls and the empirical correlations equation(2.27) and (2.28b). The values of the  $k_*$  corresponding to  $C_j$  are obtained by the direct comparisons of the logarithmic mean velocity profiles in the fully turbulent region calculated from the equation(2.26) of van Driest's

theory and are tabulated in Table 3.1. For the lower Reynolds number flow the slope of the logarithmic mean velocity profiles deviates from the von Karman's logarithmic velocity law for a smooth wall. Therefore for  $Re_D = 10,000$  the  $k_*$  corresponding to  $C_j$  is obtained approximately in the range of  $40 < y^+ < 100$ . In Figure 3.8 the experimental data of Ligrani and Moffat<sup>84</sup> for boundary layer flow on rough surfaces are shown. The present result corresponding to  $k_*$  of van Driest's theory predicts a little higher  $k_*$  than that of experimental data. But the overall effect of  $C_j$  being different from 1.0 results in the shift of the logarithmic velocity profile for the smooth wall.

Figures 3.12, 3.13 and 3.14 demonstrate the near-wall behavior of Reynolds shear stress. The effect of the wall roughness on the Reynolds shear stress is shown respectively in Figures 3.12, 3.13, and 3.14 for  $Re_D = 10,000$ ,  $50,000$  and  $500,000$ . The corresponding roughness Reynolds number  $k_*$  from the van Driest's formula and experimental data of Schubauer<sup>85</sup> for the smooth pipe and boundary layer flows are also shown. The near-wall variation of the Reynolds-stresses is not affected much by Reynolds number. But as the wall roughness increases a significant increment in the Reynolds-shear stresses is shown. In the laminar sublayer region ( $y^+ < 5$ ) the present calculations with  $C_j = 0.8$  and  $0.9$  predict the experimental data for the smooth surfaces very well. As Reynolds number increases the results in the fully turbulent region are independent of the roughened wall conditions and the effect of wall roughness is limited to the buffer region. For the higher Reynolds number flow in part of the buffer region and the fully turbulent region the distribution of Reynolds shear stress is consistent with the experimental data for smooth walls. The present results are consistent with the Reynolds similarity hypothesis of Townsend<sup>90</sup> which means that at sufficiently high Reynolds number turbulent motion outside the inner layer (up to five times of the roughness height) is independent of the wall roughness.

Figures 3.15, 3.16 and 3.17 show the distribution of Reynolds shear stresses along the radial directions for different  $C_j$ . For the higher Reynolds number flow the effect of wall roughness is confined to regions very close to the wall. On the contrary to the

higher Reynolds number flow (Figure 3.17), for the case of lower Reynolds number turbulent flow (Figure 3.15) the effect of the wall roughness is significant even in regions away from the wall. This may be due to the fact that the strong diffusive action transfers the effect of the wall conditions further away from the wall at lower Reynolds numbers. In the fully turbulent flow region the present results compare very well with the experimental data of Laufer<sup>83</sup> for smooth walls.

Figure 3.18(also Table 3.1) shows the functional relationship between the roughness Reynolds number  $k_*$  in equation(2.26) and the roughness parameter  $C_j$  for  $Re_D=10,000, 50,000$  and  $500,000$ . Also in the Figure the result obtained from the comparison of theories in Chapter 2 is shown. The logarithmic law velocity profiles in the fully turbulent region are compared to the results of the present algebraic model and van Driest's theory. From the numerical simulation of algebraic turbulence model the empirical functional relationship between  $k_*$  and  $C_j$  is given by:

$$k_* = 60 ( 1 - C_j^{0.8} ) \quad (3.8)$$

which is the same relationship as the result obtained in chapter 2.

## 5. CONCLUSIONS

Based on the present study the following conclusions are obtained.

- 1) A simultaneous solution technique was used successfully for the Reynolds-averaged momentum equations combined with a new algebraic turbulence model.
- 2) By introducing a new roughness parameter  $C_j$  into the damping factor of the van Driest's model for a smooth wall, a new algebraic turbulence model was obtained and it predicts mean velocity and Reynolds-shear stress for the flow

near smooth, transitionally rough and fully rough walls. The correlation between the roughness Reynolds number  $k_*$  and roughness parameter  $C_j$  is found and it is shown that  $C_j$  is inversely related to  $k_*$  within the moderate range of the wall roughness, *i.e.*  $0.0 \leq k_* \leq 60$ .

- 3) In the logarithmic law of the wall region, the overall results obtained show good agreement with experimental data for the flow near smooth walls. Very close to the wall the introduction of the new roughness parameter predicts high values of Reynolds shear stresses compared with the experimental data for smooth walls.

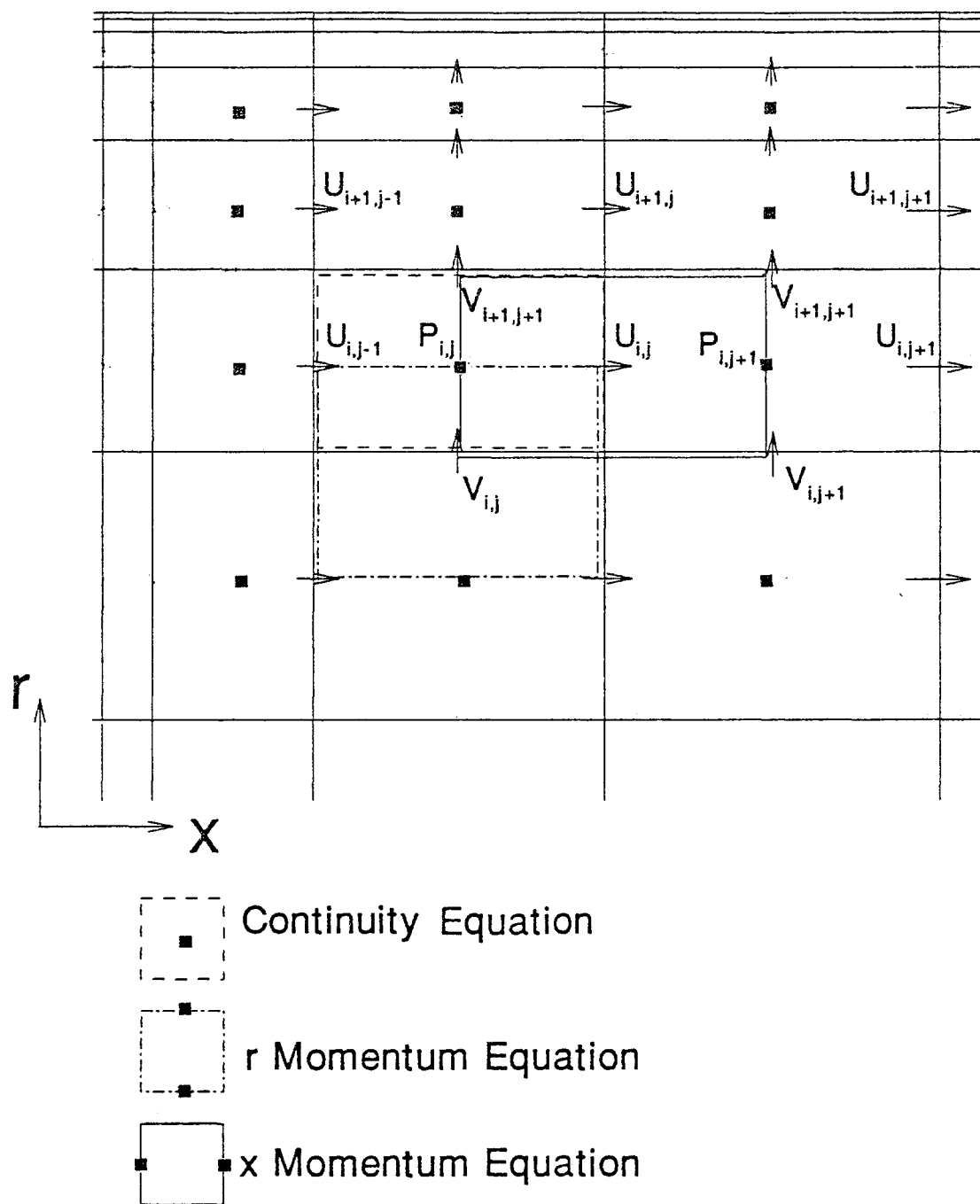


Figure 3.1 Finite difference domain for discretized governing equations

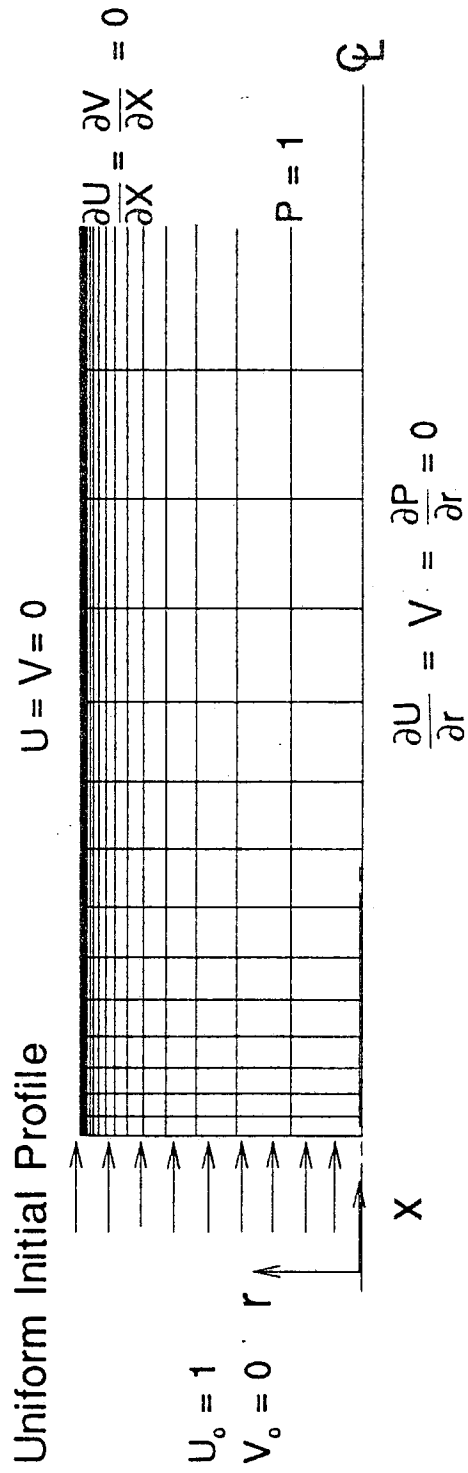


Figure 3.2 Computational geometry and boundary conditions

## Turbulent Pipe Flow

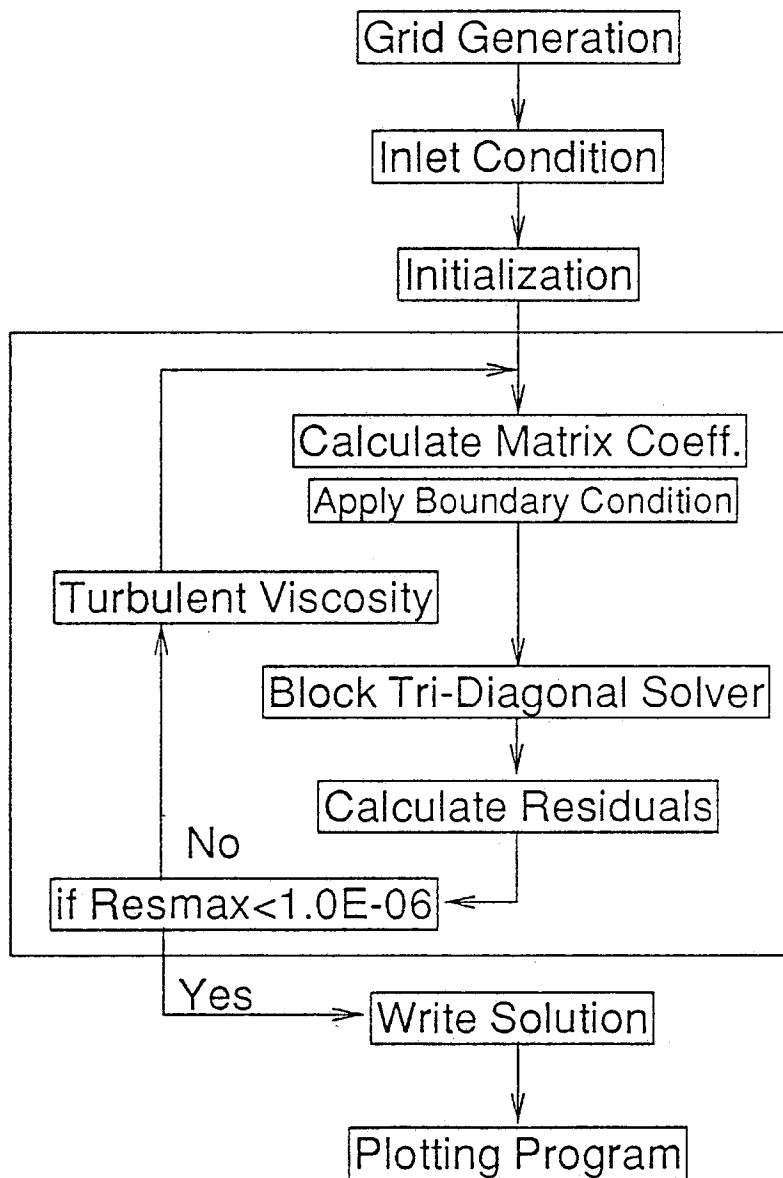


Figure 3.3 Flow chart for computational procedure



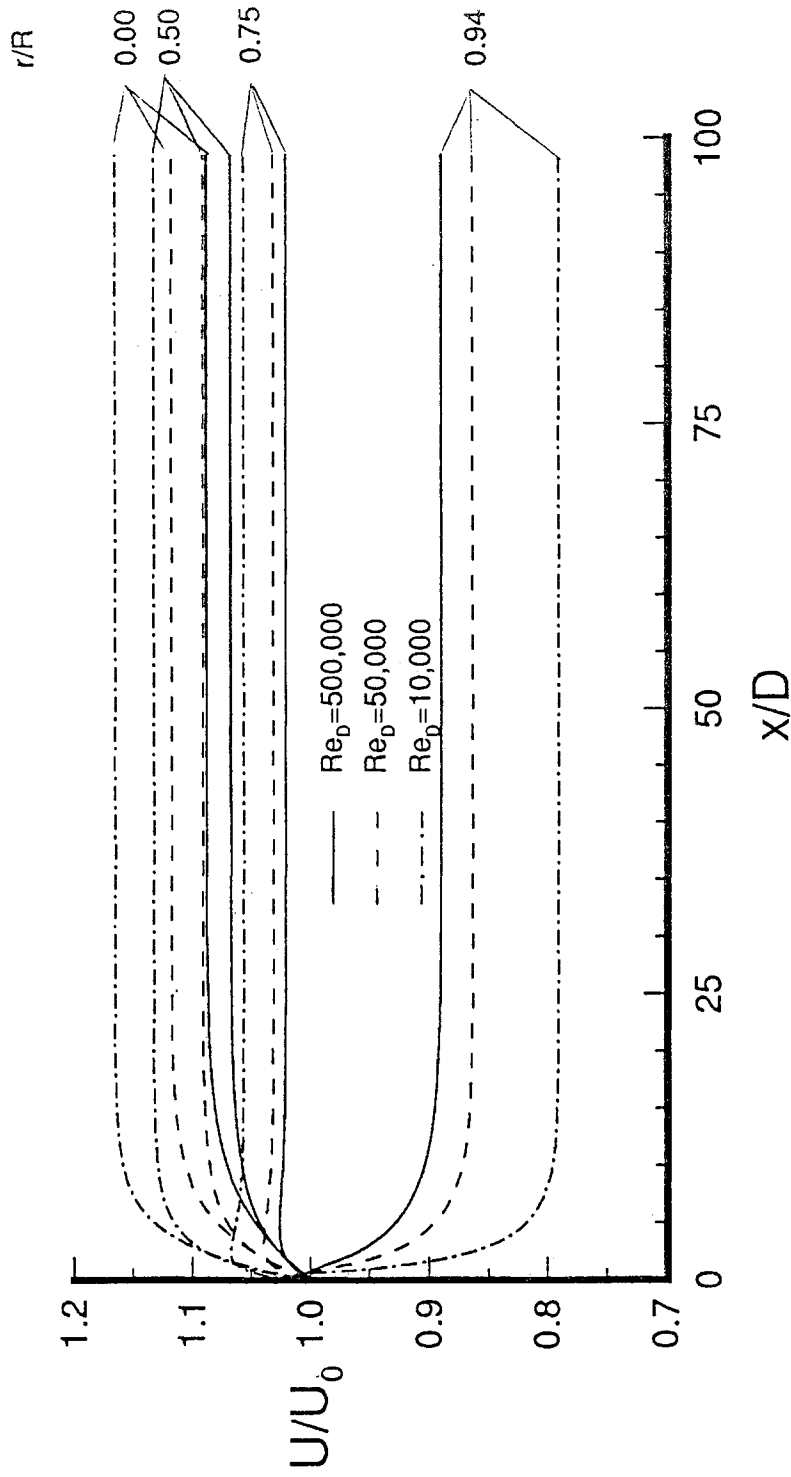


Figure 3.4 Variation of axial velocity with distance downstream of pipe inlet at  $C_j = 1.0$  for  $r/R = 0.0, 0.5, 0.75, 0.94$  for  $Re_D = 10,000, 50,000$  and  $500,000$

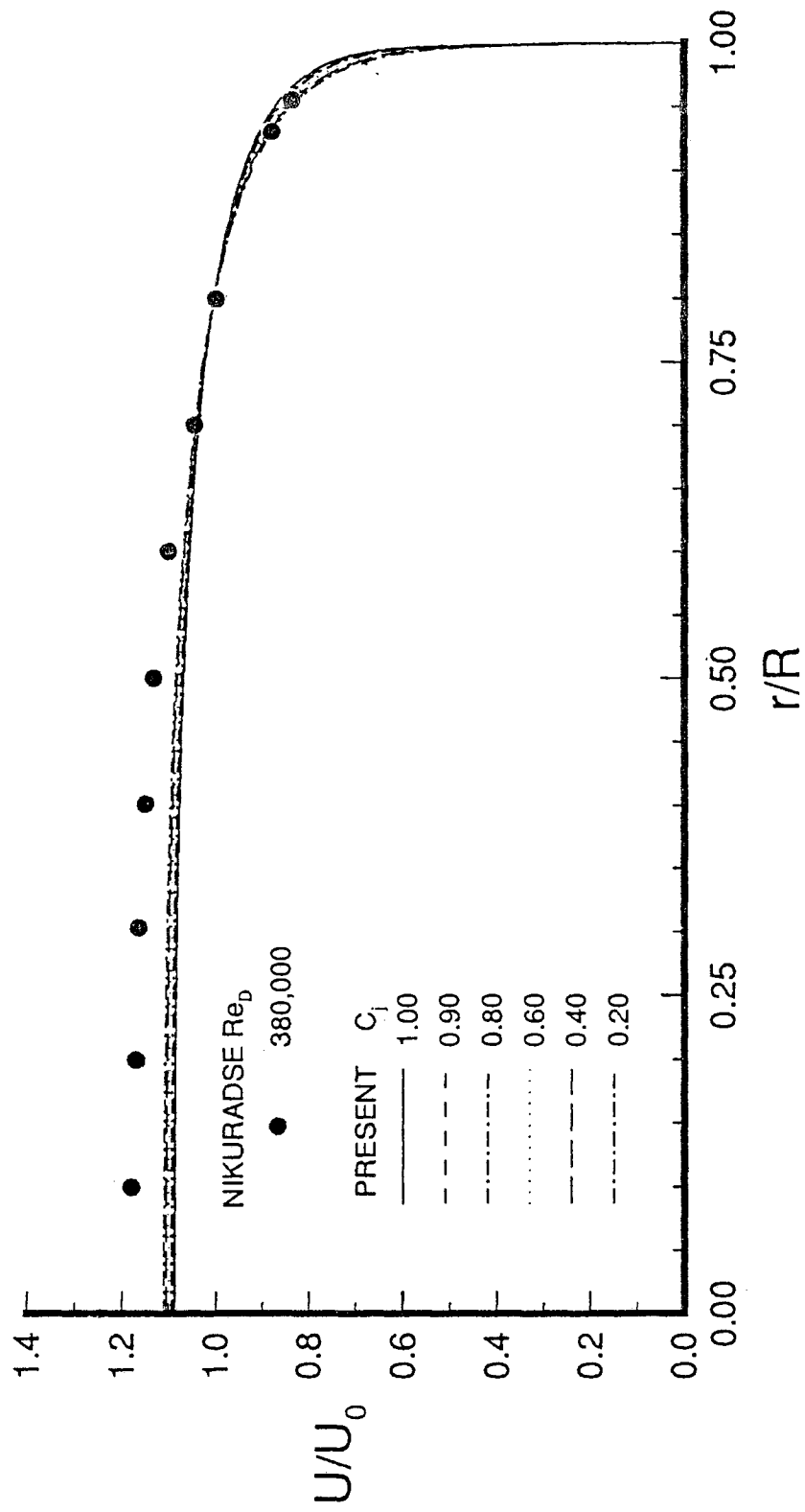


Figure 3.5 Variation of axial velocity with  $r/R$  for  $0.2 \leq C_j \leq 1.0$

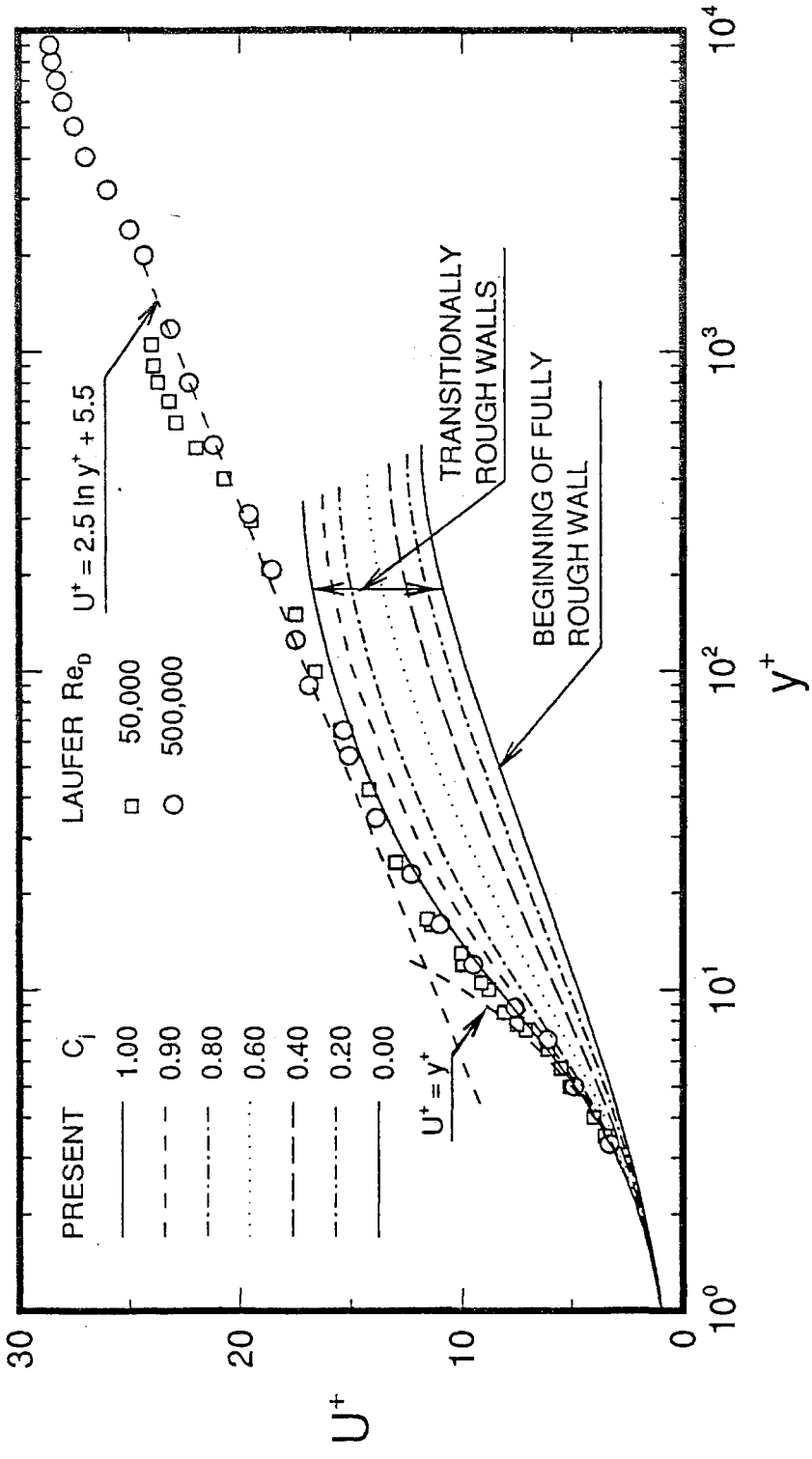


Figure 3.6 Logarithmic velocity profiles for turbulent flow near smooth and rough walls: Comparison of results of the present algebraic turbulence model ( $Re_D=10,000$ ) and experiment for a smooth pipe

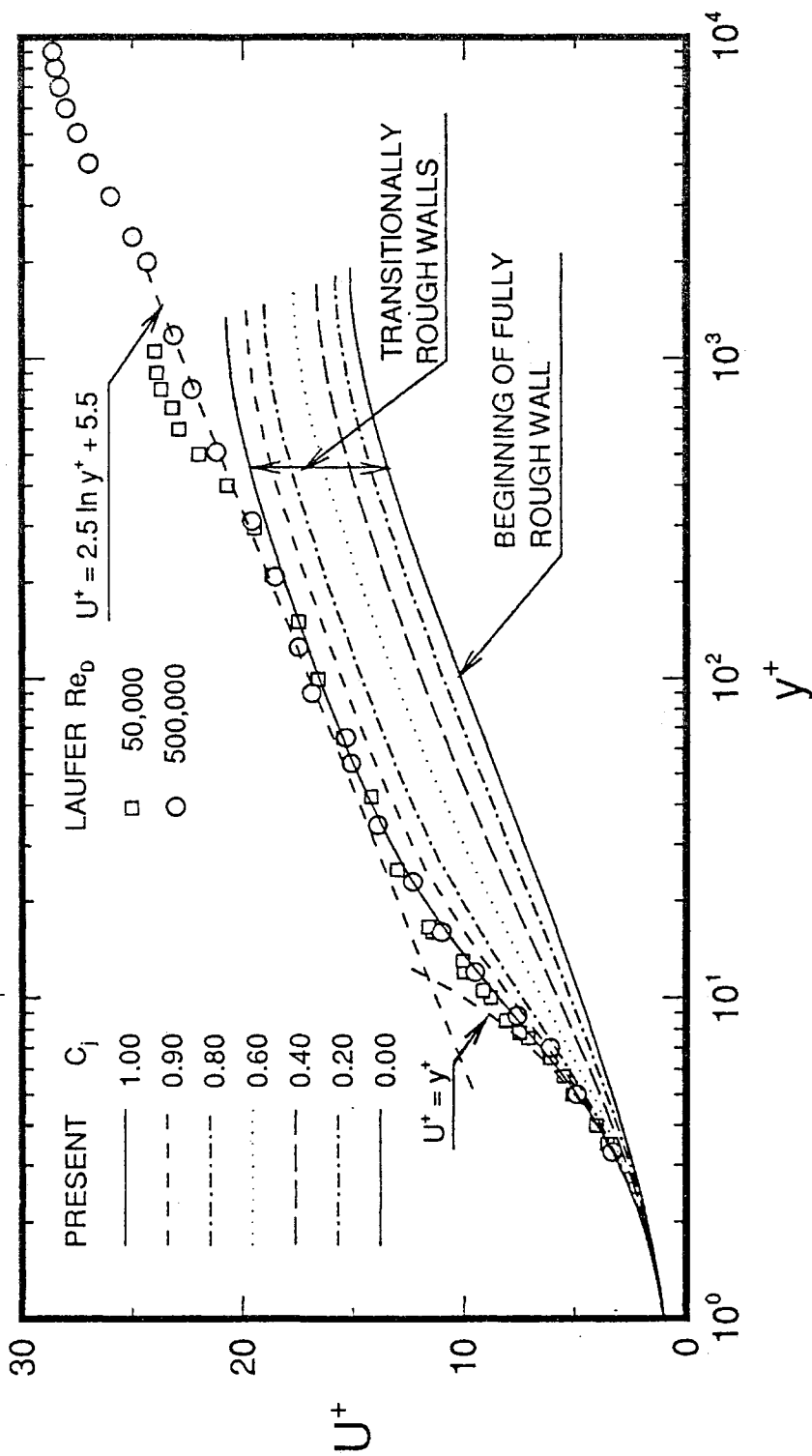


Figure 3.7 Logarithmic velocity profiles for turbulent flow near smooth and rough walls: Comparison of results of the present algebraic turbulence model ( $Re_D=50,000$ ) and experiment for a smooth pipe

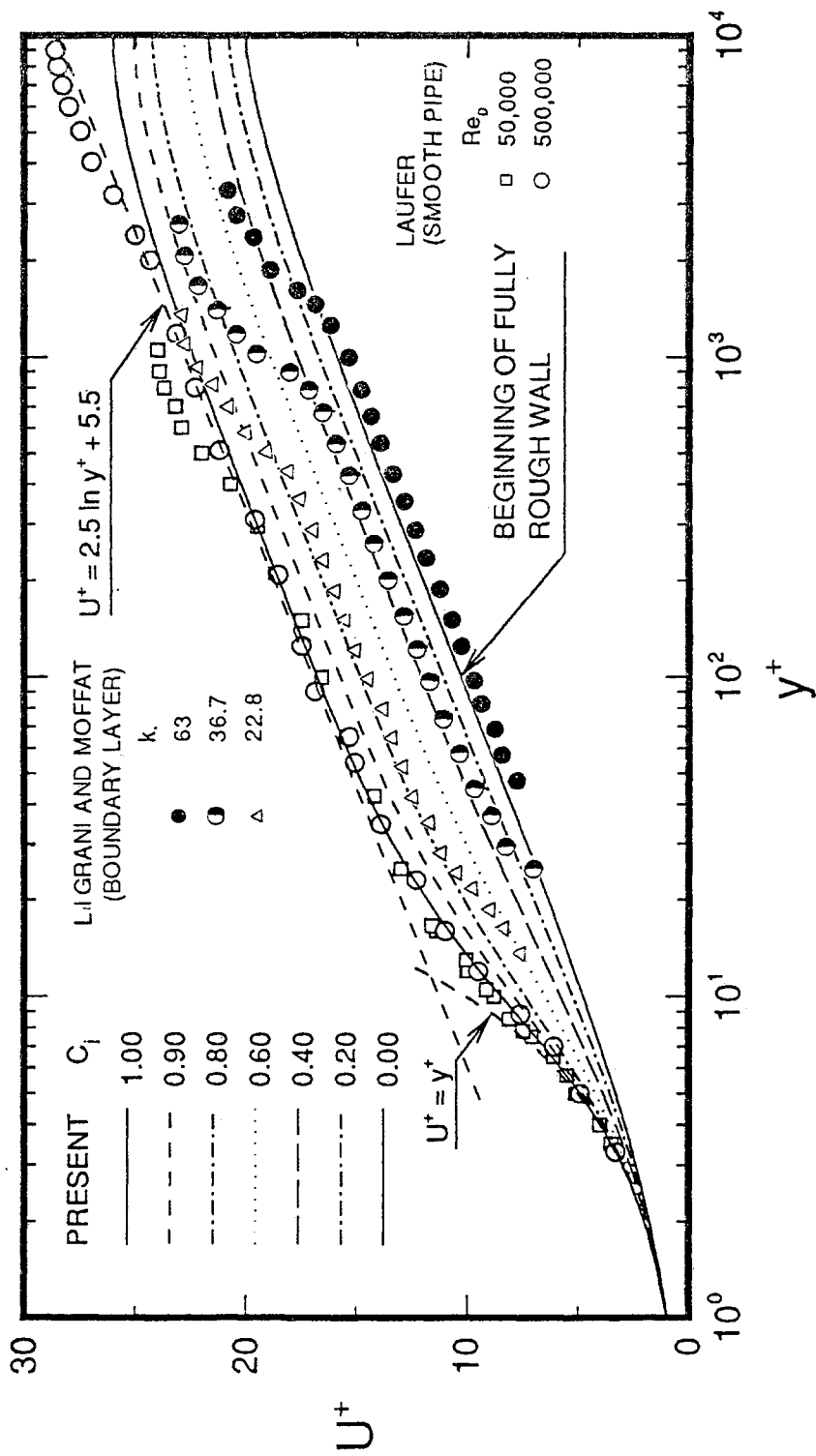


Figure 3.8 Logarithmic velocity profiles for turbulent flow near smooth and rough walls: Comparison of results of the present algebraic turbulence model ( $Re_D=500,000$ ) and experiment for smooth and rough surfaces

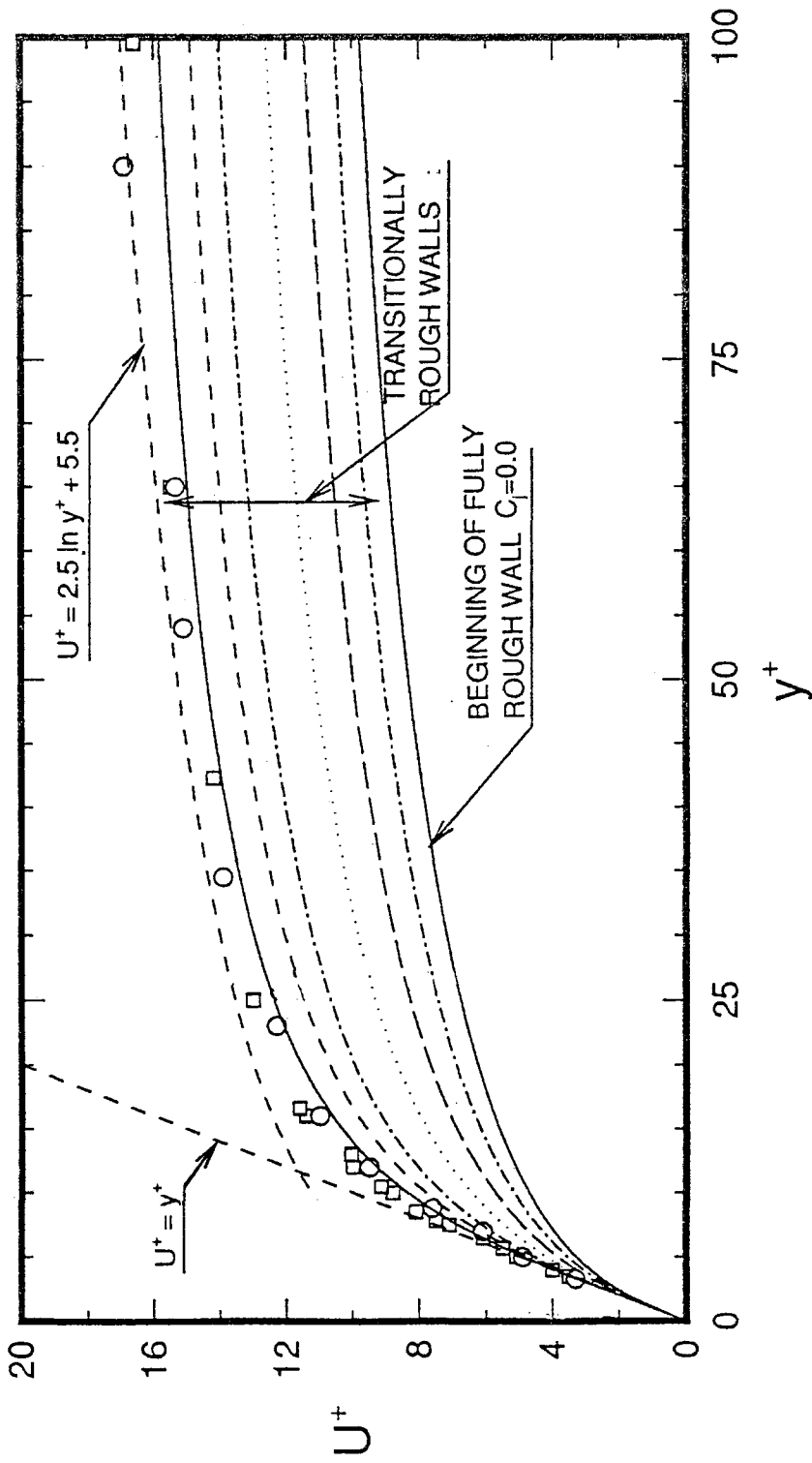


Figure 3.9 Velocity profiles for turbulent flow near smooth and rough walls: Comparison of results of the present algebraic turbulence model ( $Re_D=10,000$ ) and experiment for a smooth pipe (Notations are the same as in Figure 3.6)

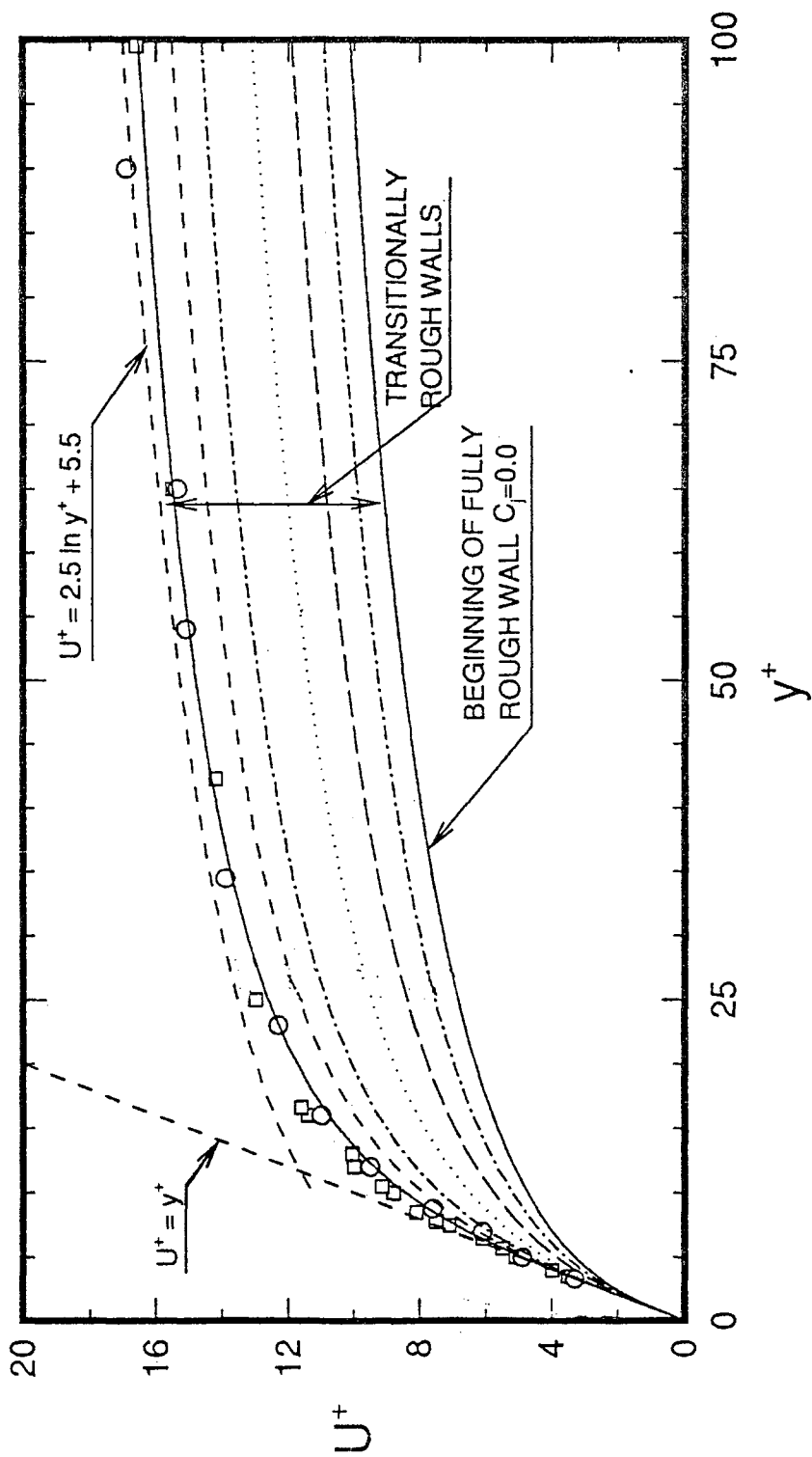


Figure 3.10 Velocity profiles for turbulent flow near smooth and rough walls: Comparison of results of the present algebraic turbulence model ( $Re_D=50,000$ ) and experiment for a smooth pipe (Notations are the same as in Figure 3.6)

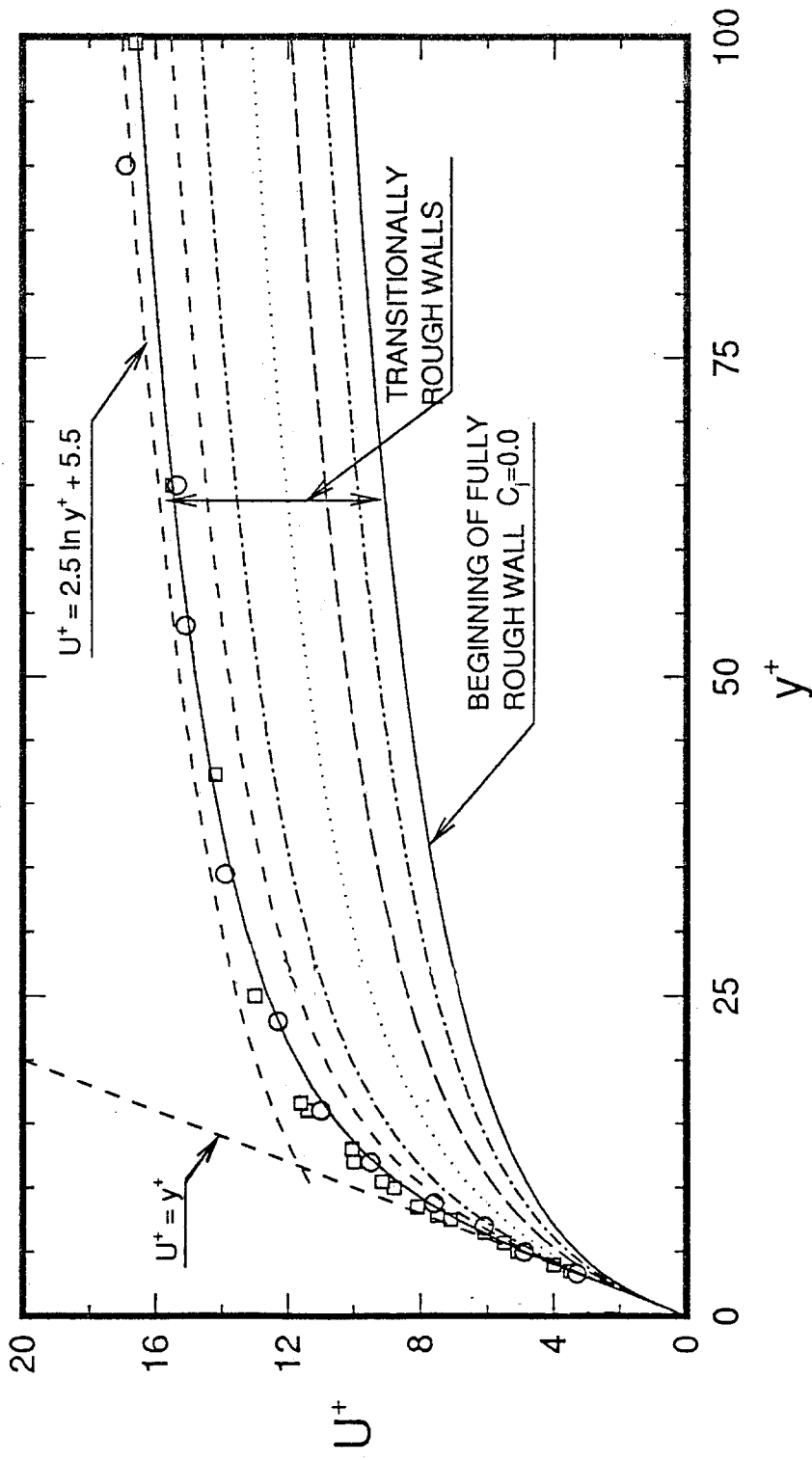


Figure 3.11 Velocity profiles for turbulent flow near smooth and rough walls: Comparison of results of the present algebraic turbulence model ( $Re_D=500,000$ ) and experiment for a smooth pipe (Notations are the same as in Figure 3.6)



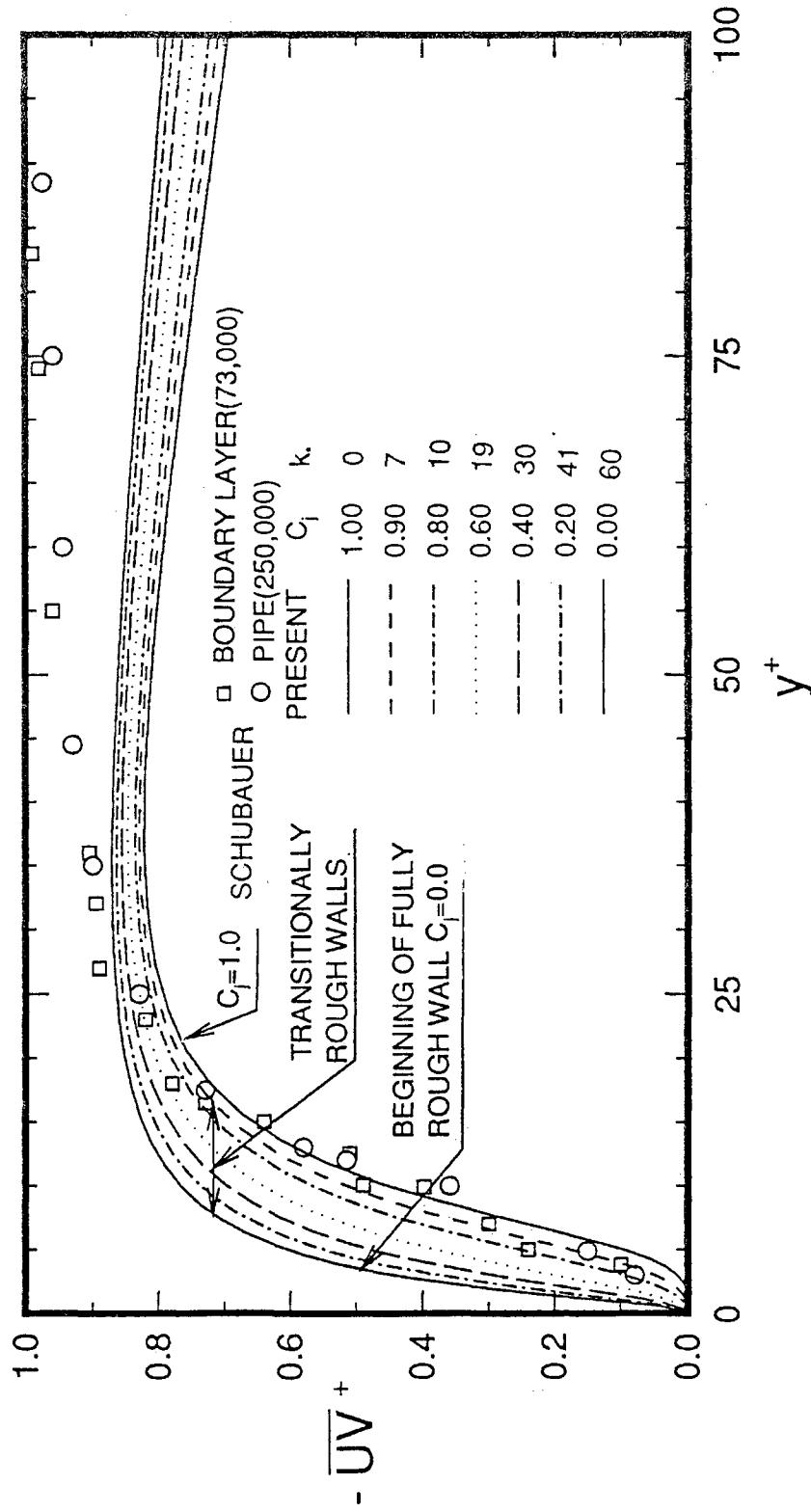


Figure 3.12 Near-wall distribution of Reynolds shear stress for flow near smooth and rough walls: Comparison of results of the present algebraic turbulence model ( $Re_D=10,000$ ) and experiment for smooth surfaces

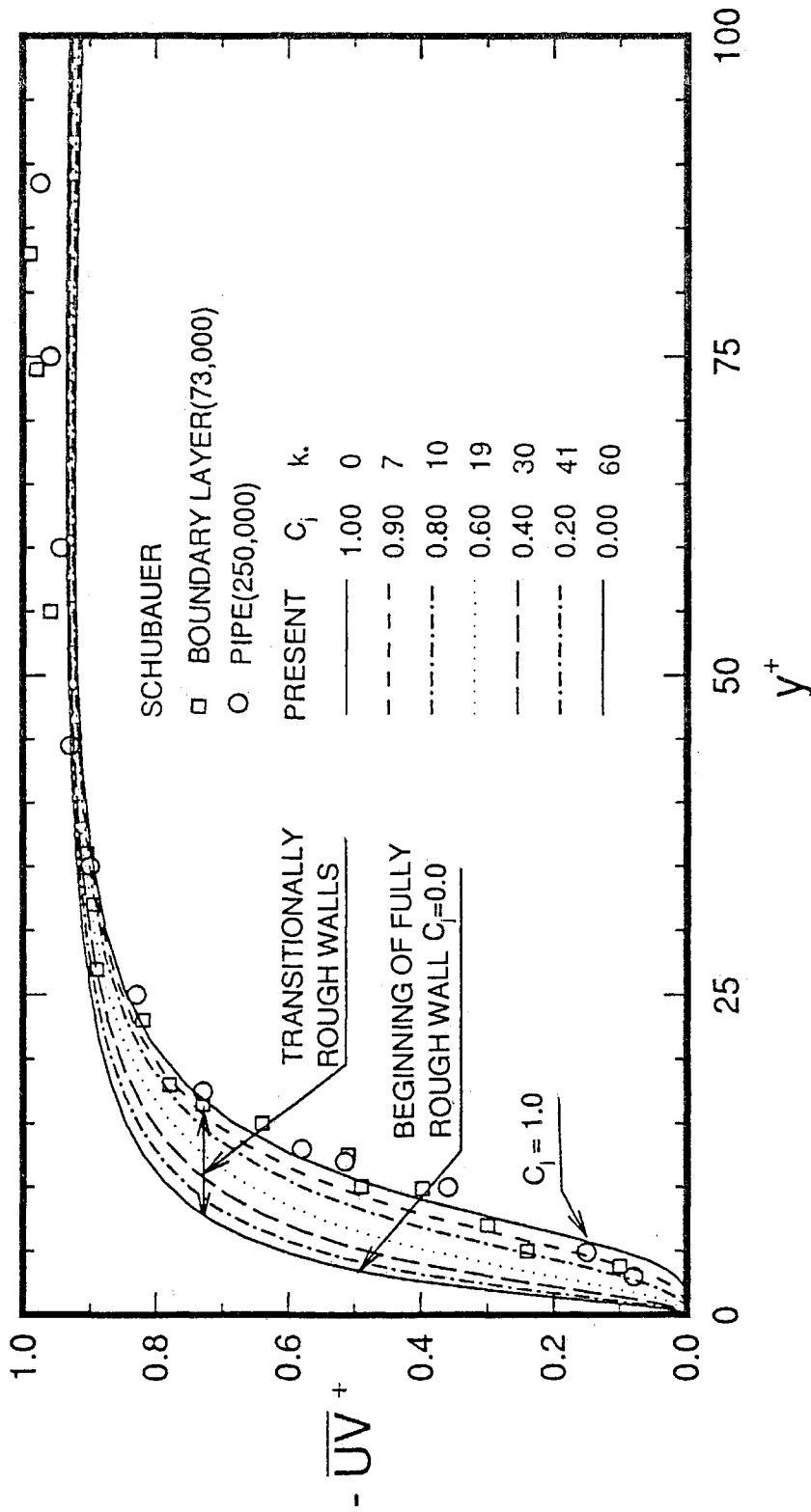


Figure 3.13 Near-wall distribution of Reynolds shear stress for flow near smooth and rough walls: Comparison of results of the present algebraic turbulence model ( $Re_D=50,000$ ) and experiment for smooth surfaces

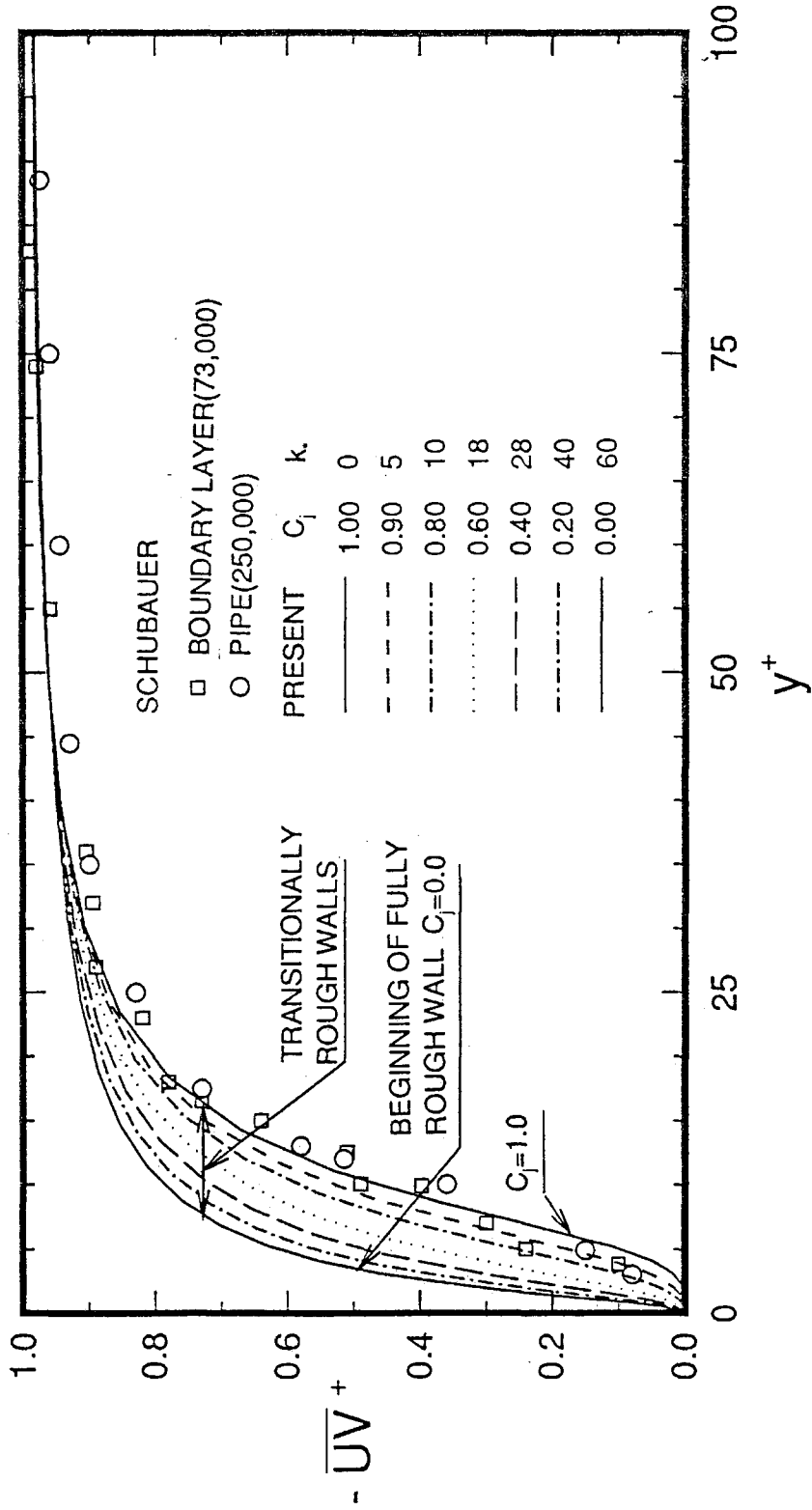


Figure 3.14 Near-wall distribution of Reynolds shear stress for flow near smooth and rough walls: Comparison of results of the present algebraic turbulence model ( $Re_D=500,000$ ) and experiment for smooth surfaces

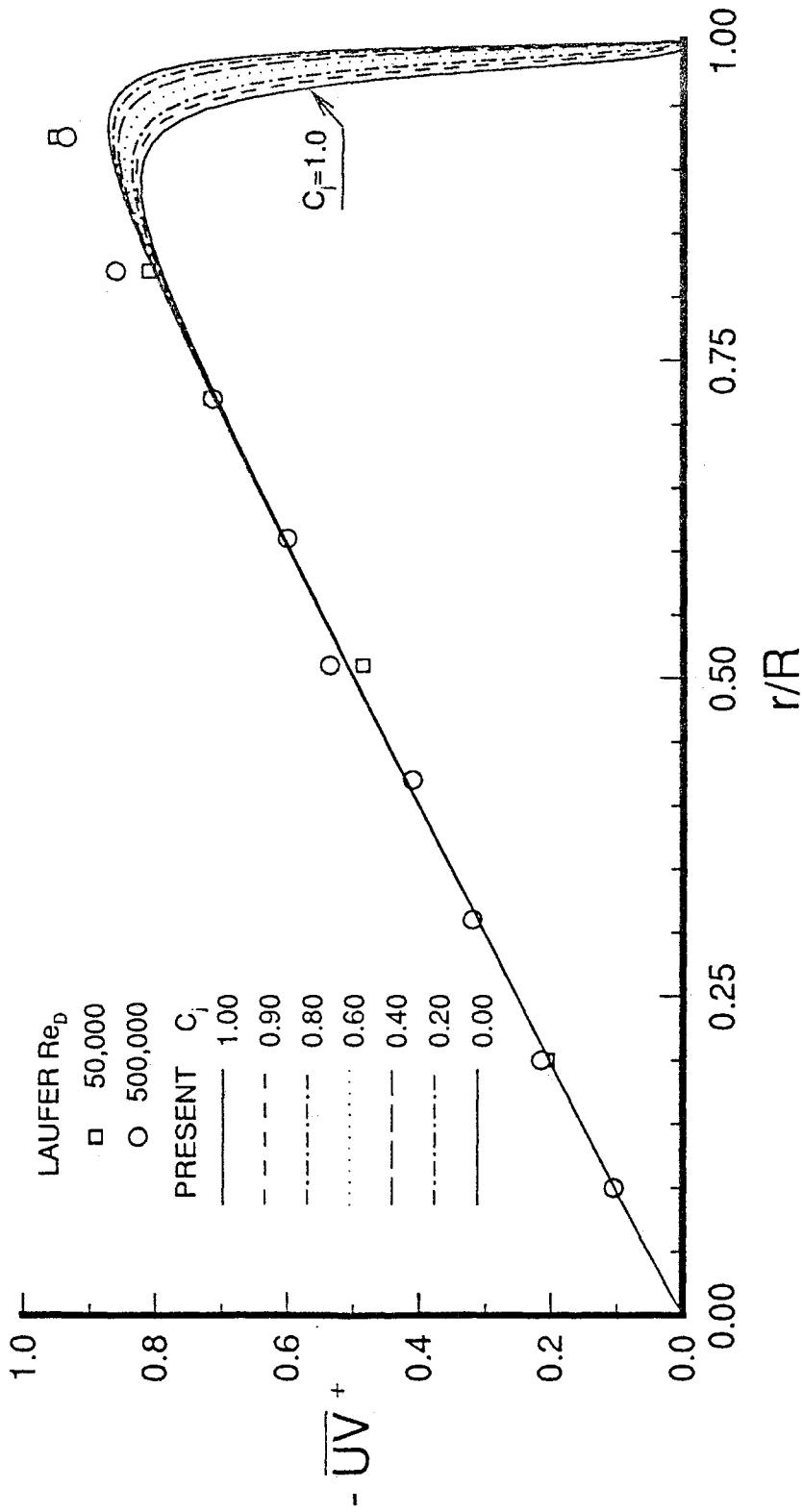


Figure 3.15 Variation of Reynolds shear stress with  $r/R$  for  $0.0 \leq C_j \leq 1.0$ :  
 Comparison of results of the present algebraic turbulence  
 model ( $Re_D = 10,000$ ) and experiment for a smooth pipe

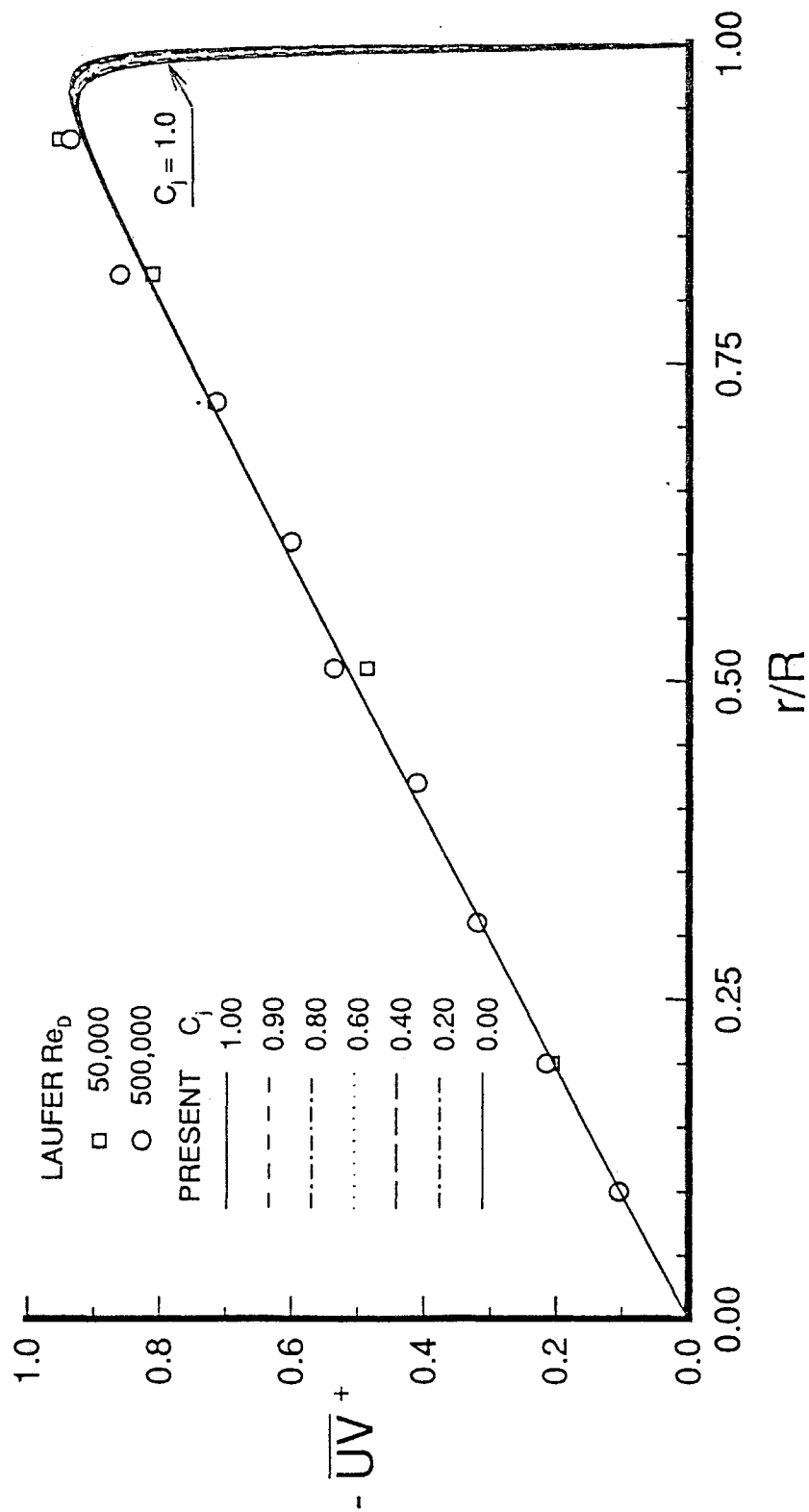


Figure 3.16 Variation of Reynolds shear stress with  $r/R$  for  $0.0 \leq C_j \leq 1.0$ :  
 Comparison of results of the present algebraic turbulence  
 model ( $Re_D = 50,000$ ) and experiment for a smooth pipe

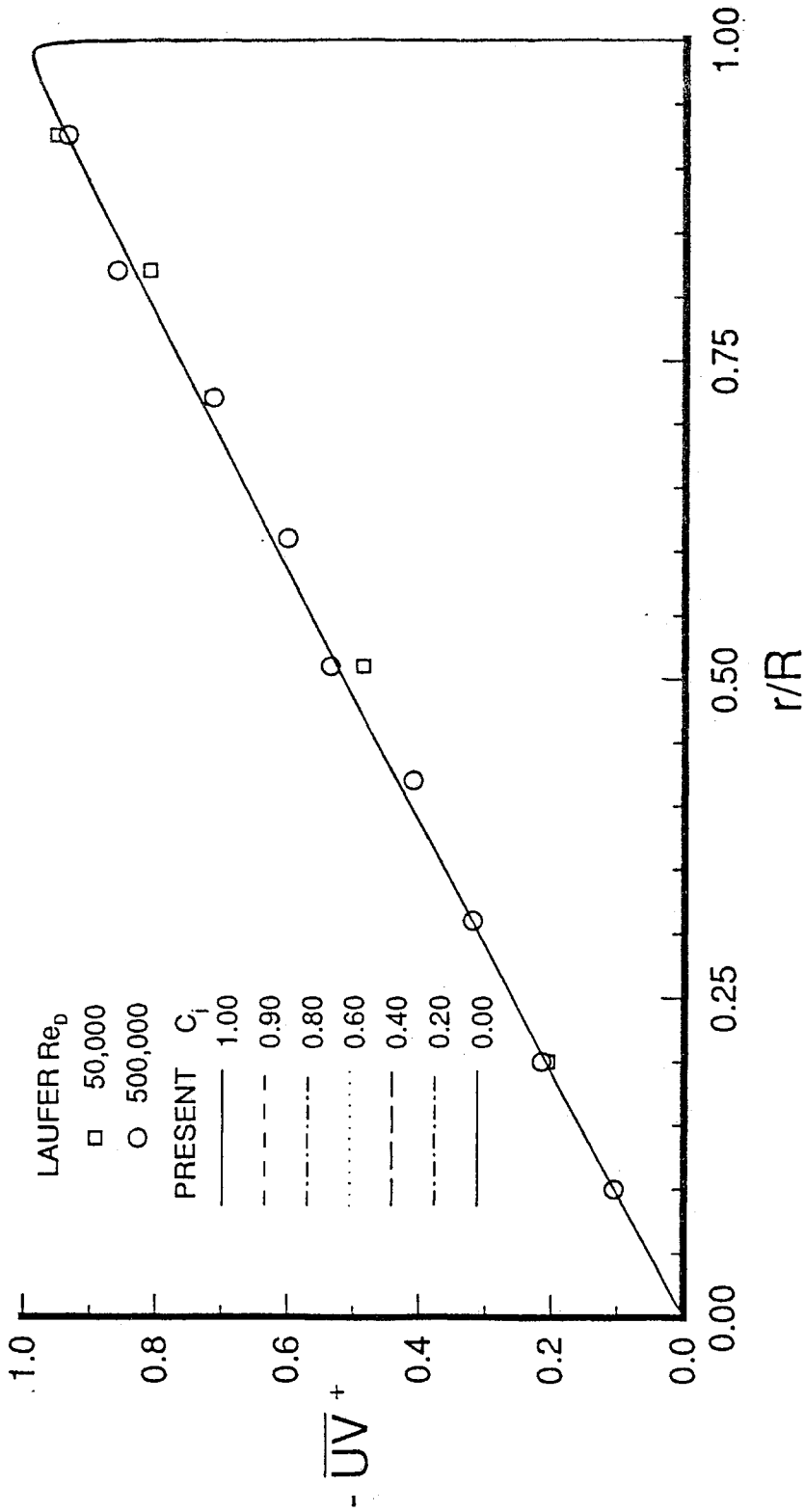


Figure 3.17 Variation of Reynolds shear stress with  $r/R$  for  $0.0 \leq C_i \leq 1.0$ :  
 Comparison of results of the present algebraic turbulence  
 model ( $Re_D = 500,000$ ) and experiment for a smooth pipe

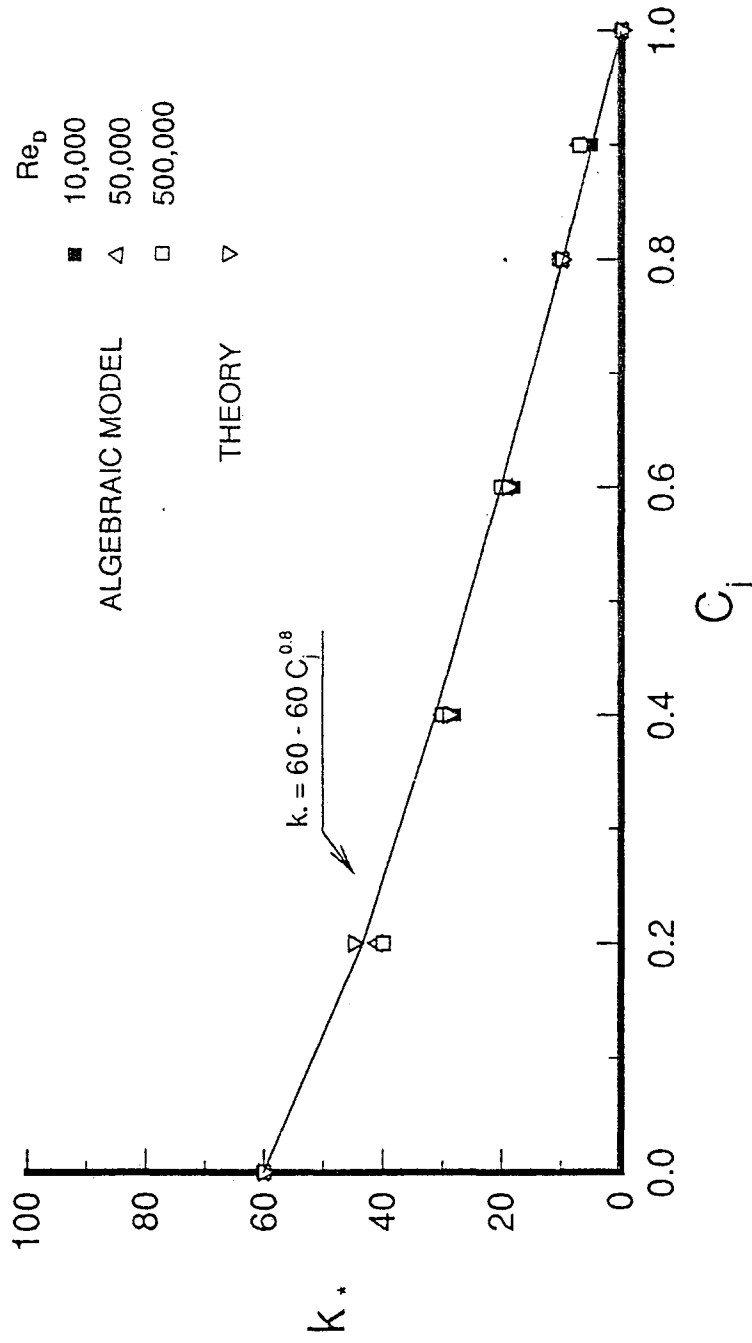


Figure 3.18 Functional relationship between roughness Reynolds number  $k_*$  (van Driest's theory) and roughness parameter  $C_j$  (algebraic turbulence model)

Table 3.1 Comparison of roughness parameter  $C_j$  (algebraic turbulence model) and roughness Reynolds number  $k_*$  (van Driest's theory)

Algebraic Turbulence Model					
$Re_D = 10,000$		$Re_D = 50,000$		$Re_D = 500,000$	
$C_j$	$k_*$	$C_j$	$k_*$	$C_j$	$k_*$
1.0	0	1.0	0	1.0	0
0.9	7	0.9	7	0.9	5
0.8	10	0.8	10	0.8	10
0.6	20	0.6	19	0.6	18
0.4	30	0.4	30	0.4	28
0.2	40	0.2	41	0.2	40
0.0	60	0.0	60	0.0	60



# Chapter 4

## Computation 2

### $k - \varepsilon$ Low-Reynolds Number Turbulence Model

#### 1. INTRODUCTION

The development of high-speed computers and new computational methods has made the computation of more complex mathematical models for fluid flow problems possible. But some of the well-known and simple flows have served over and over again as standard test cases for the evaluation of numerical solution procedures and mathematical models. One benchmark problem is a turbulent pipe flow. Since the historic dye experiment was first carried out by Reynolds<sup>91</sup> there have been many studies of the turbulent flow in a pipe.

The roughness effect on a turbulent flow in a pipe is not only of fundamental interest in fluid dynamics but is also of practical importance. In the earlier experiments sand grain type roughness was employed by Nikuradse<sup>30</sup>, Hama<sup>92</sup>, and Grass<sup>93</sup>. In experiments in which repeated rib (or groove) roughness configurations were used the geometrical parameter used to describe the roughness pattern is the roughness element spanwise aspect ratio ( $W/k$ ), where  $W$  is the spanwise distance in the cavity between ribs and  $k$  is the height of roughness element. Perry and Joubert<sup>94</sup>, Liu, Kline and Johnston<sup>95</sup>, Perry, Schofield and Joubert<sup>96</sup>, Antonia and Luxton<sup>97</sup>, Wood and Antonia<sup>98</sup> studied boundary layer flow over  $d$ -type roughness ( $W/k < 1$ ). Ligrani and Moffat<sup>84</sup>, Pimenta, Moffat and Kays<sup>99</sup>, Coleman, Moffat and Kays<sup>100</sup>, Siuru and Logan<sup>101</sup> studied characteristics of boundary layer flow developing over  $k$ -type roughness surface ( $W/k > 1$ ). But experimental data for rough surfaces including turbulent energy and Reynolds-stresses, do not exist in large quantities. Especially scarce are near-wall data for rough surfaces because of the difficulties in measurement. The small amount of data obtained are for slightly different flow conditions, such as boundary layer flows<sup>84,93</sup>. Experimental data for smooth pipes can be found in the works of Laufer<sup>83</sup>, Schubauer<sup>85</sup>, Nikuradse<sup>89</sup>, Barbin and Jones<sup>102</sup>, Lawn<sup>103</sup>, Richman and Azad<sup>104</sup>.

In the present study a  $k$ - $\epsilon$  low-Reynolds number turbulence model is developed. The low-Reynolds number turbulence model of Lam and Bremhorst<sup>23</sup> is modified and incorporated into the code. The new computational parameter  $C_j$  and a modelling constant  $A_C$  are introduced into a damping factor within a combined damping function  $f_\mu$ . The same test problem as that for the algebraic turbulence model, *i.e.* a steady state, incompressible, developing turbulent flow in a pipe, is selected to evaluate the newly developed numerical code and turbulence model. The simultaneous solution technique, which was not successful for the  $k$ - $\epsilon$  turbulence model, according to several researchers<sup>70,72</sup>, is successfully used here. All flow properties ( $U, V, P, k$  and  $\epsilon$ ) are solved simultaneously using a line-by-line iterative solution method for distances up to

100 pipe diameters downstream for bulk Reynolds numbers of 10,000, 38,000, 50,000, 380,000 and 500,000. The bulk Reynolds number,  $Re_D$ , is based on the uniform inlet velocity,  $u_0$ , the pipe diameter,  $D$ , and the kinematic viscosity of fluid,  $\nu$ .

Initially  $C_j$  is treated as a purely computational parameter. The results show that with a given set of boundary conditions computations agree well with other numerical and experimental results for a certain range of  $C_j$ . Further investigations revealed that  $C_j$  has a physical interpretation. It is found that it can serve as a measure of the wall roughness for a given turbulent flow. This encouraged the comparison with van Driest's earlier work<sup>7</sup>, in which continuous velocity and shear distributions for turbulent flow near smooth and rough walls were studied. An empirical relationship was eventually developed to relate  $C_j$  to the roughness Reynolds number  $k_*$  based on the friction velocity,  $u_\tau$ , equivalent sandgrain roughness scale  $k_s$  and kinematic viscosity of fluid  $\nu$ . The mean velocities, turbulent kinetic energy, its dissipation rate and the Reynolds-stresses are demonstrated. Comparisons are made with the results of van Driest's theory and available experimental data for smooth and rough walls.

## 2. PROBLEM FORMULATION

### 2.1 Governing Equations

The governing equations are fully elliptic in cylindrical, axisymmetric coordinates. The following equations are written in nondimensionalized form. The flow properties are normalized with following scales:

$$X = \frac{x}{D}, \quad r = \frac{y}{D}, \quad U = \frac{\bar{u}}{u_0}, \quad V = \frac{\bar{v}}{u_0},$$

$$P = \frac{\bar{p}}{\rho u_0^2}, \quad k = \frac{K}{u_0^2}, \quad \varepsilon = \frac{ED}{u_0^3}, \quad (4.1)$$

Continuity Equation;

$$\frac{\partial U}{\partial X} + \frac{1}{r} \frac{\partial rV}{\partial r} = 0 \quad (4.2)$$

X-Momentum Equation;

$$\begin{aligned} U \frac{\partial U}{\partial X} + V \frac{\partial U}{\partial r} = & - \frac{\partial P}{\partial X} + \frac{1}{\text{Re}_D} \frac{\partial}{\partial X} \left[ (1+2v_t) \frac{\partial U}{\partial X} \right] - \frac{2}{3} \frac{\partial k}{\partial X} \\ & + \frac{1}{\text{Re}_D} \left[ \frac{1}{r} \frac{\partial}{\partial r} r \left[ \frac{\partial V}{\partial r} + v_t \left( \frac{\partial U}{\partial r} + \frac{\partial V}{\partial X} \right) \right] \right] \end{aligned} \quad (4.3)$$

r-Momentum Equation;

$$\begin{aligned} U \frac{\partial V}{\partial X} + V \frac{\partial V}{\partial r} = & - \frac{\partial P}{\partial r} + \frac{1}{\text{Re}_D} \frac{\partial}{\partial X} \left[ (1+v_t) \frac{\partial V}{\partial X} + v_t \frac{\partial U}{\partial r} \right] \\ & + \frac{1}{\text{Re}_D} \left[ \frac{1}{r} \frac{\partial}{\partial r} \left[ (1+2v_t) r \frac{\partial V}{\partial r} \right] \right] - \frac{2}{3} \frac{1}{r} \frac{\partial rk}{\partial r} \end{aligned} \quad (4.4)$$

k-Equation;

$$\begin{aligned} U \frac{\partial k}{\partial X} + V \frac{\partial k}{\partial r} = & \frac{1}{\text{Re}_D} \frac{\partial}{\partial X} \left[ \left( 1 + \frac{v_t}{\sigma_k} \right) \frac{\partial k}{\partial X} \right] \\ & + \frac{1}{\text{Re}_D} \left[ \frac{1}{r} \frac{\partial}{\partial r} \left[ \left( 1 + \frac{v_t}{\sigma_k} \right) r \frac{\partial k}{\partial r} \right] \right] + \frac{1}{\text{Re}_D} P_k - \epsilon \end{aligned} \quad (4.5)$$

$\varepsilon$ -Equation;

$$U \frac{\partial \varepsilon}{\partial X} + V \frac{\partial \varepsilon}{\partial r} = \frac{1}{\text{Re}_D} \frac{\partial}{\partial X} \left[ \left(1 + \frac{v_t}{\sigma_\varepsilon}\right) \frac{\partial \varepsilon}{\partial X} \right] \\ + \frac{1}{\text{Re}_D} \left[ \frac{1}{r} \frac{\partial}{\partial r} \left[ \left(1 + \frac{v_t}{\sigma_\varepsilon}\right) r \frac{\partial \varepsilon}{\partial r} \right] \right] + \frac{1}{\text{Re}_D} \frac{\varepsilon}{k} C_{\varepsilon 1} f_1 P_k - C_{\varepsilon 2} f_2 \frac{\varepsilon^2}{k} \quad (4.6)$$

where the production of turbulent kinetic energy is

$$P_k = v_t \left[ 2 \left[ \left( \frac{\partial U}{\partial X} \right)^2 + \left( \frac{\partial V}{\partial r} \right)^2 + \left( \frac{V}{r} \right)^2 \right] + \left( \frac{\partial U}{\partial r} + \frac{\partial V}{\partial X} \right)^2 \right] \quad (4.7)$$

and the turbulent viscosity and Reynolds number are

$$v_t = \text{Re}_D C_\mu f_\mu \frac{k^2}{\varepsilon}, \quad \text{Re}_D = \frac{\rho u_0 D}{\mu} \quad (4.8)$$

where  $C_\mu = 0.09$ ,  $\sigma_k = 1.0$ ,  $\sigma_\varepsilon = 1.3$ ,  $\sigma_{\varepsilon 1} = 1.44$ , and  $\sigma_{\varepsilon 2} = 1.92$  as recommended in reference 19.

## 2.2 Low-Reynolds Number Turbulence Model

According to Lam and Bremhorst<sup>23</sup> a damping function  $f_\mu$  can be obtained by using the Hassid-Poreh<sup>105</sup> one equation turbulence model employed by Gibson, Spalding and Zinser<sup>106</sup> in which the turbulent viscosity and the dissipation rate of turbulent kinetic energy are given by

$$v_t = 0.2274 y_n K^{1/2} (1 - e^{-0.01189 R_k}) \quad (4.9)$$

$$E = 0.4 \frac{K^{3/2}}{y_n} (1 - e^{-0.01189 R_k}) + 2 \nu \frac{K}{y_n^2} \quad (4.10)$$

where  $y_n$  is the normal distance from the wall. Combining equations (4.9) and (4.10) to eliminate  $y_n$  the expression for turbulent viscosity  $\nu_t$  can be obtained:

$$\nu_t = \frac{0.09}{2} \frac{K^2}{E} (1 - e^{0.01189 R_k})^2 \left[ 1 + \sqrt{1 + 50 \frac{\nu E}{K^2} (1 - e^{-0.01189 R_k})^{-2}} \right] \quad (4.11)$$

Comparing this with equation (4.8) for  $C_\mu = 0.09$  the damping function becomes

$$f_\mu = 0.5 (1 - e^{0.01189 R_k})^2 \left[ 1 + \sqrt{1 + \frac{50}{R_t (1 - e^{-0.01189 R_k})^2}} \right] \quad (4.12)$$

Lam and Bremhorst suggested the simpler equation

$$f_\mu = (1 - e^{-A_\mu R_k})^2 \left( 1 + \frac{A_t}{R_t} \right) \quad (4.13)$$

which makes  $f_\mu$  a function of both  $R_k$  and  $R_t$ . For the fully turbulent region,  $f_\mu$  will tend to unity at large distances from the wall but the  $R_k$  dependence near the wall is retained. But for this form of  $f_\mu$  a singularity exists at the wall. As the wall is approached the quantities  $R_k$  and  $R_t$  become zero. Therefore the first term in equation (4.13),  $(1 - e^{-A_\mu R_k})$ , becomes zero while the second term,  $(1 + \frac{A_t}{R_t})$  becomes infinite.

But the former one asymptotes to zero faster than the second one approaches infinity, *i.e.*

$$\lim_{y \rightarrow 0} f_\mu \rightarrow 0 \quad (4.14)$$

The numerical results of Lam and Bremhorst's model are shown in Figure 4.3 and Figure 4.4. The disappearance of the damping function  $f_\mu$  might cause unrealistic overshoot of the production term in the equation(4.6) in which the damping function  $f_1$  is an inverse function of  $f_\mu$ .

$$f_1 = 1 + \left(\frac{A_{cl}}{f_\mu}\right)^3 \quad (4.15)$$

The other damping function  $f_2$  is affected indirectly by the turbulence Reynolds number  $R_k$  and tends to zero as  $R_t$  becomes zero.

$$f_2 = 1 - e^{-R_t^2} \quad (4.16)$$

The turbulence Reynolds numbers are defined as follows:

$$R_k = \frac{K^{1/2}y_n}{\nu}, \quad R_t = \frac{K^2}{\nu E} \quad (4.17)$$

And Lam and Bremhorst obtained the modelling constants by numerical trial and error:

$$A_{cl} = 0.05, \quad A_\mu = 0.0165, \quad A_t = 20.5 \quad (4.18)$$

In spite of the singularity problem with  $f_\mu$ , the robustnesses of Lam and Bremhorst's model are demonstrated. The experimental evidence and computational results from several turbulence models shown in Figure 2 of reference 20(also see Figure 4.3 in present results) show that although among them the model of Lam and Bremhorst is best, it still fails to predict the non-zero value of  $f_\mu$  at the wall because of the disappearance of the damping factor at wall.

### 2.3 New Computational Parameter $C_j$ and Modelling Constant $A_C$

In the present study a computational parameter  $C_j$  is introduced into a damping factor of  $f_\mu$ . In addition, an arbitrary constant,  $A_C$ , is added to the second term of  $f_\mu$ . The effects of  $C_j$  and  $A_C$  on the mean axial velocity, the turbulent kinetic energy and the dissipation rate of turbulent kinetic energy are shown in Figures 4.10, 4.11 and 4.10.  $A_C$  is introduced to ensure the vanishing of  $v_t$  at the wall. The new damping function  $f_\mu$  is defined as follows:

$$f_\mu = [ 1 - C_j e^{-A_\mu R_k} ]^2 \left( 1 + \frac{A_t}{A_C + R_t} \right) \quad (4.19)$$

The damping function  $f_\mu$  will now vary depending on not only  $R_k$  and  $R_t$  but also  $C_j$  and  $A_C$ , and as the wall is approached, it becomes a non-zero value if  $C_j$  is not 1.0. In case of  $C_j$  other than 1.0, for example, with the limit case of  $C_j = 0.0$  and  $A_C = 0.1$ , the second term in equation(4.19) will be 206 at the wall which will result in the same magnitude for  $f_\mu$ . Furthermore, at the first grid point, which is usually on the order  $y^+ = 0.5$ , the magnitude of the second term of  $f_\mu$  in equation(4.19) with  $C_j = 0.0$  and  $A_C = 0.0$  becomes larger than that with  $C_j = 0.0$  and  $A_C = 0.1$ . However at grid points other than the first one the computational results do not show any significant differences in the value of  $f_\mu$ . It is important to show that for  $C_j$  close to 0.0, a non-zero finite value of  $f_\mu$  at wall does lead to an approximately zero value of turbulent viscosity even for very small  $A_C$ . This might be shown in the following manner. Consider the turbulent eddy viscosity expression shown in equation (4.8) as written below:

$$v_t = Re_D C_\mu f_\mu \frac{k^2}{\epsilon} \quad (4.8)$$



At the wall  $f_\mu$  is non-zero and finite except where  $C_j=1.0$ . The quantity  $C_\mu$  is an empirical constant. Analysis of the experimental data<sup>20</sup> shows that the rate of dissipation of the turbulent kinetic energy is non-zero finite at wall and the turbulent kinetic energy within the laminar sublayer is proportional to the second power of wall distance:

$$\epsilon^+ = 2(A^+ + 2B^+y^+ + \dots) \quad (4.20)$$

$$k^+ = A^+y^{+2} + B^+y^{+3} + \dots \quad (4.21)$$

where  $A^+$  and  $B^+$  are experimental values. Therefore at very small distances from the wall the turbulent viscosity should be proportional to  $y^{+4}$ . Consequently

$$\lim_{y \rightarrow 0} v_t = 0 \quad (4.22)$$

The sensitivity of  $f_\mu$  and the turbulence properties to the value of  $C_j$  has been tested and the results will be demonstrated later.

## 2.4 Computational Grid and Boundary Conditions

The set of the fully elliptic governing differential equations is solved numerically for a steady state, incompressible, two dimensional, developing turbulent pipe flow with uniform inlet conditions for the mean velocities and other turbulence properties. The low-Reynolds number turbulence model (compared to high-Reynolds number versions in which wall functions are used to avoid the calculation of laminar sublayer region) needs a very fine grid near the wall. To resolve the large gradient of mean velocities and turbulence properties in the near-wall region, a nonuniform grid system is essential. The positions of the grid system are carefully determined by modifying an exponentially stretching transformation used in ARC2D code<sup>87</sup> to generate a finer

grid near the wall and inlet regions. In the fully turbulent region far away from the wall a uniform grid is used. Most of the results demonstrated are at the fully developed region *i.e.*  $x/D=80$ . Several fine grid systems are used for the streamwise direction but the streamwise grid does not affect the fully developed profiles of the mean variables. Furthermore with the selected streamwise grid system the results in the developing regions (which are not shown in the present dissertation but may be found in the study of Jang and Oyibo<sup>75</sup>) show reasonable agreement with experimental data and other numerical results. The grid system in the radial direction is crucial for resolving the details of the near-wall variation of turbulent properties. Depending on the Reynolds number, the distance to the first grid point from the wall should be adjusted to get a reliable convergent solution. In the present study the computation was very sensitive to the location of the first grid point away from the wall. The slightest change of the first grid position towards the wall often caused a convergence problem or a negative turbulent kinetic energy. For Reynolds numbers of 50,000 and 500,000 with  $C_j=0.9$  and  $A_C=0.0$  in a  $120 \times 50$  grid system, grid independent results were achieved for typical positions of the first grid point of 0.00038 and 0.00004 times the pipe radius, respectively. This put at least 10 grid points within the laminar sublayer region ( $y^+ < 5$ ) and 22 grid points within the buffer region ( $y^+ < 40$ ).

The boundary conditions for the mean velocities and pressure are the same as for the cases studied with the algebraic turbulence model. The pipe centreline is assumed to be an axis of symmetry. Along the wall no-slip conditions are enforced for mean velocity components and the turbulent kinetic energy is made to vanish there as well. A symmetry condition is implemented for the dissipation rate of turbulent kinetic energy. Thus the finite value of the dissipation rate of turbulent kinetic energy at wall is calculated during the iteration procedures. In the cases of  $C_j < 1.0$ , which are for rough walls, the effects of wall roughness are accounted for in the transport equations through the turbulent viscosity which is related to the modified damping function  $f_\mu$  while the wall boundary conditions (at  $y=0$ ) are approximated by smooth wall

expression. At the inlet, uniform values for the mean velocity and turbulent kinetic energy are specified, *i.e.*  $U_0=1$ ,  $V_0=0$ ,  $k_0=0.005$  along the radial direction at two axial stations. For the dissipation rate of turbulent kinetic energy the empirical relation,  $\epsilon_0=C_\mu k_0^{1.5}/0.03R$ , is used, where  $R$  is the nondimensionalized radius of the pipe. At the exit for all flow properties, except the mean pressure, fully developed conditions are specified, *i.e.* the axial gradient of all flow properties are zero. For mean pressure, an arbitrary value is specified, *i.e.*  $P = 1$ . The details of the computational geometry, boundary conditions, inlet conditions and exit conditions are shown in Figure 4.1.

### 3. SOLUTION METHOD

The solution method and the staggered grid system used in this Chapter are the same as for the cases studied with the algebraic turbulence model in Chapter 3. The quantities  $k$  and  $\epsilon$  are calculated at the same grid positions as  $P$ . The discretized grid positions for the calculation of each of the flow properties are shown in Figure 4.2. The turbulent viscosity is evaluated at the same positions as  $k$  and  $\epsilon$  at the end of each global iteration process for the whole computational domain using the newly obtained mean velocities and turbulence properties. A relaxation method is used for the convergence of  $k$ ,  $\epsilon$  and  $v_t$ . No relaxation technique is used for  $U, V$  and  $P$ . Typical relaxation constants are 0.4, 0.4 and 0.3 for  $k$ ,  $\epsilon$  and  $v_t$  respectively. Due to the staggered grid and the finite difference scheme used for the continuity equation, the residual of a discretized continuity equation always becomes machine accuracy  $10^{-15}$  at any stage of the solution procedure, the convergence is checked for the Reynolds-averaged momentum equations, the turbulent kinetic energy equation and the dissipation rate equation of the turbulent kinetic energy. A series of grid sensitivity runs were performed on nonuniform grids. Grid independence of the solution was confirmed by comparing the results for  $80 \times 30$ ,  $100 \times 40$ ,  $120 \times 40$  and  $120 \times 50$  grids. Even though,

for the fully turbulent region, the results for the  $80 \times 40$  grid are in good agreement with experimental data, to assure the grid independence of the near-wall turbulence properties the results of  $120 \times 50$  are compared with available experimental data. In general, for  $C_j < 0.9$  with a proper grid system, 250 iterations are sufficient to give a convergent solution. But as  $C_j$  is close to 1.0 the number of iterations are increased. It took 15.9 CPU seconds for one iteration on the UNIX convex machine. When the total residual of discretized equations becomes less than  $10^{-6}$  the iteration process is stopped.

## 4. RESULTS AND DISCUSSIONS

The sensitivity of various turbulence properties to the values of  $C_j$  and  $A_C$  was tested, motivated by a suggestion of Wilcox<sup>107</sup>. The modified low-Reynolds turbulence model with new computational parameters  $C_j$  and  $A_C$  should properly predict the behavior of near-wall turbulent flows.

### 4.1 Sensitivity Test of $C_j$ and $A_C$

In Figure 4.3 the smooth wall experimental data and numerical results of other turbulence models<sup>20</sup> for the damping function  $f_\mu$  are compared with the results of the present calculation for  $C_j = 0.9$ ,  $A_C = 0.0$ , and  $Re_D = 380,000$ . The model of Lam and Bremhorst produces better results than the other turbulence models but fails in the region very close to the wall. None of the models tested predicts the near-wall variation of  $f_\mu$ , but close examination shows that the present result compares reasonably with the trend of experimental data, although this is not as marked further out in the boundary layer.

A numerical approach to model the near-wall variation of  $f_\mu$  itself is rare. Based on the author's review, one case appears to be the modification of the van Driest model<sup>7</sup> carried out by Miner, Swean, Handler and Leighton<sup>108</sup> using results from the direct numerical simulation of turbulent channel flow reported by Handler, Hendricks and Leighton<sup>109</sup>. By shifting  $f_\mu$  upward and adjusting the origin of the wall coordinate  $y^+$  Handler *et al* modified the standard van Driest model to give better agreement with the result of the direct numerical simulation arriving at the form

$$f_\mu = f_0 + (1-f_0)(1-\exp[-(y^+-y_0^+)/A])^2 \quad (4.23)$$

where 0.04 and 8 are specified for  $f_0$  and the effective origin  $y_0^+$  respectively. Using the above modified van Driest function with  $C_\mu=0.115$  instead of  $C_\mu=0.09$  the results for the near-wall turbulence properties near a smooth wall were improved. In Figure 4.4 the empirical data<sup>20</sup>, the result of the direct numerical simulation and the result of the modified van Driest formula are compared with the present results for several values of  $C_j$ . The modified van Driest model more closely follows the result of direct numerical simulation. But of course it is modelled to fit the result of direct numerical simulation which is a turbulent channel flow at a low Reynolds number, *i.e.*  $Re_R=2,215$ , where  $Re_R$  is based on the initial laminar centreline velocity and the half-width of channel. However equation(4.23) does not include the effect of rough walls. In the present results, the introduction of two new computational parameters into the damping function  $f_\mu$  is in good agreement with both the trends of experimental data and the results of the direct numerical simulation. The result for  $C_j = 1$  and  $A_C = 0$  is the same as that of Lam and Bremhorst's model. Obviously from Figures 4.3 and 4.4 near the wall the present result with  $C_j=0.9$  compares well with experimental data and the results of the direct numerical simulation.

Figure 4.5 demonstrates the development of the axial mean velocity. In this Figure the developing axial mean velocity for  $Re_D=380,000$  at different radial positions, *i.e.*  $r/R=0.0, 0.5, 0.75, 0.94$  from the inlet to 100 pipe diameter downstream is shown and compared with the experimental data of Barbin and Jones<sup>102</sup>. Comparing with the developing process of mean velocity obtained by using algebraic turbulence model (see Figure 3.3) the present result shows that the fully developed flow starts around  $x/D = 50$ . The  $k-\varepsilon$  two equation turbulence model is superior to the algebraic turbulence model to predict the developing process of turbulent properties. Except for the core region and  $r/R=0.94$  the present results, with  $C_j$  close to 1.0 and  $A_C = 0$ , reproduce the experimental data well. Overall the mean axial velocity is gradually approaching to the experimental data of Nikuradse<sup>89</sup> as shown in Figure 4.7. This is similar to results obtained with other turbulence models<sup>20</sup> shown in references 16, 17 and 18.

In Figures 4.6 and 4.7 the radial distribution of mean velocity are shown for  $Re_D = 10,000$  and  $380,000$  respectively. The effect of the mean velocity on  $C_j$  are also shown together with the experimental data of Nikuradse<sup>89</sup> for a smooth pipe. The present results match with the experiment data. As  $C_j$  decreases the mean velocities near the centreline increases while near the wall they decrease. Higher  $C_j$  gives the fuller mean velocity profile which is consistent to the result of the algebraic turbulence model.

In Figures 4.8 and 4.9 the axial variations of the turbulent kinetic energy and turbulent viscosity with  $C_j=0.9, 0.95, \text{ and } 1.0$  are shown for  $Re_D=380,000$  at various radial positions. The results are very sensitive to  $C_j$ . Different from the developing process of the mean velocity as the  $C_j$  increases overall levels of turbulent kinetic energy and turbulent viscosity decrease regardless to the radial positions.

Figures 4.10, 4.11 and 4.12 show the sensitivity of mean velocity, turbulent kinetic energy and its dissipation rate on  $C_j$  and  $A_C$  for  $Re_D=500,000$ . The results in

these Figures confirm the independence of mean velocity and turbulence properties from the values of  $A_C$ . The effect of  $C_j$  to turbulent kinetic energy and its dissipation rate are discussed in the following Figures.

Figure 4.13 and Figure 4.14 demonstrate the sensitivity of the near-wall behavior of the turbulent kinetic energy normalized by the friction velocity  $u_\tau$  to a wide range of values of the computational parameter  $C_j$ . For  $Re_D=50,000$  and  $500,000$  the present results are compared with the empirical correlation, *i.e.*  $k^+=0.05y^+$ , for the flow in the laminar sublayer region of smooth walls and several experimental data for smooth walls, the scatter of which is very wide. It is seen that for the cases for  $0.9 \leq C_j \leq 1.0$   $k^+$  has the maximum value of 4.5 around  $y^+=15$ , which is in fair agreement with the empirical data for smooth walls shown by Patel, *et al.*<sup>20</sup>. In that range, as  $C_j$  decreases the turbulent kinetic energy slightly increases and the location of the maximum value moves closer to the wall. But when  $C_j$  is less than 0.9 the maximum value of turbulent kinetic energy decreases and eventually the turning point of turbulent kinetic energy disappears. Away from the wall ( $y^+=100$ ) all the numerical results asymptote to 3.4 which is close to the 3.3 of the empirical data of Patel *et al.* In the range of  $0.0 \leq C_j \leq 0.2$  the turbulent kinetic energy is not sensitive to  $C_j$  over the entire cross-sectional area of pipe. Figure 4.15 shows the results of smooth walls ( $C_j=1.0$ ) for various  $Re_D$ , which are in fair agreement with experimental data.

In Figure 4.16 and Figure 4.17 the variation of turbulent kinetic energy along the pipe radius for  $Re_D=10,000$  and  $380,000$  are shown with the experimental data of Lawn<sup>103</sup>. In the fully turbulent region the numerical data are not sensitive to the computational parameter  $C_j$ . Contrary to the higher Reynolds number results, for the same  $C_j$  the lower Reynolds number results show that the effect of  $C_j$  penetrates farther region from the wall due to the strong diffusion transfer. This is clearly shown in Figure 4.18 where the results for a smooth wall are plotted for several Reynolds numbers.

In Figures 4.19 and 4.20 the variations of the dissipation rate of turbulent kinetic energy along the pipe radius are demonstrated for  $Re_D = 10,000$  and  $380,000$ . For different  $C_j$  the dissipation rate of turbulent kinetic energy in the fully turbulent region is not affected as can be seen. But in the near wall region the dissipation rate of turbulent kinetic energy is very sensitive to the  $C_j$ , which has already been shown in Figure 4.12. The present results away from the wall show reasonable agreement with the smooth wall experimental data of Lawn<sup>103</sup>. Figure 4.21 shows the comparisons of the present results for several  $Re_D$  with  $C_j = 1.0$  and experimental data of Lawn.

## 4.2 Physical Meaning of $C_j$ as a Roughness Function

So far we have demonstrated that the near-wall behavior of turbulence properties is very sensitive to  $C_j$  but that the turbulence properties in the fully turbulent region, except for mean axial velocity, are not affected by  $C_j$ . Still it is not clear if the variations of turbulence properties with respect to  $C_j$  have any physical significance in fluid dynamics, and what functional relationship exists between  $C_j$  and known physical flow properties. To answer these questions we have to go back to the origin of the damping factor.

Recalling van Driest's theory as described in Chapter 2, the flow near transitionally rough walls has a mean velocity gradient and profile given by

$$\frac{\partial u^+}{\partial y^+} = \frac{2}{1 + \sqrt{1 + 4K^2 y^{+2} [1 - \exp(-y^+/26) + \exp(-60y^+/26k_*)]^2}} \quad (2.25)$$

$$u^+ = \int_0^{y^+} \frac{2dy^+}{1 + \sqrt{1 + 4K^2 y^{+2} [1 - \exp(-y^+/26) + \exp(-60y^+/26k_*)]^2}} \quad (2.26)$$



Equations (2.25) and (2.26) reduce to the expressions for the smooth wall (equations (2.15) and (2.16)) and the beginning of fully rough wall (equations (2.21) and (2.22)) if  $k_*$  equals 0 and 60, respectively.

For the  $k$ - $\varepsilon$  two equation approach, the present model with  $C_j=1.0$  and  $A_C=0.0$  corresponds to the original  $k$ - $\varepsilon$  turbulence model of Lam and Bremhorst. In Figures 4.22 to 4.25 the variations of  $u^+$  with  $y^+$  as a function of the roughness parameter,  $C_j$ , in the semi-logarithmic coordinates and linear coordinates, are compared with van Driest's equation(2.26) and the experimental data of Laufer<sup>83</sup> for smooth walls obtained for  $Re_D = 50,000$  and  $500,000$  respectively. In Figures 4.22 and 4.23 the experimental data of Ligrani and Moffat<sup>84</sup> for boundary layer flow over a rough surface are shown. The present results of  $C_j=1.0$ , which is the same as the original Lam and Bremhorst's model, reasonably predict the smooth wall data of Laufer and with  $C_j = 0.8$ , the analytic equation(2.22) or equation(2.26) with  $k_* = 60$  for the flow near the beginning of a fully rough wall. The present results corresponding to the  $k_*$  of van Driest's theory predicts a little discrepancy in magnitude but it is shown that the effect of the wall roughness results in the shift of the logarithmic velocity profile for the smooth wall. The results for the smooth wall with various  $Re_D$  are also shown in Figures 4.26 and 4.27.

One interpretation of the computational parameter  $C_j$  is clear: it is related to the roughness Reynolds number,  $k_*$  and predicts the turbulence properties for the flow near smooth- transitionally rough- and fully rough walls. Consequently the introduction of  $C_j$  suggests a new near-wall turbulence model for the flow over smooth and rough walls. Therefore we now call the computational parameter  $C_j$  a roughness function. As  $C_j$  decreases from 1.0 the surface of the wall is getting rougher and rougher, consequently the flow near the wall is stirred up and higher effective wall shear stress is obtained. The variation of computed friction velocities with respect to  $C_j$  for various Reynolds number are shown in Figure 4.28. The friction velocity

increases as  $C_j$  decreases, but for  $C_j$  less than 0.2 the friction velocity does not vary with  $C_j$ . Within the moderate range of the wall roughness  $0.2 < C_j < 1.0$  the damping factor is still able to predict the turbulence properties very close to the wall, but for the very rough wall  $C_j < 0.2$  the effect of the wall damping factor disappears. Recalling the theoretical approach shown in Chapter 2, where the beginning of fully rough wall is obtained at  $k_* = 60$ , the present result indicates a much higher roughness Reynolds number for the beginning of fully rough wall. By simple comparison of the damping factor between van Driest's model and the present  $k$ - $\epsilon$  model we might expect that the result of the present calculation with  $C_j = 0.0$  would be comparable with that of van Driest's equation (2.22). But that is inappropriate because the results of the present  $k$ - $\epsilon$  two equation model involve transport and history effects of  $k$  and  $\epsilon$  and the empirical constants which are appeared in the turbulence modelling process are evaluated differently. In this range of  $C_j \leq 0.2$ , the wall is so rough that the turbulent phenomena are expected to get closer to the wall. This should perhaps explain why  $v_t$  is finite near the wall (as shown Figure 4.29 and Figure 4.30), while the mathematical form of the  $v_t$  gives zero at wall.

In Figure 4.31 the skin friction coefficient vs relative roughness size is compared with experimental data of Nikuradse<sup>30</sup>. The present results are in good agreement with the experimental data.

Now, from direct comparison of mean velocity profiles in the logarithmic law region from the present  $k$ - $\epsilon$  model with those of van Driest's theory a functional relationship between the new roughness parameter and roughness Reynolds number can be found. As shown in Figure 4.32 (also in Table 4.1) linear empirical relationships between the new roughness parameter  $C_j$  and roughness Reynolds number  $k_*$  are obtained by

for  $Re_D = 50,000$

$$k_* = 250-250C_j \quad (4.24)$$

for  $Re_D = 500,000$

$$k_* = 200-200C_j \quad (4.25)$$

The relationship between  $C_j$  and  $k_*$  gives a different slope depending on the Reynolds number.

Figures 4.33 and 4.34 demonstrate the dependence of the near-wall behavior of Reynolds shear stresses for different roughness function  $C_j$  at  $Re_D = 50,000$  and  $500,000$ . Also shown is the Reynolds shear stress of van Driest for the beginning of a fully rough wall. In the laminar sublayer region the present calculations with  $C_j = 0.9$  and  $0.95$  predict the experimental data for smooth walls. The Reynolds shear stresses are increased by the effect of wall roughness. In the fully turbulent region the distribution of Reynolds shear stress is consistent with the experimental data for smooth walls.

In Figure 4.35 at a fixed  $C_j$ , *i.e.*  $C_j = 1.0$ , it is seen that very close to the wall the distribution of Reynolds shear stress is not affected by the Reynolds number but in the fully turbulent region the result of  $Re_D = 10,000$  deviates from the experimental data. This is because the  $k$ - $\epsilon$  turbulence model is modelled with the assumption of high Reynolds number therefore the empirical constants used in the  $k$ - $\epsilon$  turbulence model are obtained from the experimental data of high Reynolds number flows.

Figure 4.36 and Figure 4.37 show the distribution of Reynolds shear stress in the cross-sectional area for  $Re_D = 10,000$  and  $380,000$  and the experimental data of Ligrani and Moffat<sup>84</sup> for boundary layer flow over rough surfaces. Even though the present result shows discrepancy with the data of Ligrani and Moffat it is seen that the roughness of the wall does not affect the Reynolds shear stress in the fully turbulent regions and that the present results match with the experimental data of Laufer for a smooth pipe. In Figure 4.38 the results for smooth walls at various Reynolds numbers are shown. The numerical results match with the experimental data of Laufer.

Figures 4.39 and 4.40 show the sensitivities of the ratio of  $P_k$  to  $\varepsilon$  with  $C_j$  for  $Re_D=50,000$  and  $500,000$ . Also shown are the empirical data of Patel, *et al.* These figures indicate that very close to the wall the rate of increase of the production of turbulent kinetic energy is faster than that of the dissipation rate of turbulent kinetic energy, which leads to the increase in the level of turbulence properties in the near-wall region. As one approaches the fully turbulent region  $P_k$  balances with  $\varepsilon$ , supporting the concept of local equilibrium.

## 5. CONCLUSIONS

Based on the present study the following conclusions are obtained.

- 1) A simultaneous solution technique has been successfully tested for a set of fully elliptic time-averaged Reynolds transport equations combined with a low-Reynolds number  $k$ - $\varepsilon$  two equation turbulence model.
- 2) By introducing new computational parameters  $C_j$  and  $A_C$  into a damping function  $f_\mu$  the prediction of the experimental curve of  $f_\mu$  is recovered. It is found that the computational parameter  $C_j$  has a functional relationship to roughness Reynolds number  $k_*$  and that  $C_j$  is inversely proportional to the roughness Reynolds number within the moderate range of the wall roughness.
- 3) In the fully turbulent region overall results obtained show good agreement with experimental data for smooth walls. Very close to the wall the introduction of the  $C_j$  less than 1.0 predicts high values of near-wall turbulence properties compared with the experimental data from smooth walls. This high level of turbulence properties is the characteristics of turbulence properties near rough walls. Due to the higher surface drag on the rough wall the mean velocity profiles on rough surface become less full than those obtained on a smooth wall. In the all of the cross sectional ares the mean velocity, different from other

turbulence properties is sensitive to the  $C_j$ .

It is concluded that the new damping function  $f_\mu$  have the ability to predict the near-wall turbulence properties on both the smooth and rough walls.

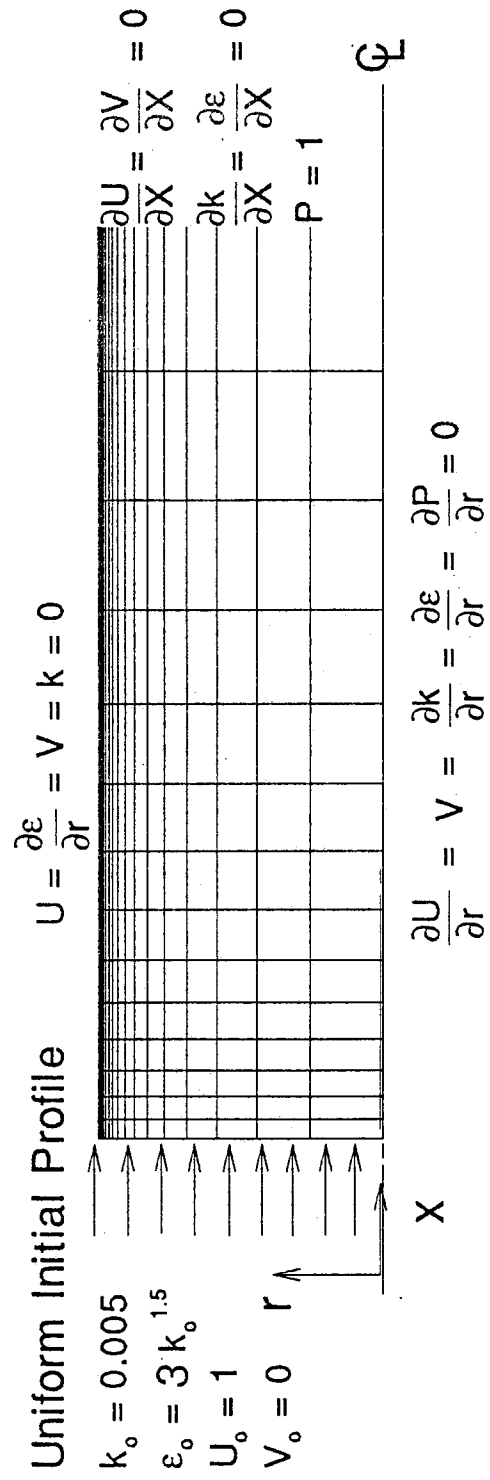


Figure 4.1 Computational geometry and boundary conditions

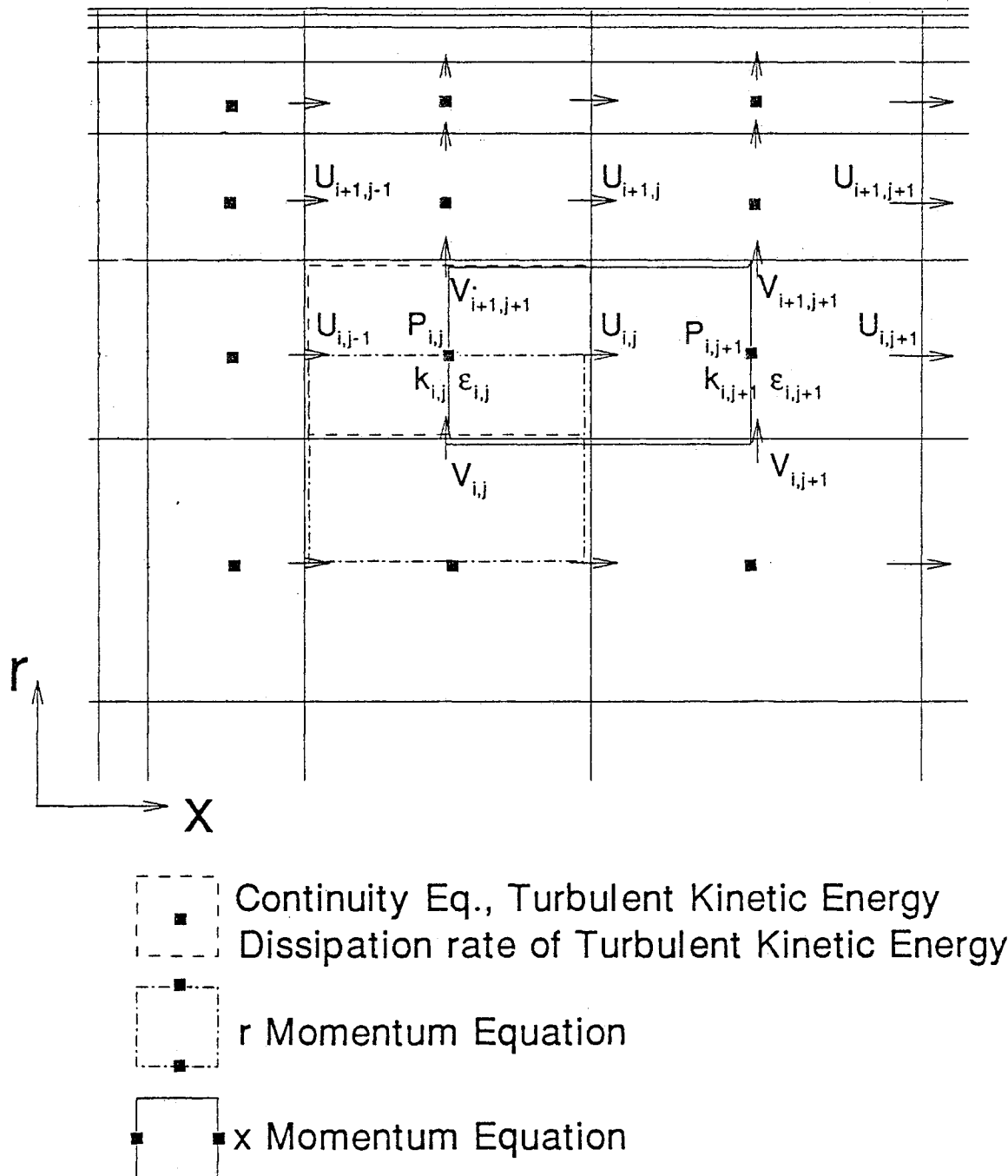


Figure 4.2 Finite difference domain for discretized governing equations

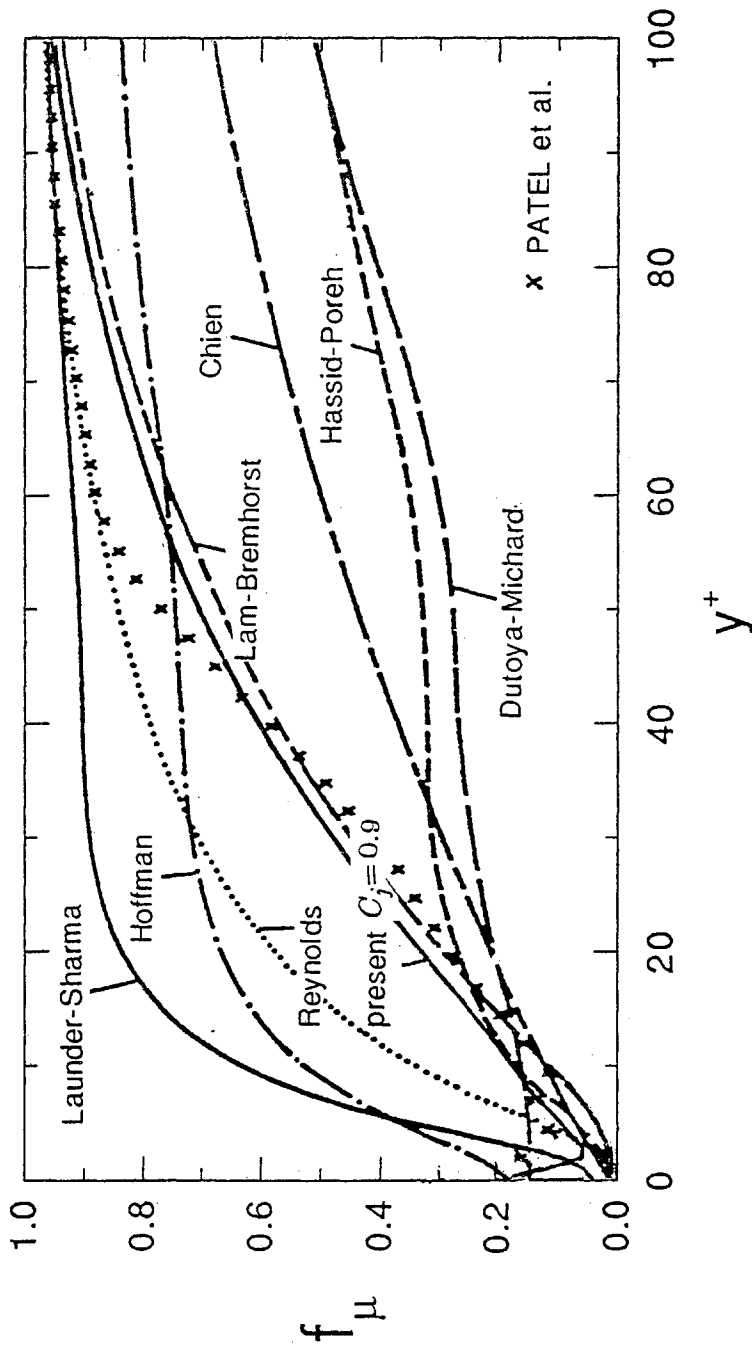


Figure 4.3 Variation of damping function  $f_\mu$  vs  $y^+$ : Comparison of results of various turbulence models and the present result with  $C_j=0.9$  and empirical data[20]



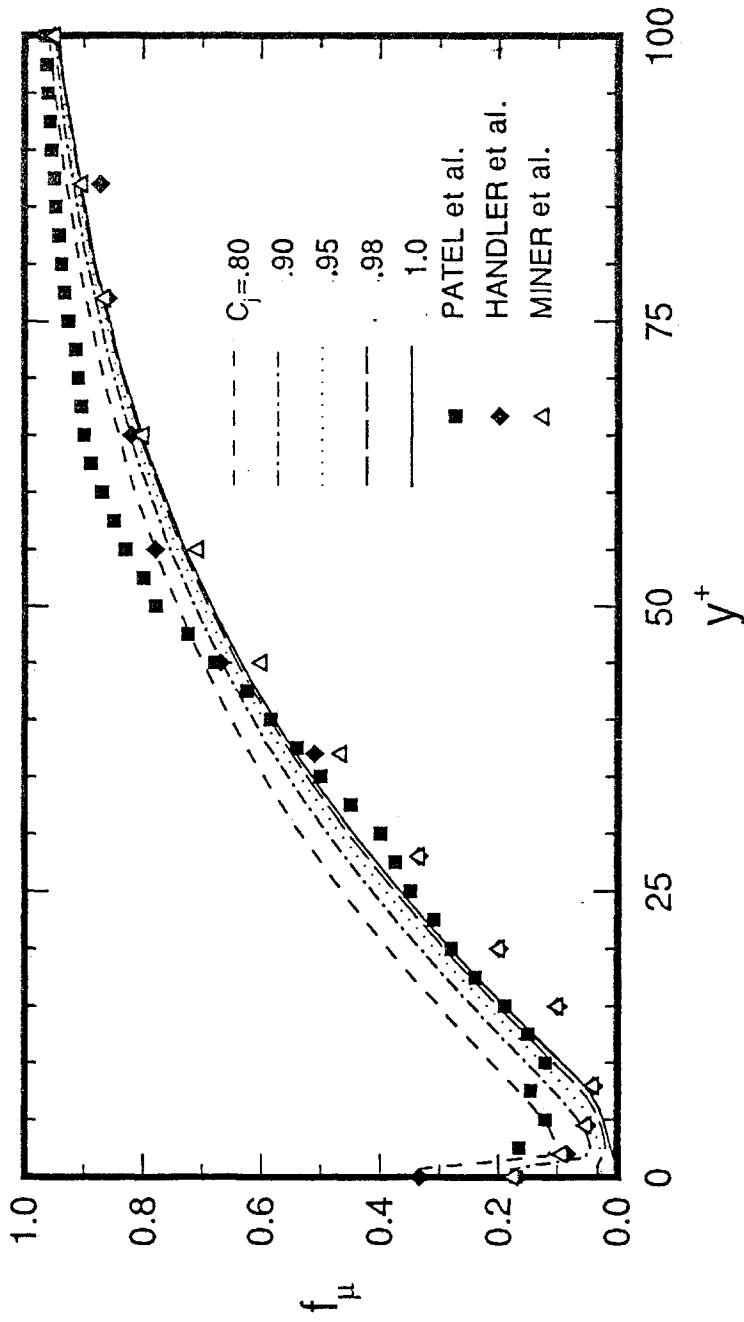


Figure 4.4 Variation of damping function  $f_\mu$  vs  $y^+$ : Comparison of results of the present calculations, empirical data[20] ■ , modified van Driest's model[109] ◆ , and direct numerical simulation[110] △

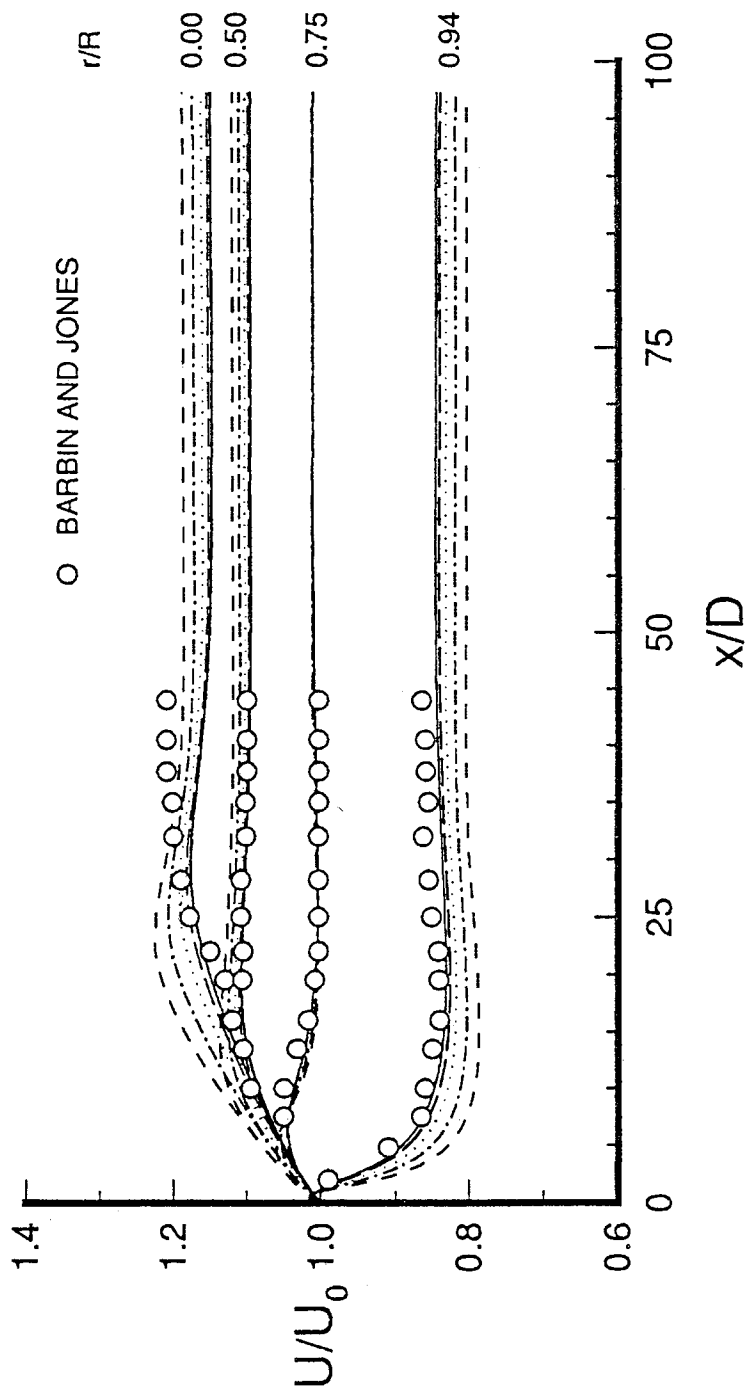


Figure 4.5 Variation of axial velocity with distance downstream of pipe inlet at  $C_j=1.0$  for  $r/R=0.0, 0.5, 0.75, 0.94$  for  $Re_D=380,000$  (Notations for lines are the same as in Figure 4.6)

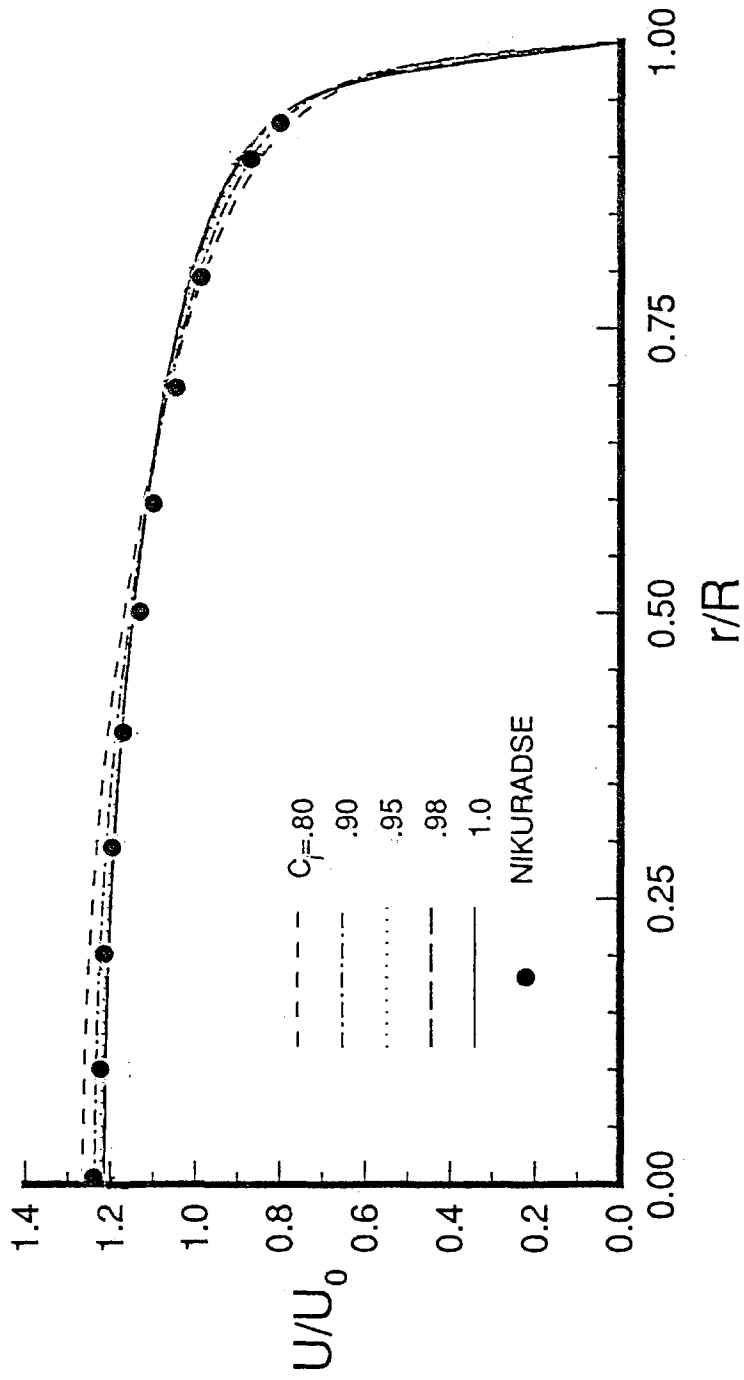


Figure 4.6 Variation of axial velocity with  $r/R$  for different  $C_j$  at  $x/D=80$   
for  $Re_D=10,000$

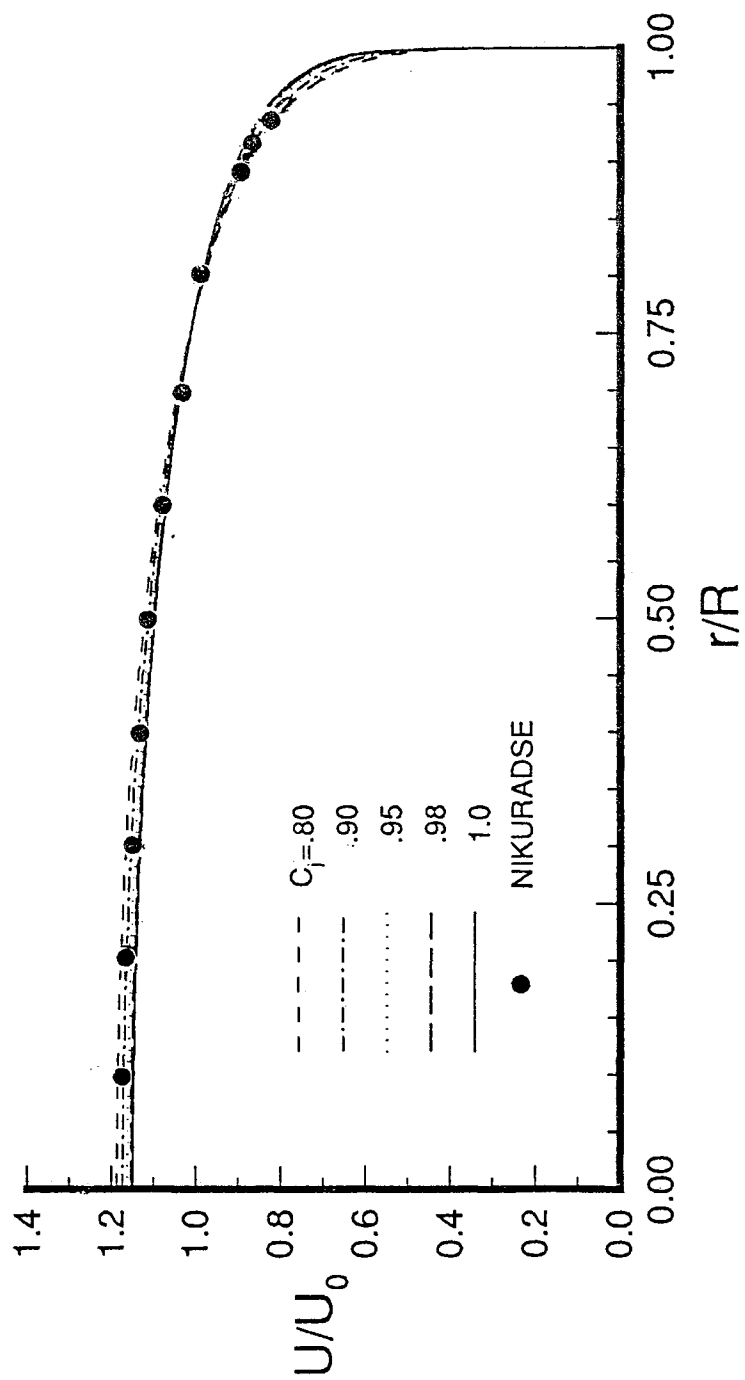


Figure 4.7 Variation of axial velocity with  $r/R$  for different  $C_j$  at  $x/D=80$   
for  $Re_D=380,000$

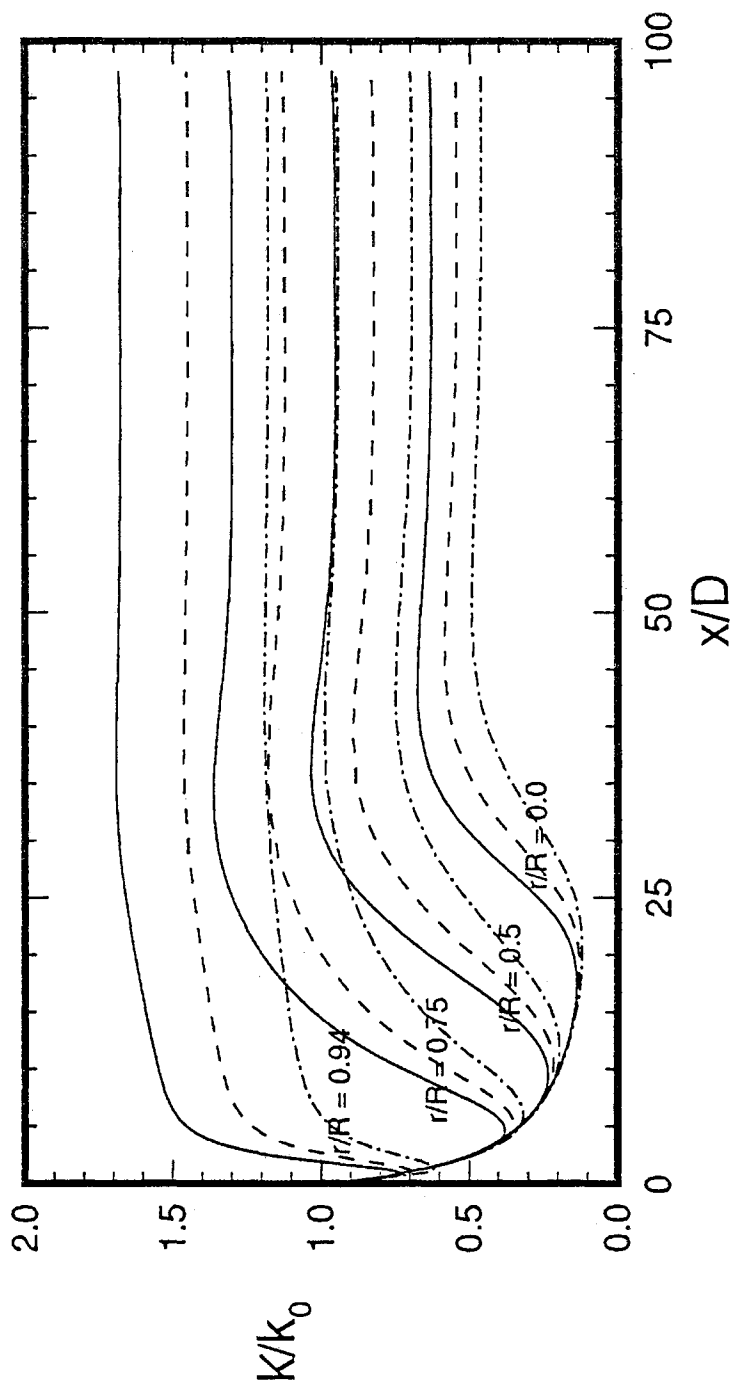


Figure 4.8 Variation of turbulent kinetic energy with distance downstream of pipe inlet at  $r/R=0.0, 0.5, 0.75, 0.94$  for  $Re_D=380,000, C_j = 0.9$  ———,  $0.95$  - - - ,  $1.0$  - · - · -

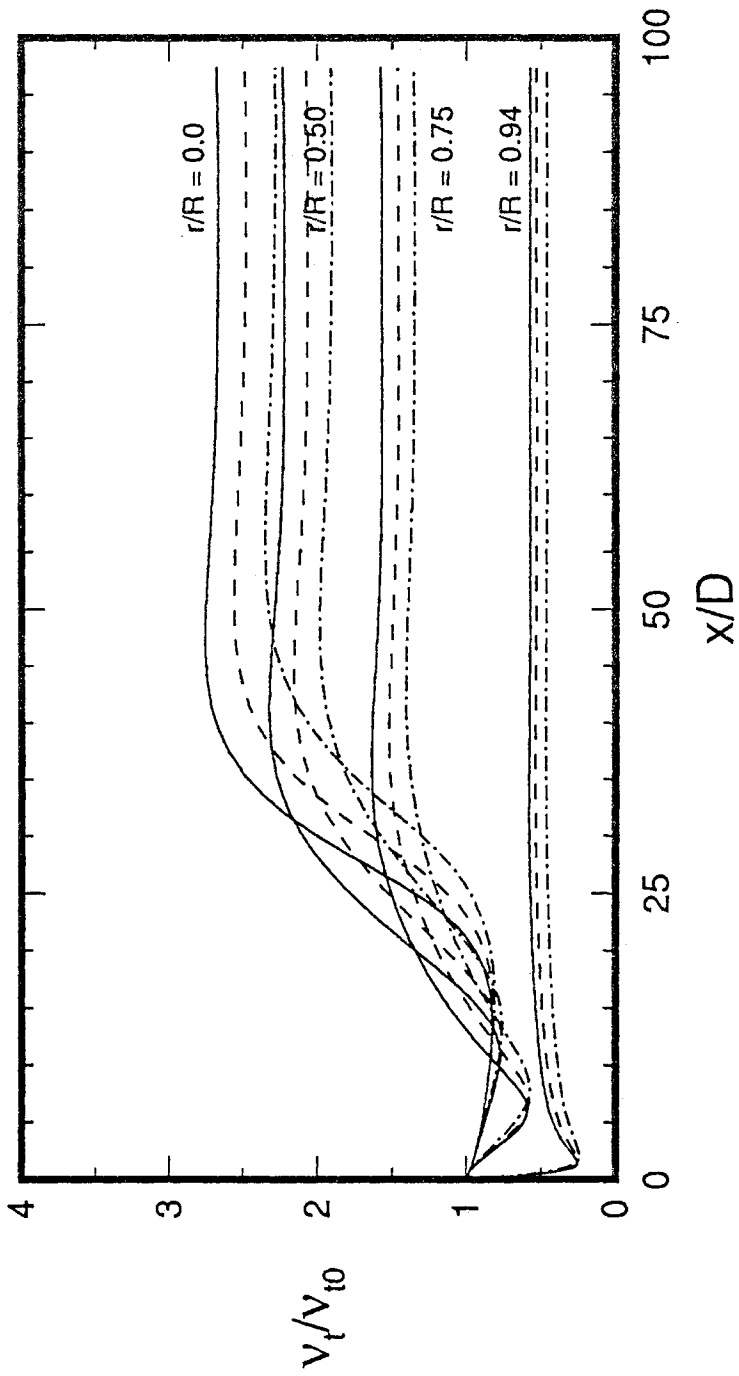


Figure 4.9 Variation of turbulent viscosity with distance downstream of pipe inlet at  $r/R=0.0, 0.5, 0.75, 0.94$  for  $Re_D=380,000$ ,  $C_j=0.9$  —,  $0.95$  ---,  $1.0$  - · - · -

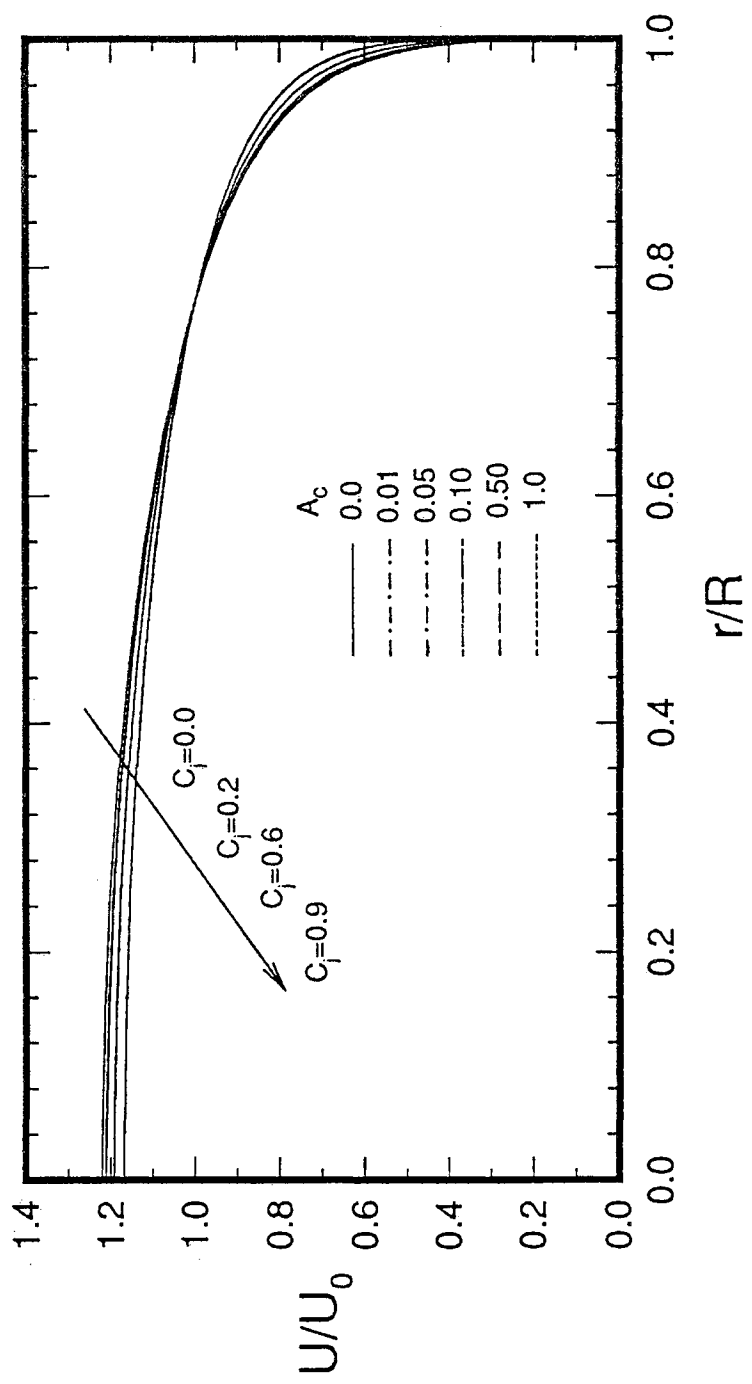


Figure 4.10 Effect of mean velocity on  $A_c$  and  $C_j$  for  $Re_D = 500,000$

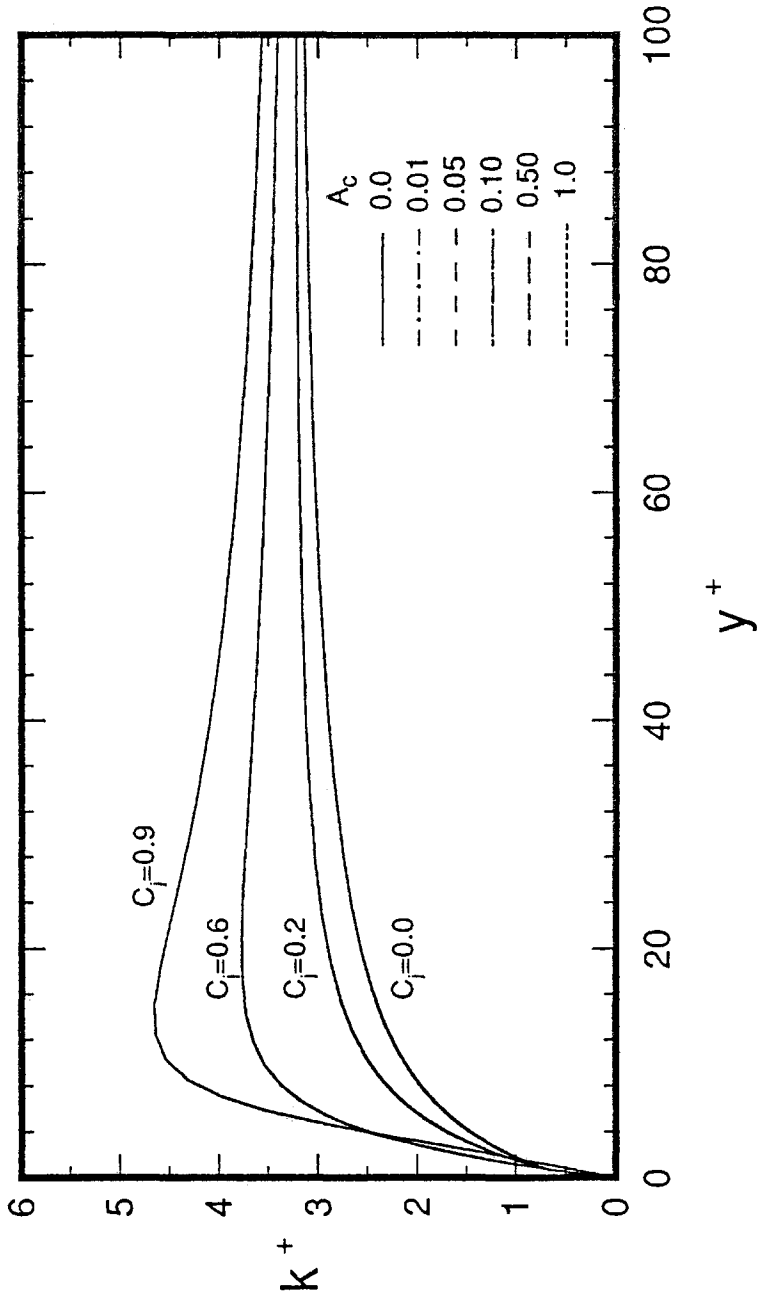


Figure 4.11 Effect of turbulent kinetic energy on  $A_c$  and  $C_j$  for

$Re_D = 500,000$



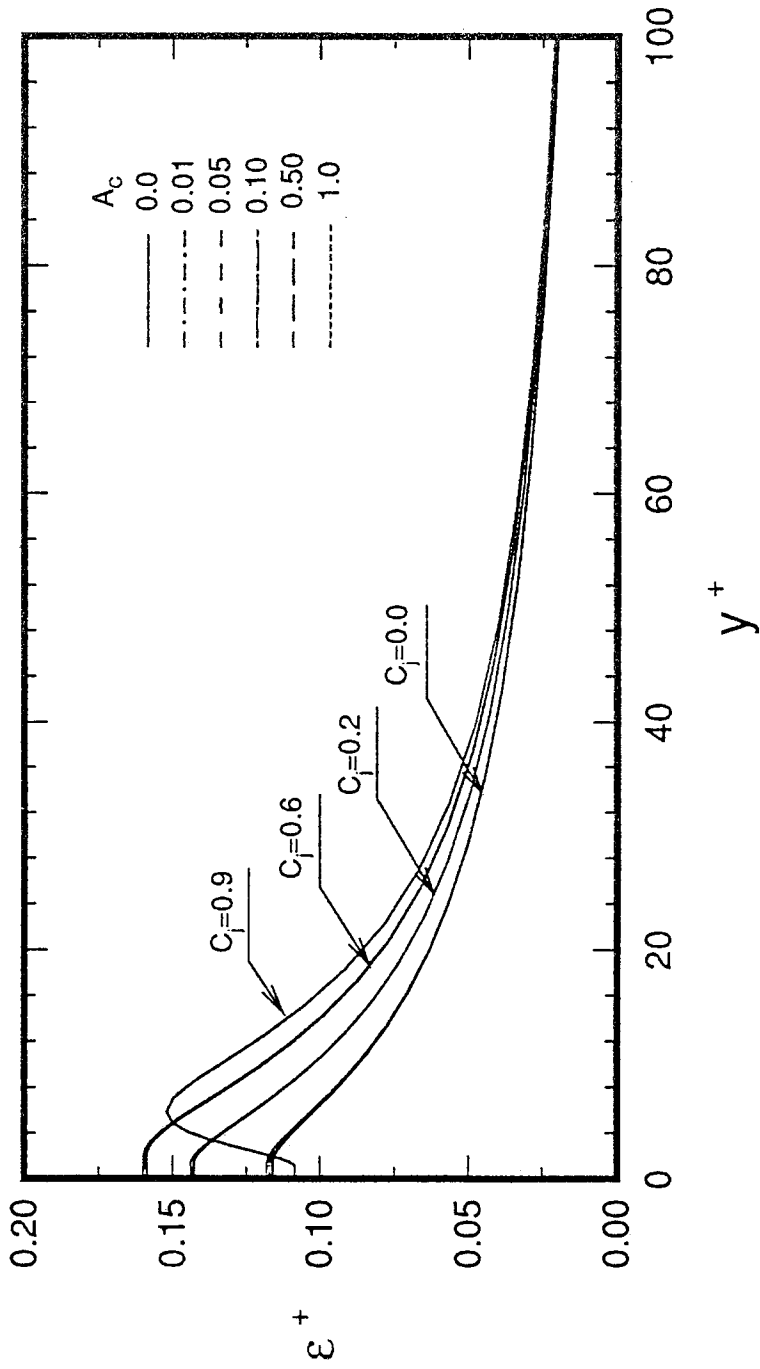


Figure 4.12 Effect of dissipation rate of turbulent kinetic energy on  $A_c$   
and  $C_f$  for  $Re_D = 500,000$

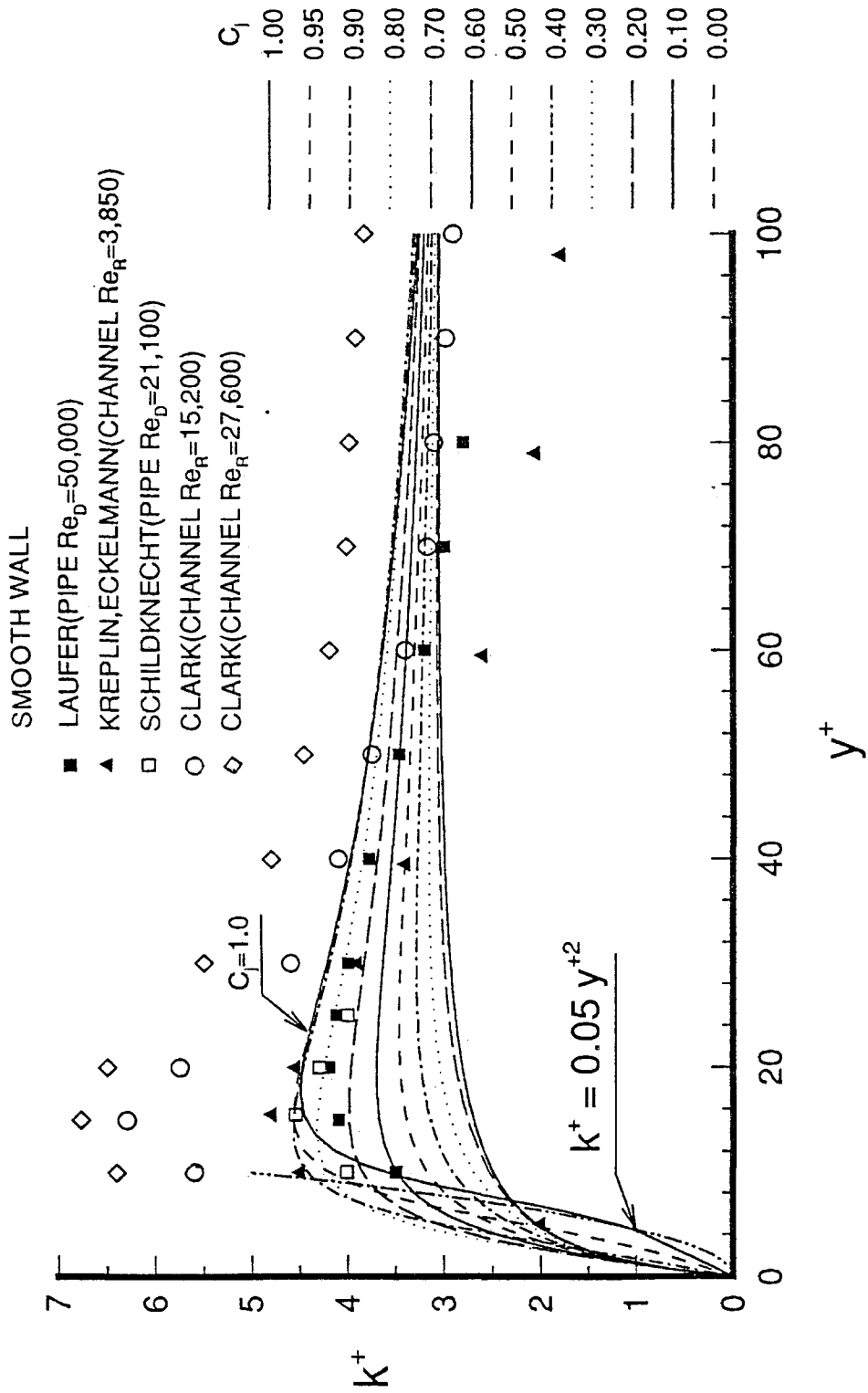


Figure 4.13 Near-wall variation of turbulent kinetic energy at different  $C_f$  for  $Re_D=50,000$

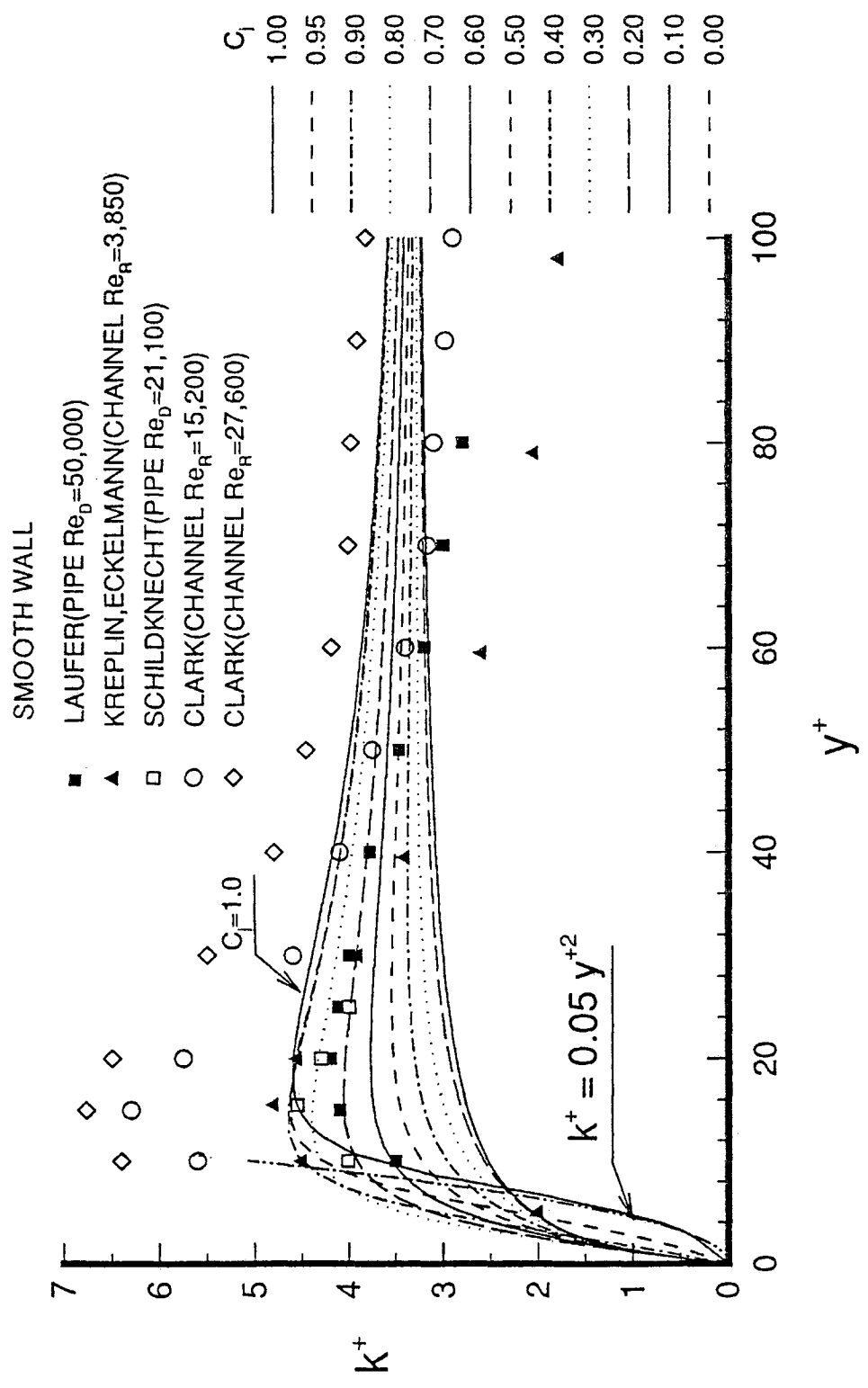


Figure 4.14 Near-wall variation of turbulent kinetic energy at different  $C_f$  for  $Re_D=500,000$

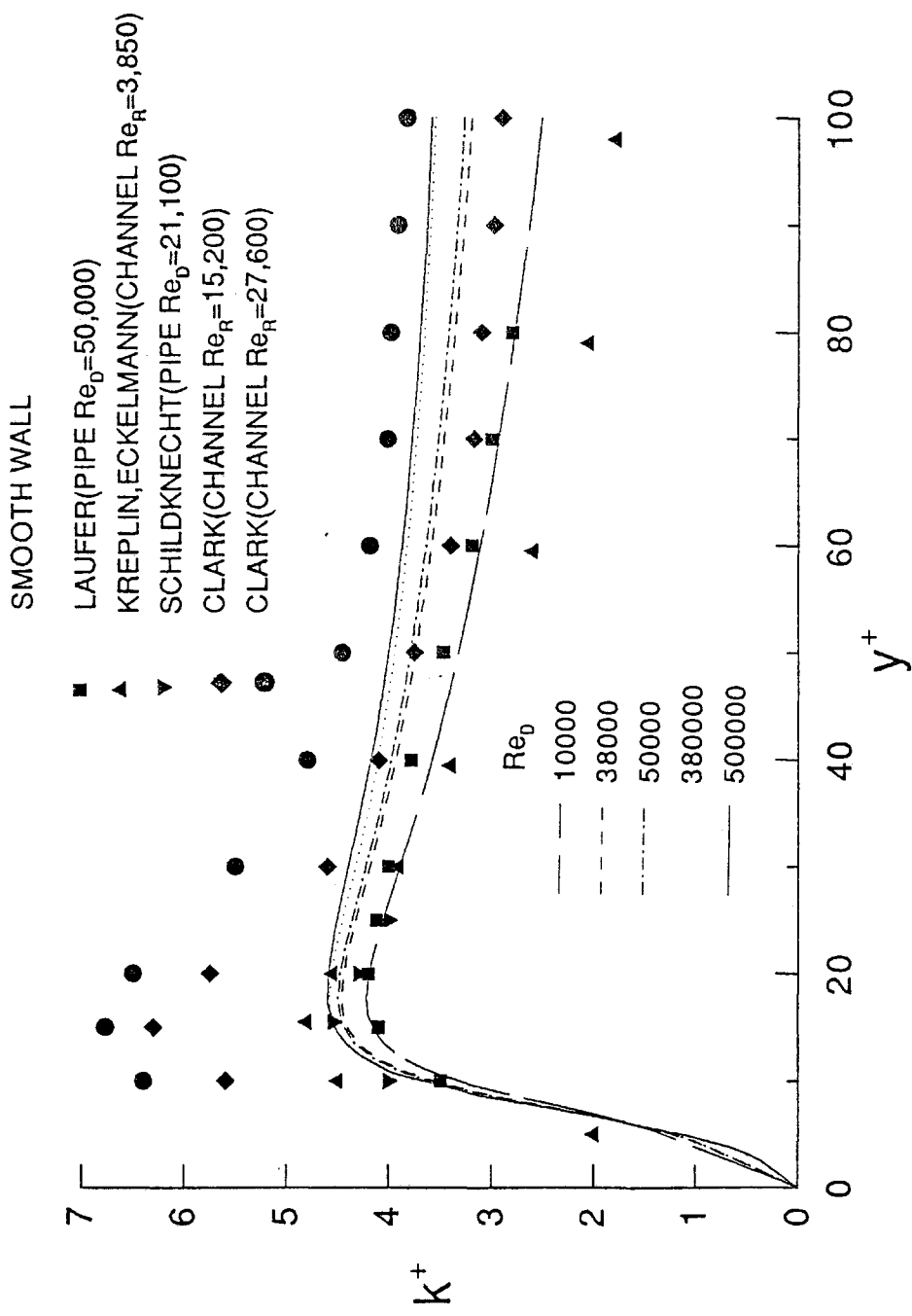


Figure 4.15 Near-wall variation of turbulent kinetic energy with  $y^+$  for  $C_j=1.0$  at  $x/D=80$  for  $Re_D=10,000, 38,000, 50,000, 380,000$  and  $500,000$

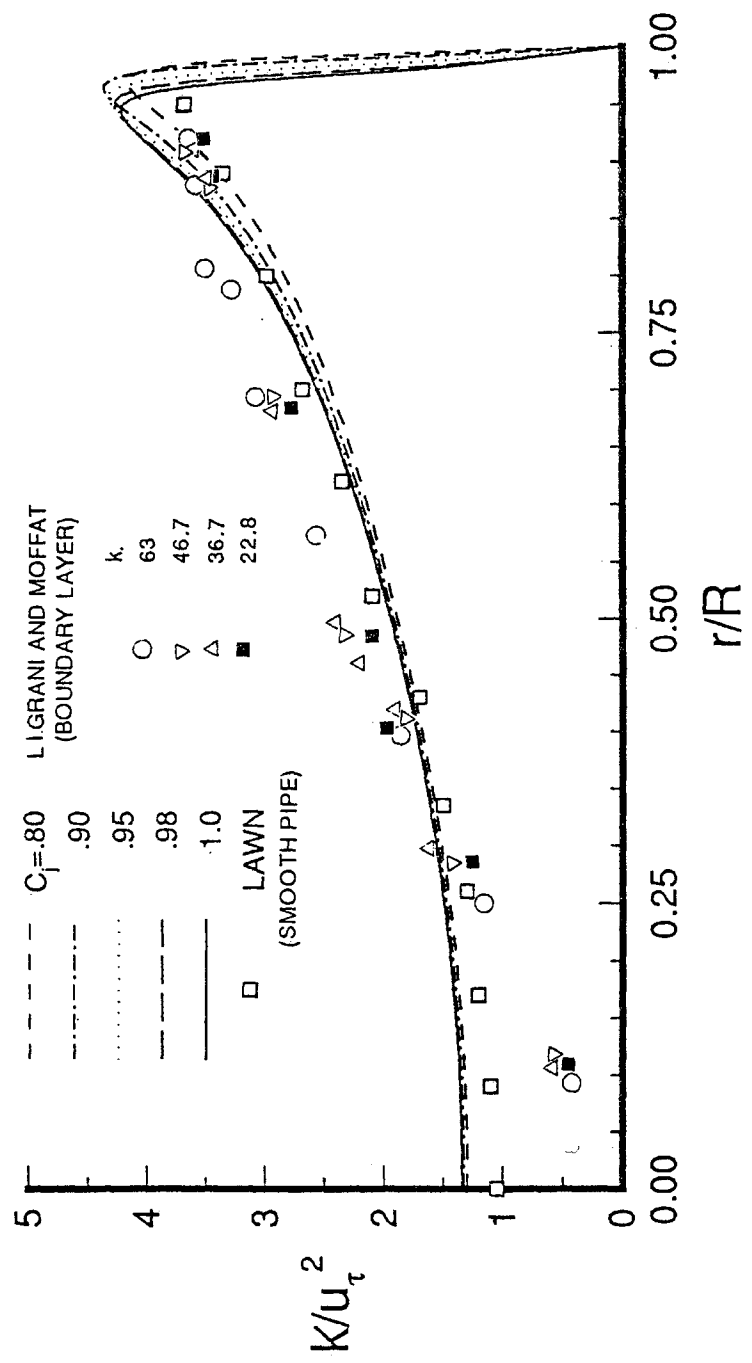


Figure 4.16 Variation of turbulent kinetic energy with  $r/R$  for different  $C_f$  at  $x/D=80$  for  $Re_D=10,000$

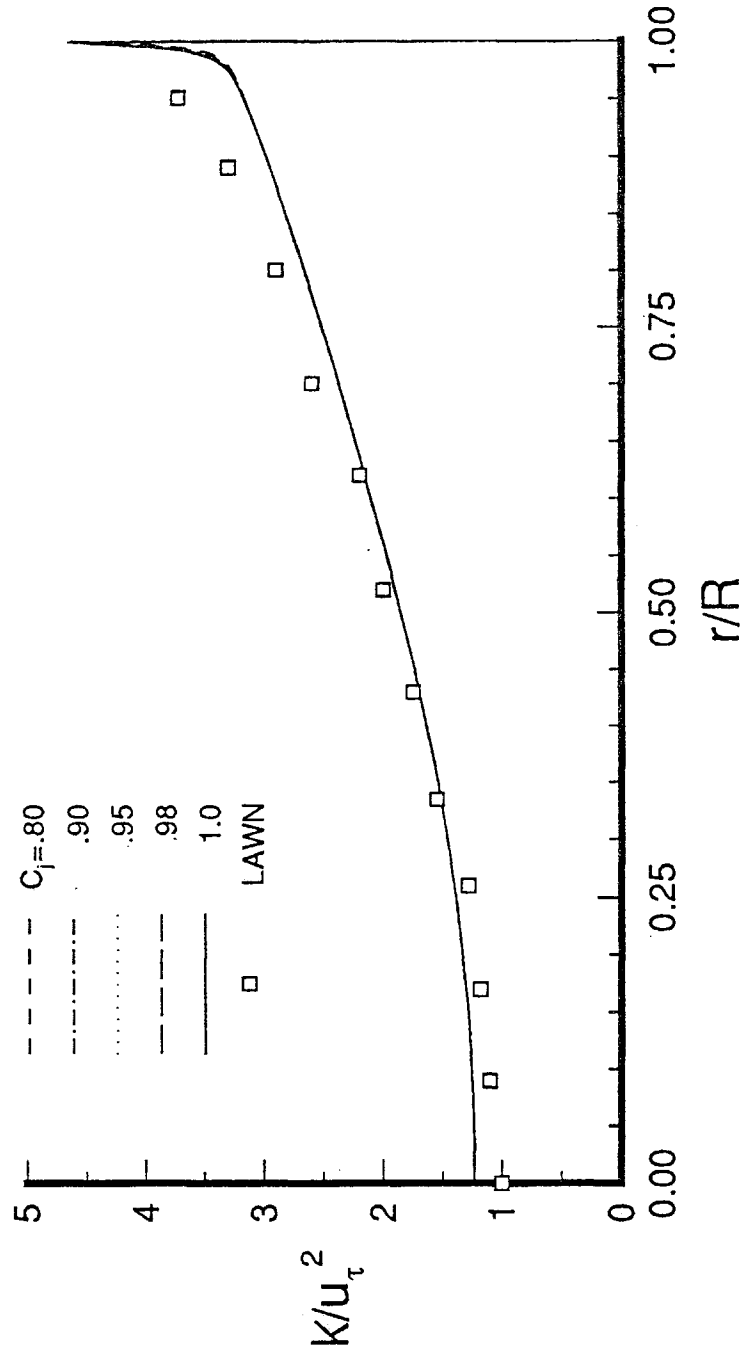


Figure 4.17 Variation of turbulent kinetic energy with  $r/R$  for different  $C_i$  at  $x/D=80$  for  $Re_D=380,000$

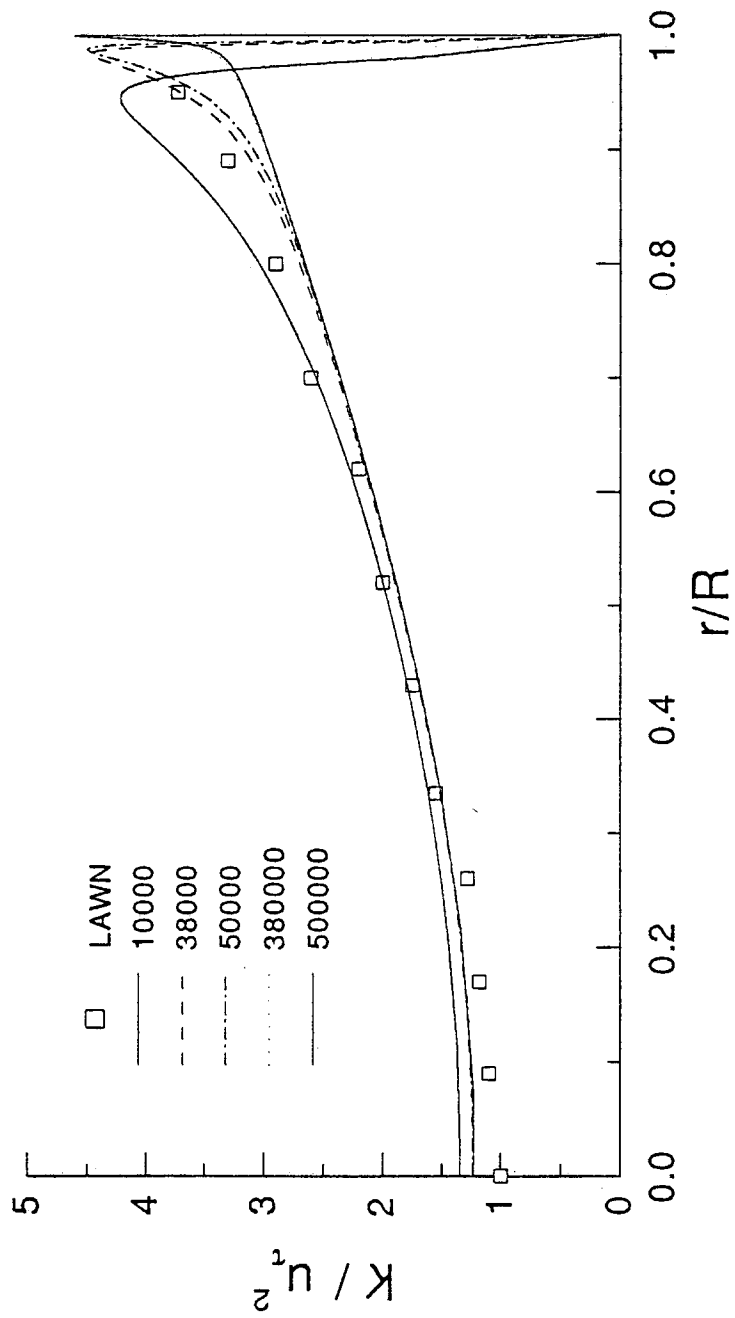


Figure 4.18 Variation of turbulent kinetic energy with  $r/R$  for  $C_j=1.0$  at  $x/D=80$  for  $Re_D=10,000, 38,000, 50,000, 380,000$  and  $500,000$

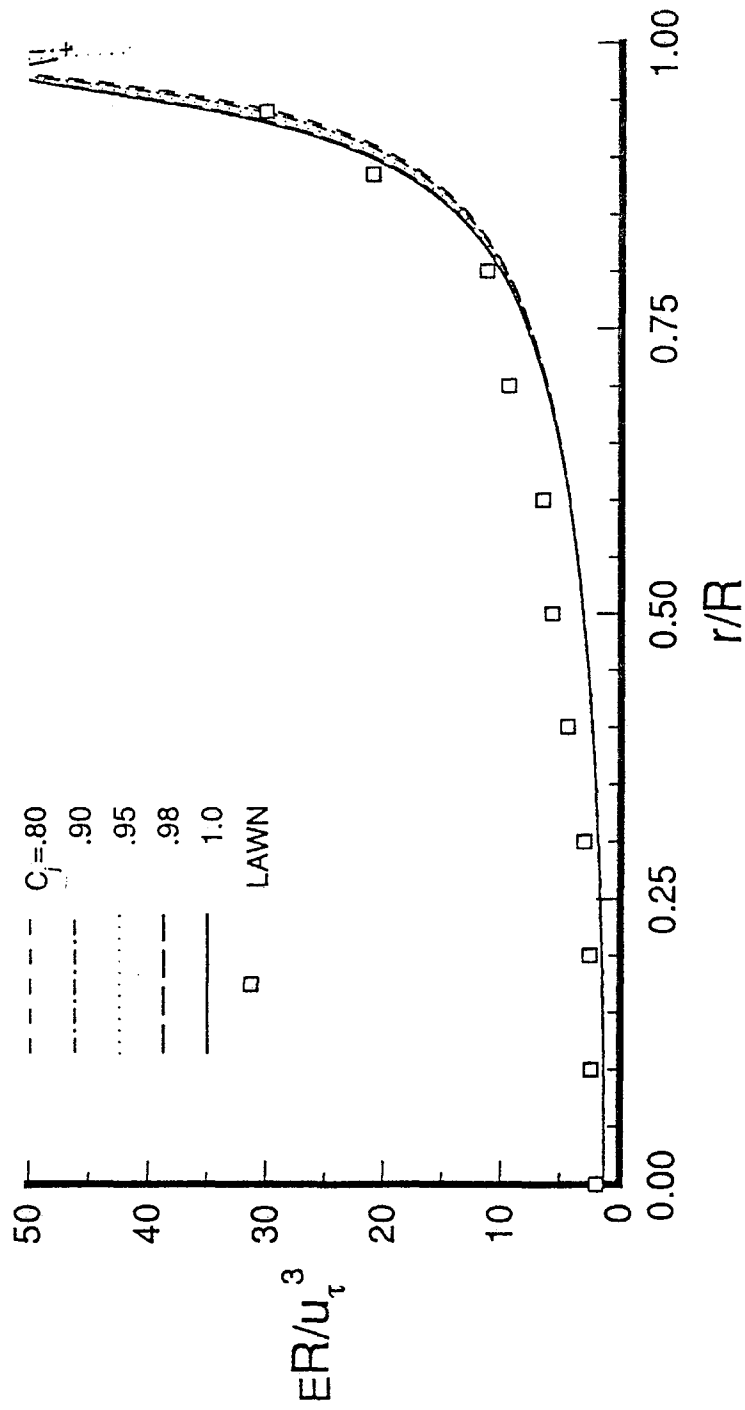


Figure 4.19 Variation of dissipation rate of turbulent kinetic energy with  $r/R$  for different  $C_j$  at  $x/D=80$  for  $Re_D=10,000$



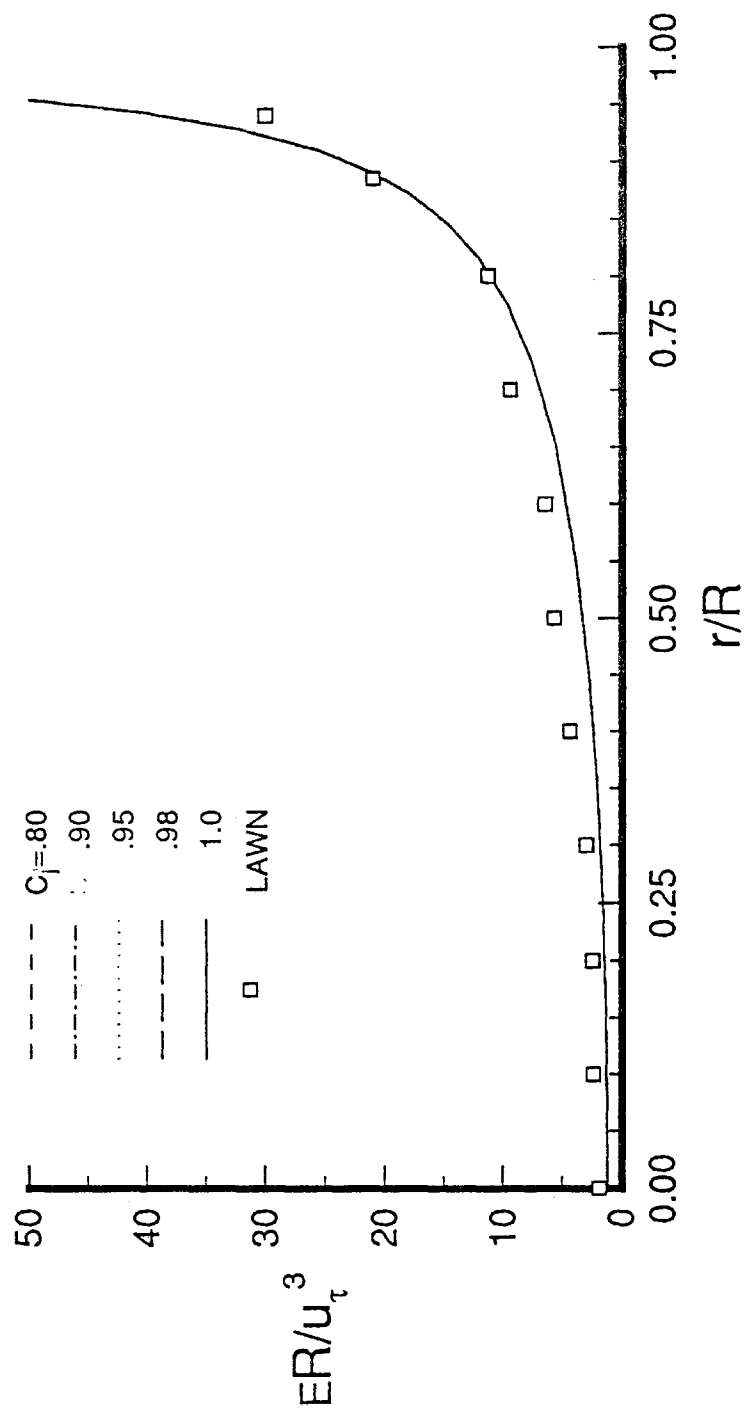


Figure 4.20 Variation of dissipation rate of turbulent kinetic energy with  $r/R$  for different  $C_j$  at  $x/D=80$  for  $Re_D=380,000$

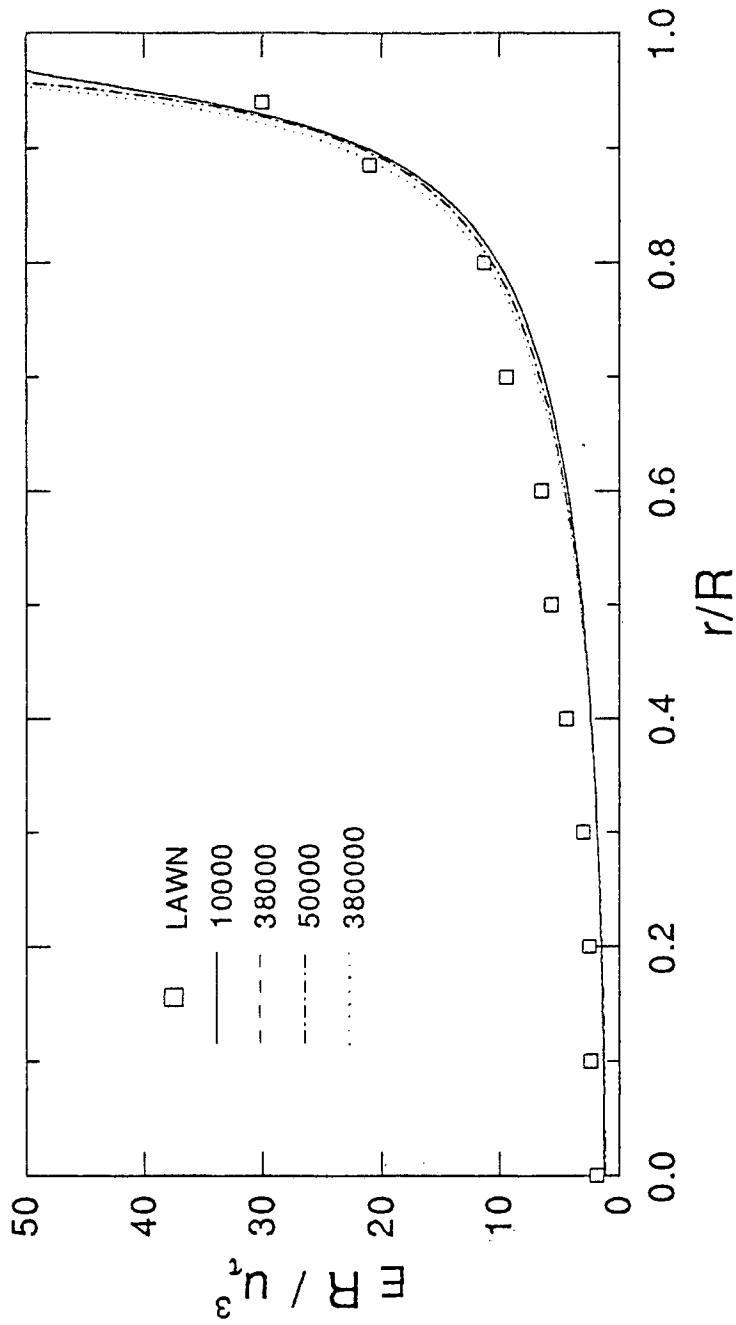


Figure 4.21 Variation of dissipation rate of turbulent kinetic energy with  $r/R$  for  $C_j=1.0$  at  $x/D=80$  for  $Re_D=10,000, 38,000, 50,000$  and  $380,000$

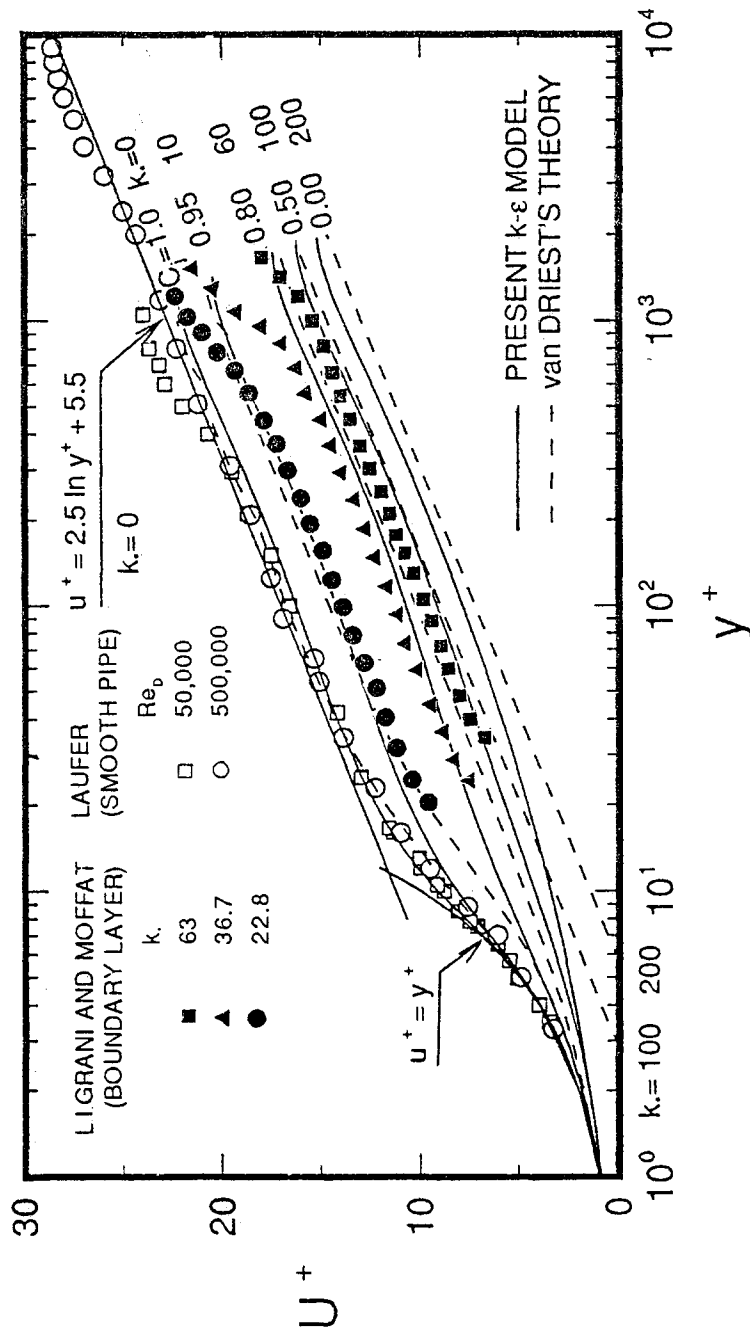


Figure 4.22 Logarithmic velocity profiles for turbulent flow near smooth and rough walls: Comparison of results of the present  $k-\epsilon$  turbulence model ( $Re_D=50,000$ ), van Driest's theory, and experimental data for smooth and rough surfaces

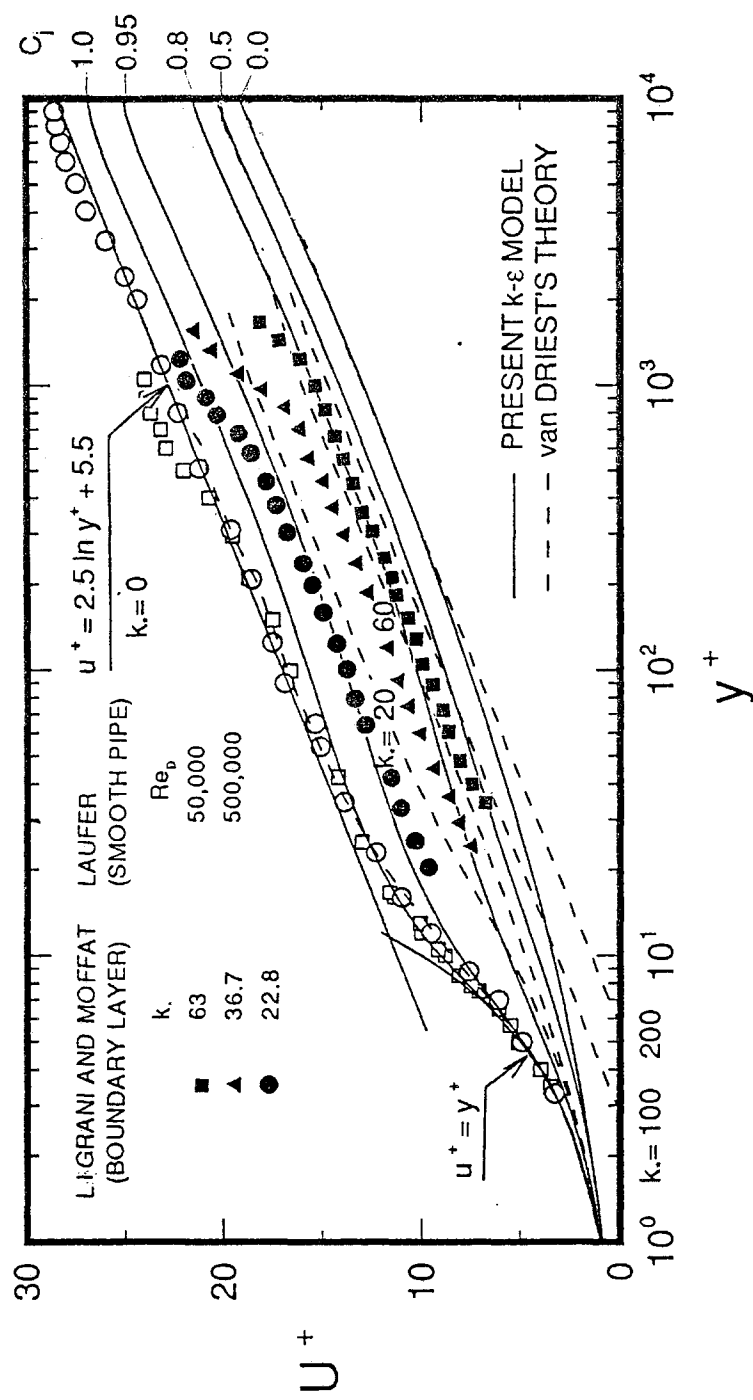


Figure 4.23 Logarithmic velocity profiles for turbulent flow near smooth and rough walls: Comparison of results of the present  $k-\epsilon$  turbulence model ( $Re_D=500,000$ ), van Driest's theory, and experimental data for smooth and rough surfaces

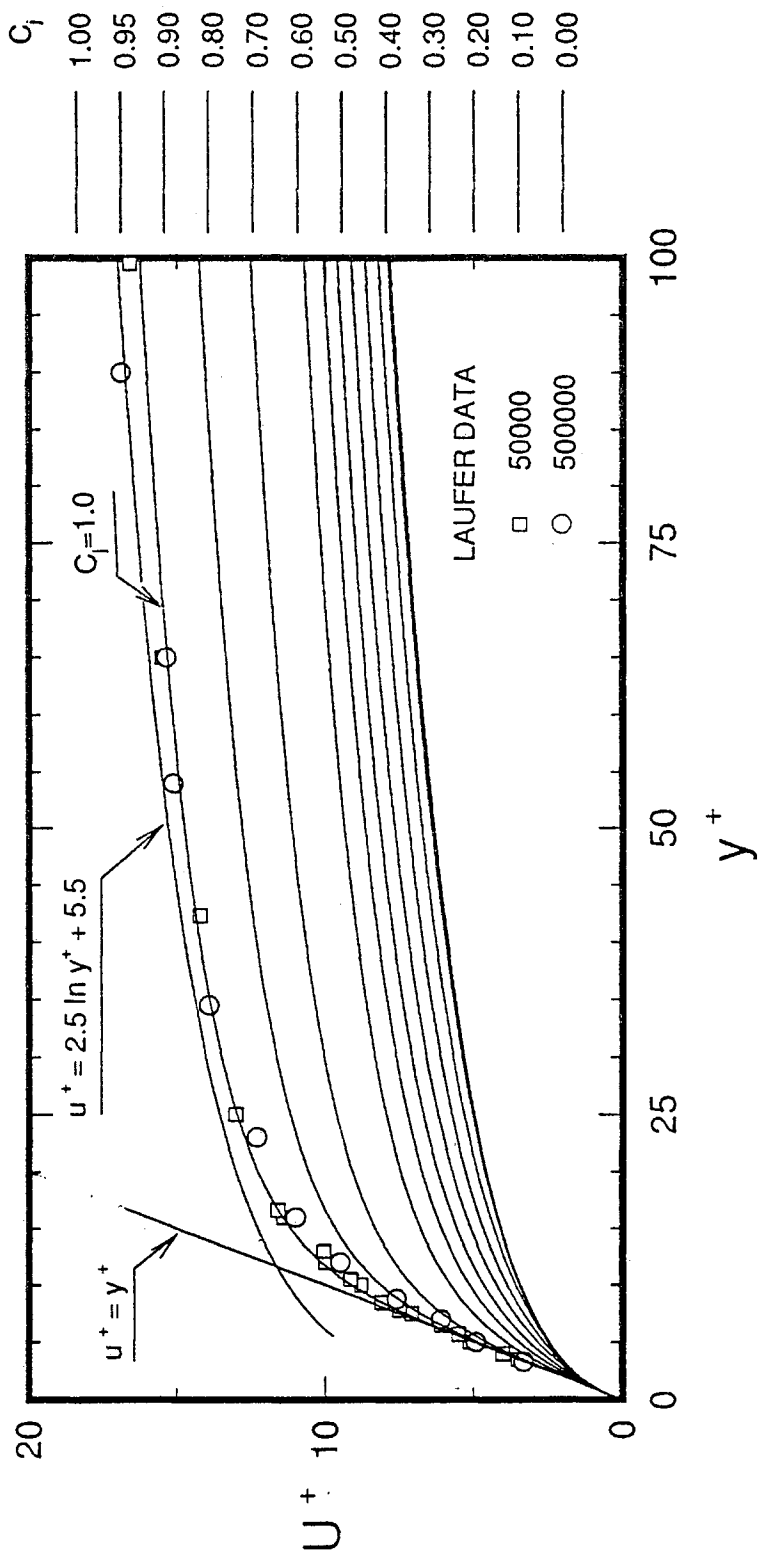


Figure 4.24 Velocity profiles for turbulent flow near smooth and rough walls: Comparison of results of the present  $k-\epsilon$  turbulence model ( $Re_D=50,000$ ) and experimental data for a smooth pipe

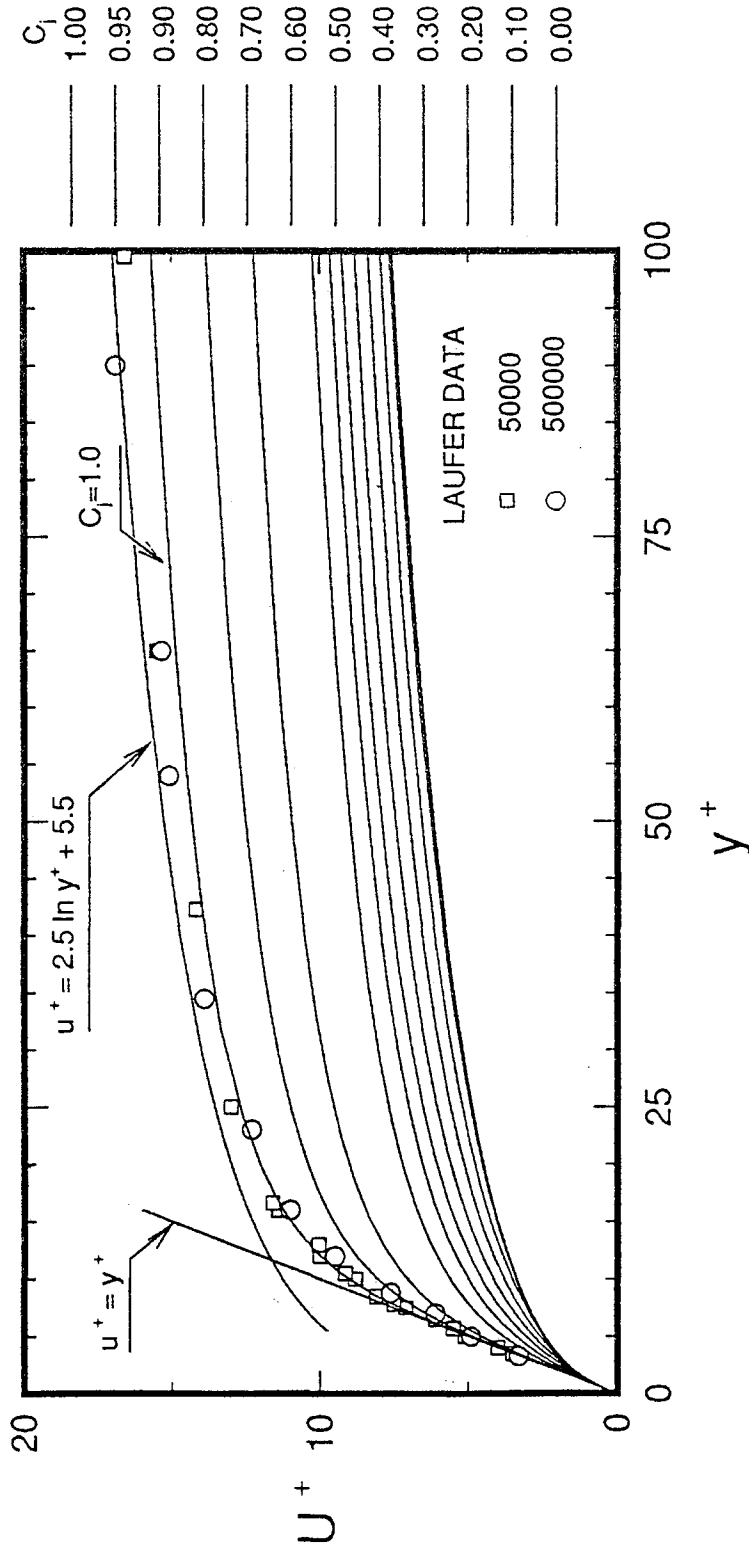


Figure 4.25 Velocity profiles for turbulent flow near smooth and rough walls: Comparison of results of the present  $k-\epsilon$  turbulence model ( $Re_D=500,000$ ) and experimental data for a smooth pipe

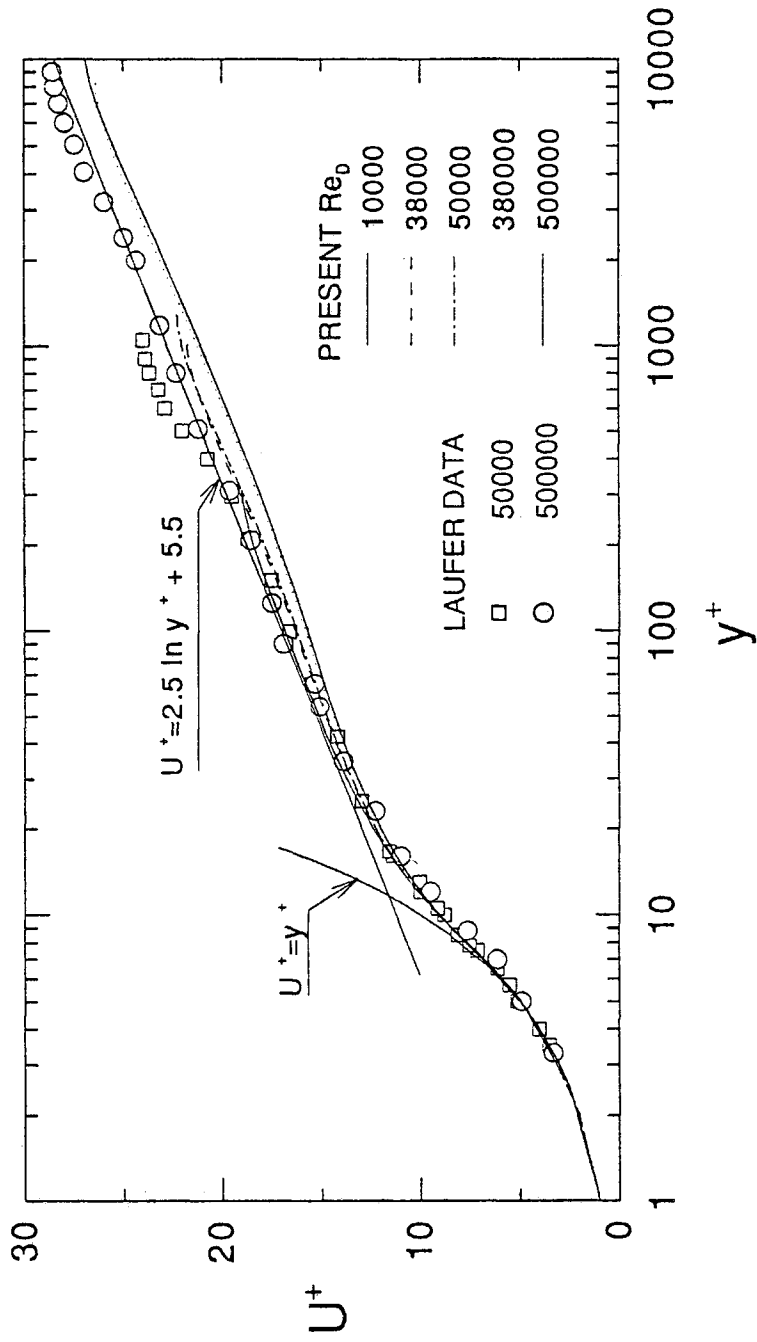


Figure 4.26 Logarithmic velocity profiles for turbulent flow near smooth and rough walls: Comparison of results of the present  $k-\epsilon$  turbulence model with  $C_j=1.0$  for  $Re_D=10,000, 38,000, 50,000, 380,000$  and  $500,000$  and experimental data for a smooth pipe

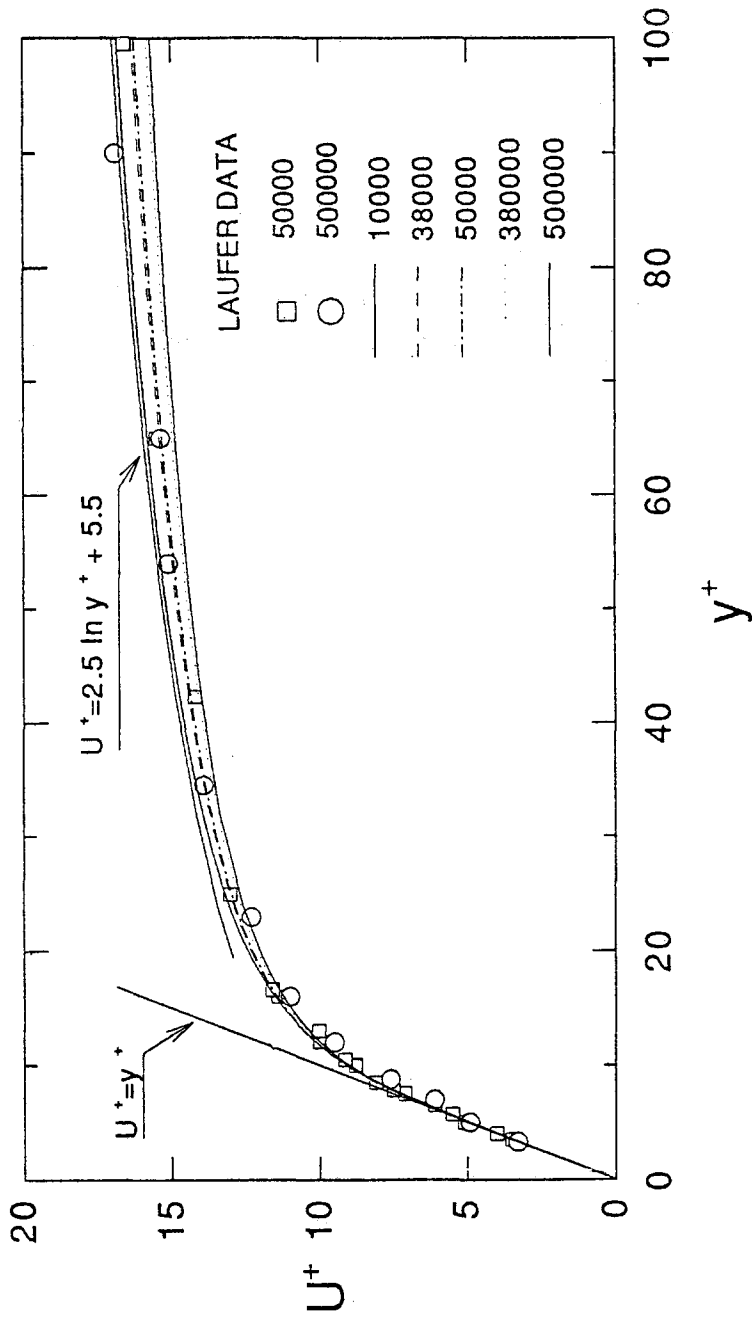


Figure 4.27 Velocity profiles for turbulent flow near smooth and rough walls: Comparison of results of the present  $k-\epsilon$  turbulence model with  $C_j=1.0$  for  $Re_D=10,000, 38,000, 50,000, 380,000$  and  $500,000$  and experimental data for a smooth pipe



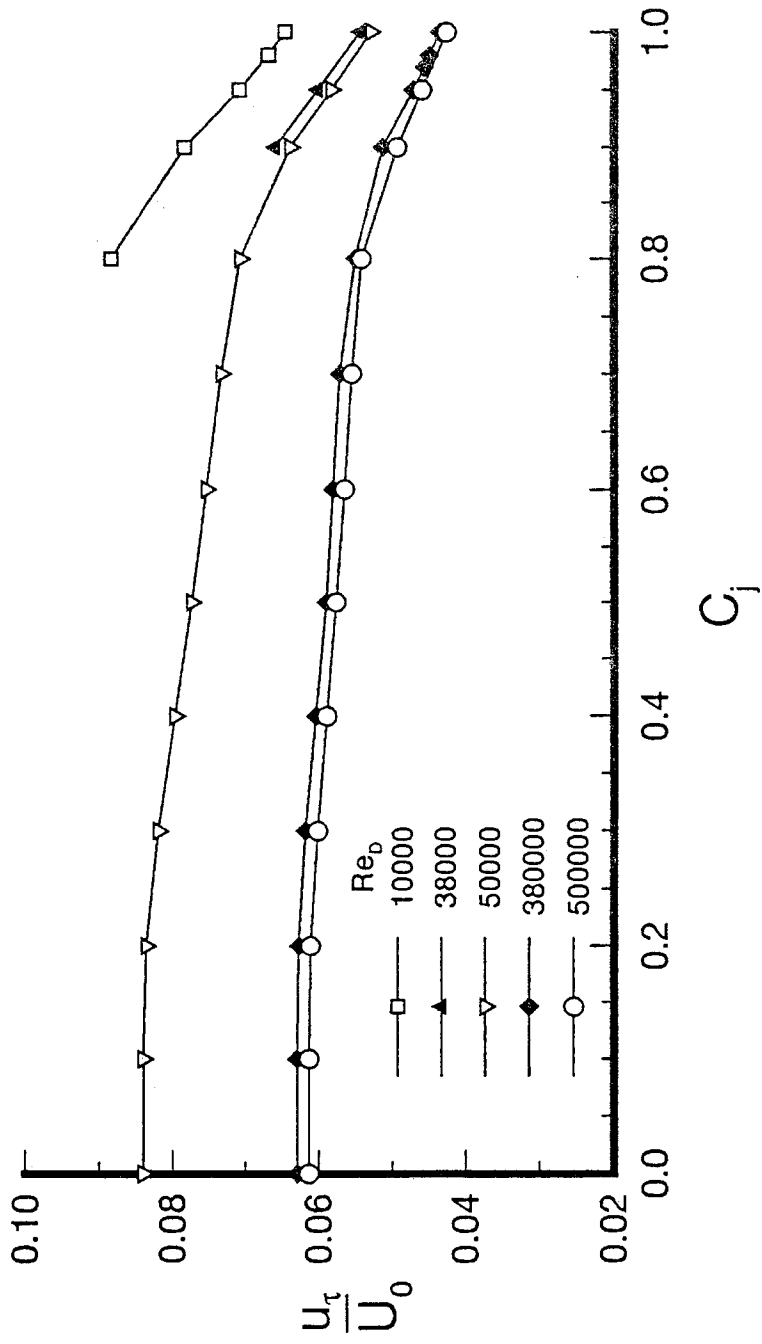


Figure 4.28 Distribution of wall shear-stresses with roughness parameter  $C_j$  for  $Re_D = 10,000, 38,000, 50,000, 380,000$  and  $500,000$

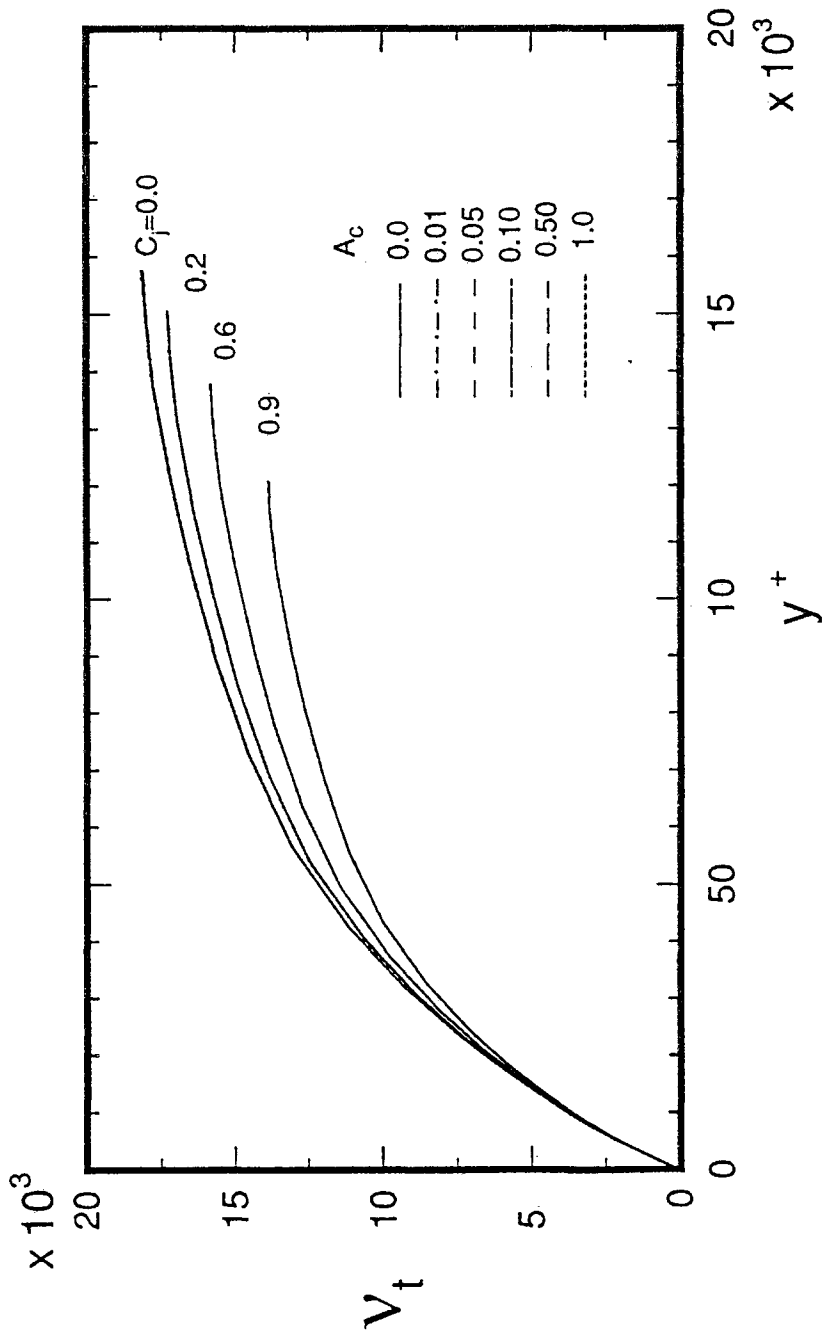


Figure 4.29 Effect of turbulent viscosity  $\nu_t$  on  $A_c$  and  $C_f$  for  $Re_D = 500,000$

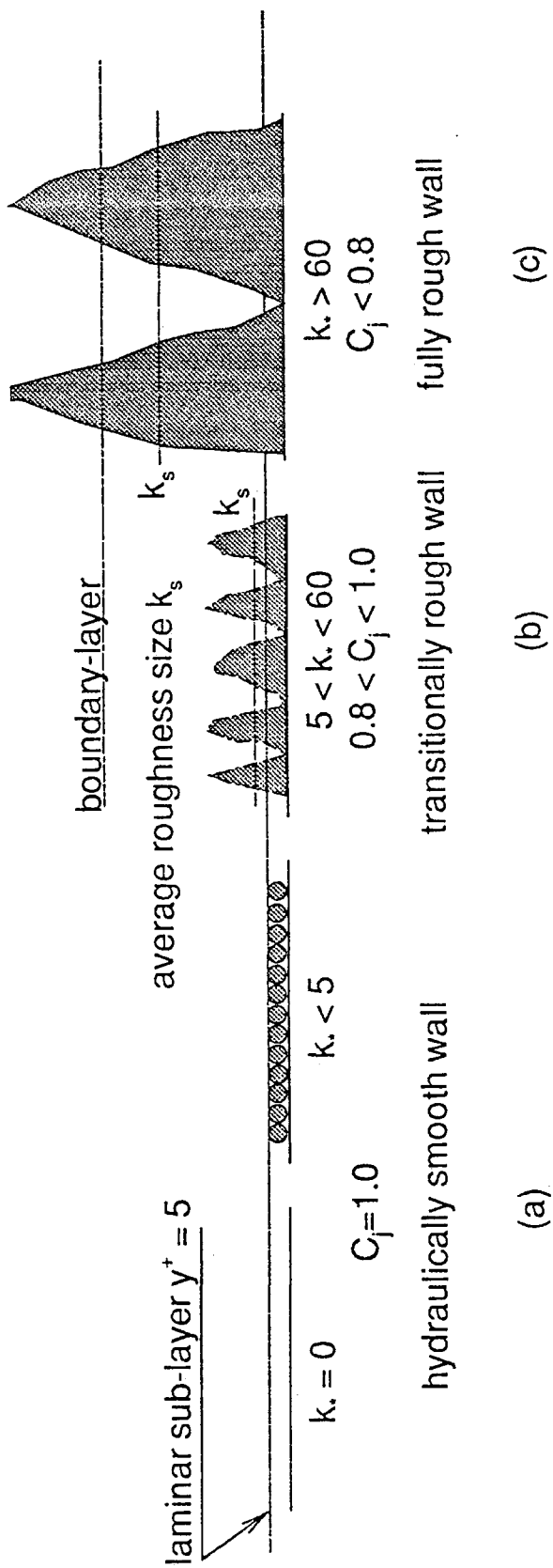


Figure 4.30 Geometry of surface roughness

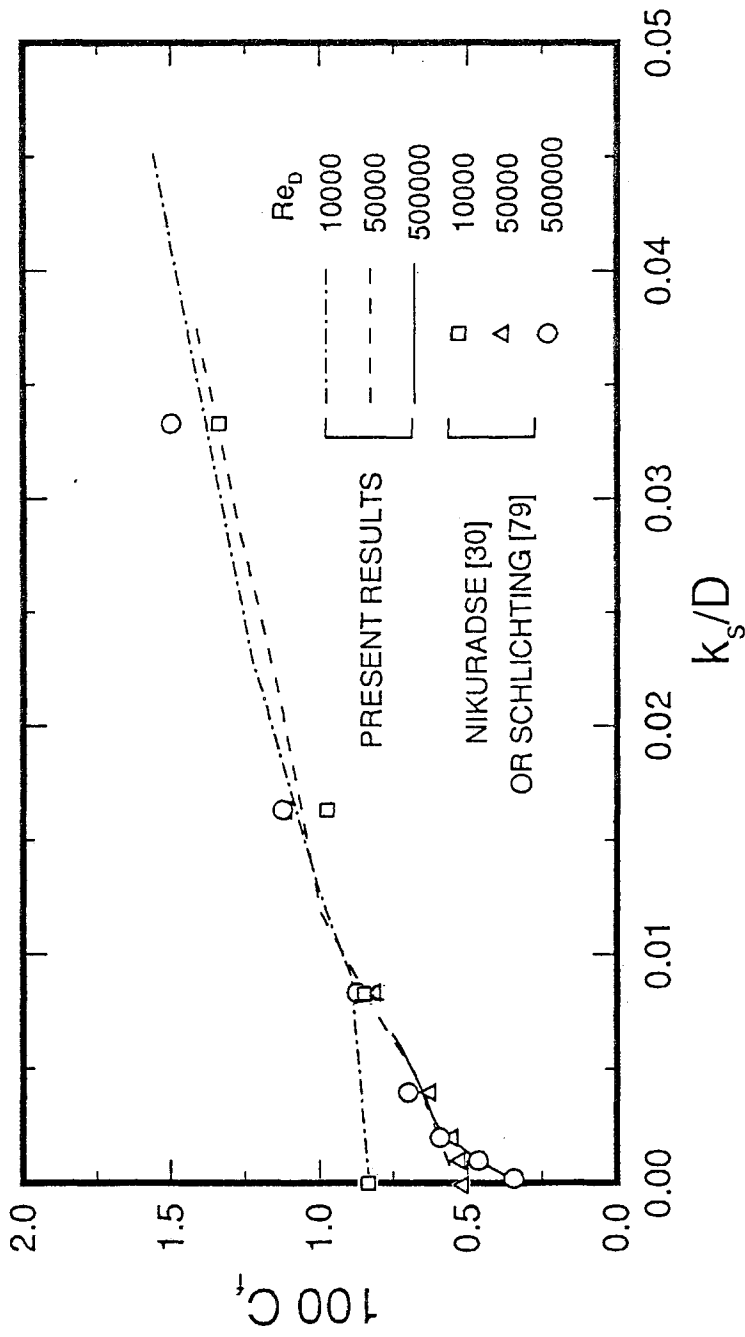


Figure 4.31 Skin friction coefficient vs relative roughness

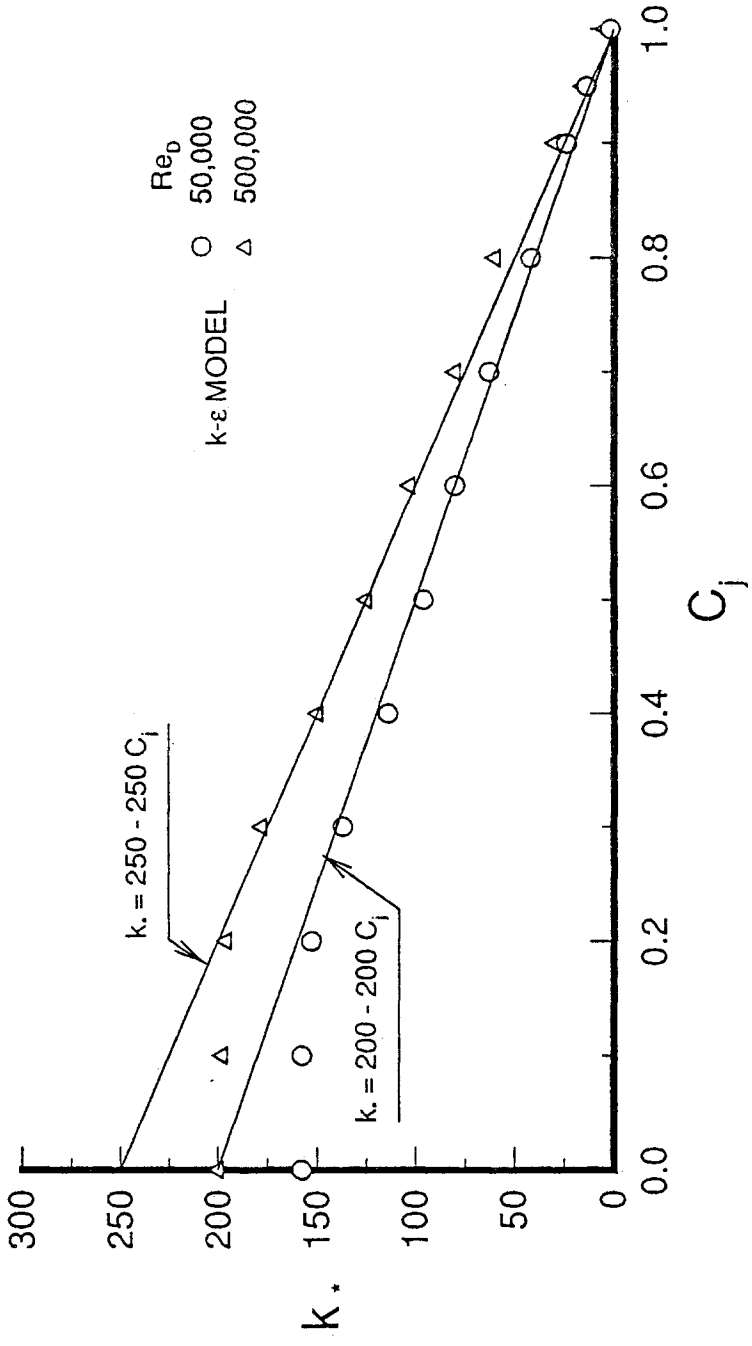


Figure 4.32 Functional relationship between roughness Reynolds number  $k^*$  (van Driest's theory) and roughness parameter  $C_j$  ( $k-\epsilon$  turbulence model)

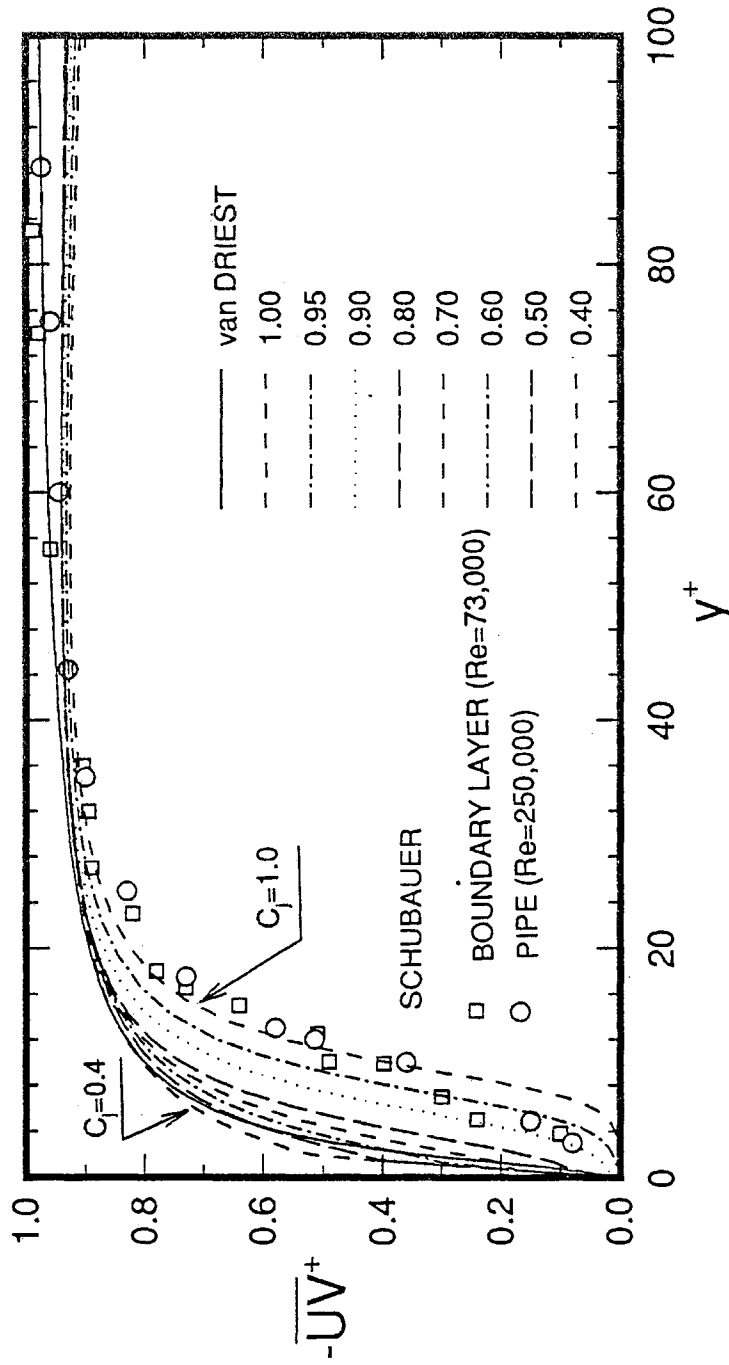


Figure 4.33 Near-wall distribution of Reynolds shear stress for flow near smooth and rough walls: Comparison of the present  $k-\epsilon$  turbulence model for  $Re_D=50,000$ , van Driest's theory, and experimental data for smooth surfaces

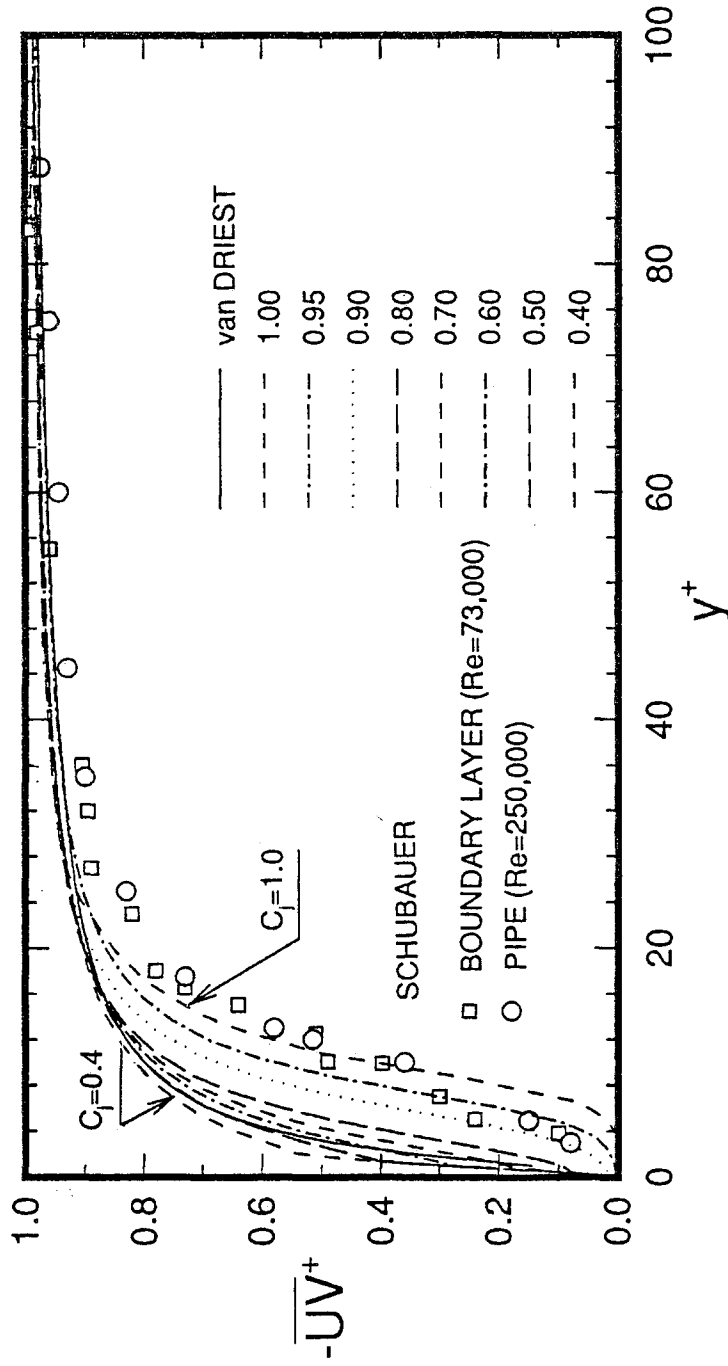


Figure 4.34 Near-wall distribution of Reynolds shear stress for flow near smooth and rough walls: Comparison of the present  $k-\epsilon$  turbulent model for  $Re_D=500,000$ , van Driest's theory, and experimental data for smooth surfaces

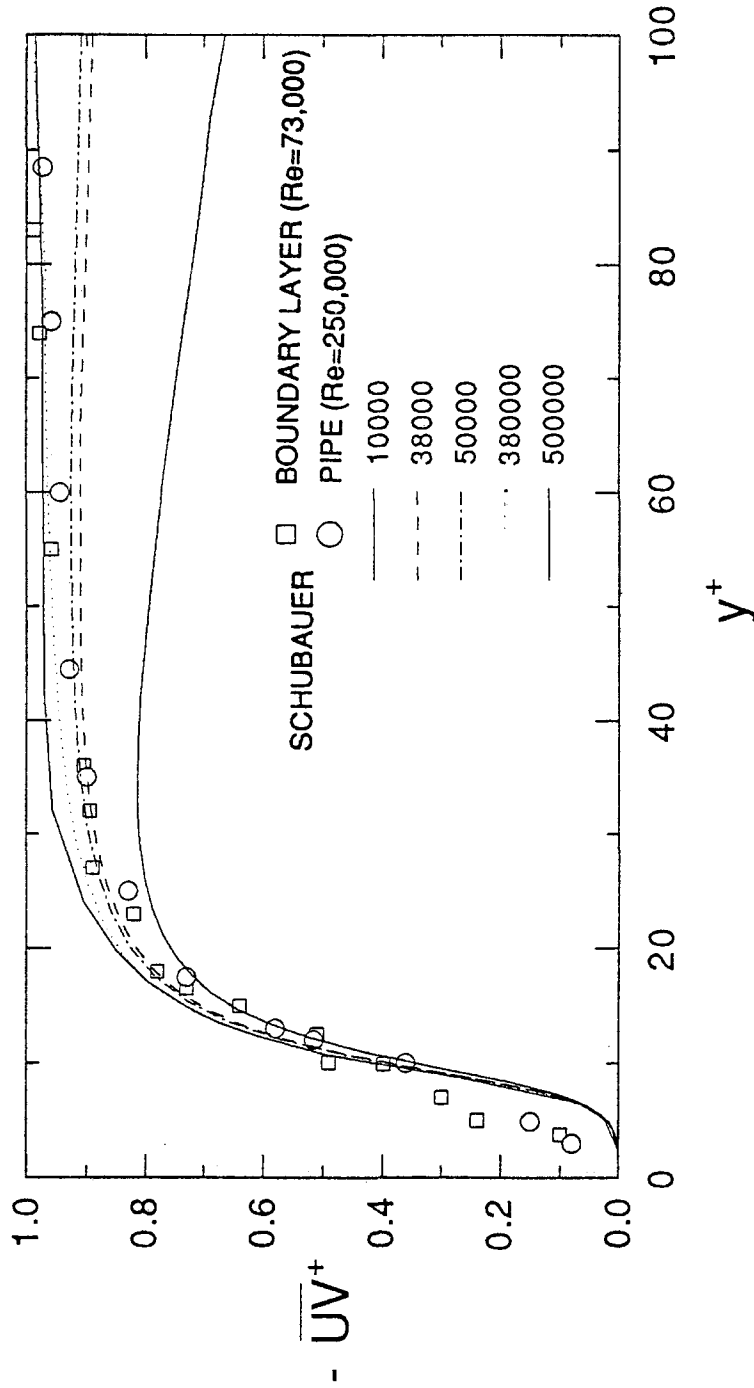


Figure 4.35 Near-wall distribution of Reynolds shear stress for flow near smooth and rough walls: Comparison of the present  $k-\epsilon$  turbulent model with  $C_j=1.0$  at  $x/D=80$  for  $Re_D=10,000, 38,000, 50,000, 380,000$  and  $500,000$  and experimental data for smooth surfaces



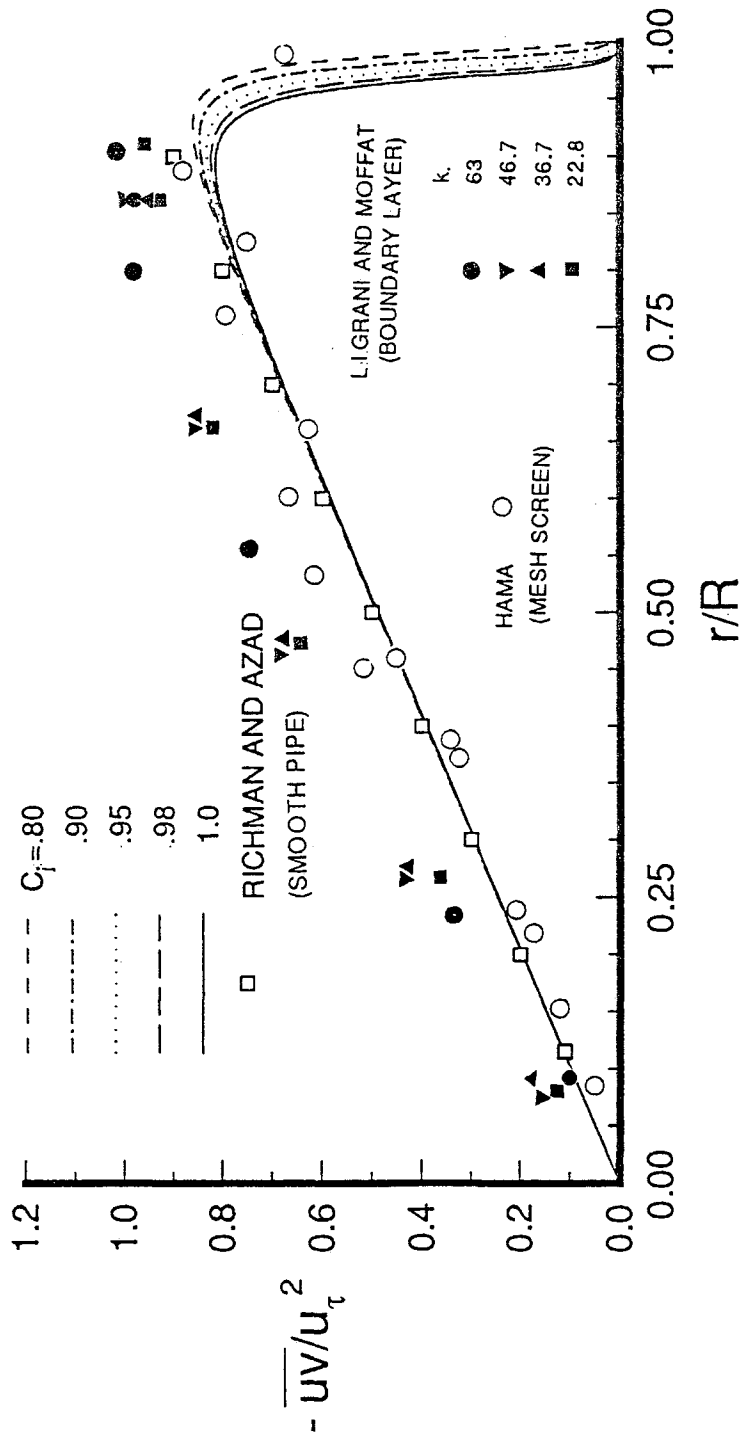


Figure 4.36 Variation of Reynolds shear stress with  $r/R$  for different  $C_j$  at  $x/D=80$  for  $Re_D=10,000$

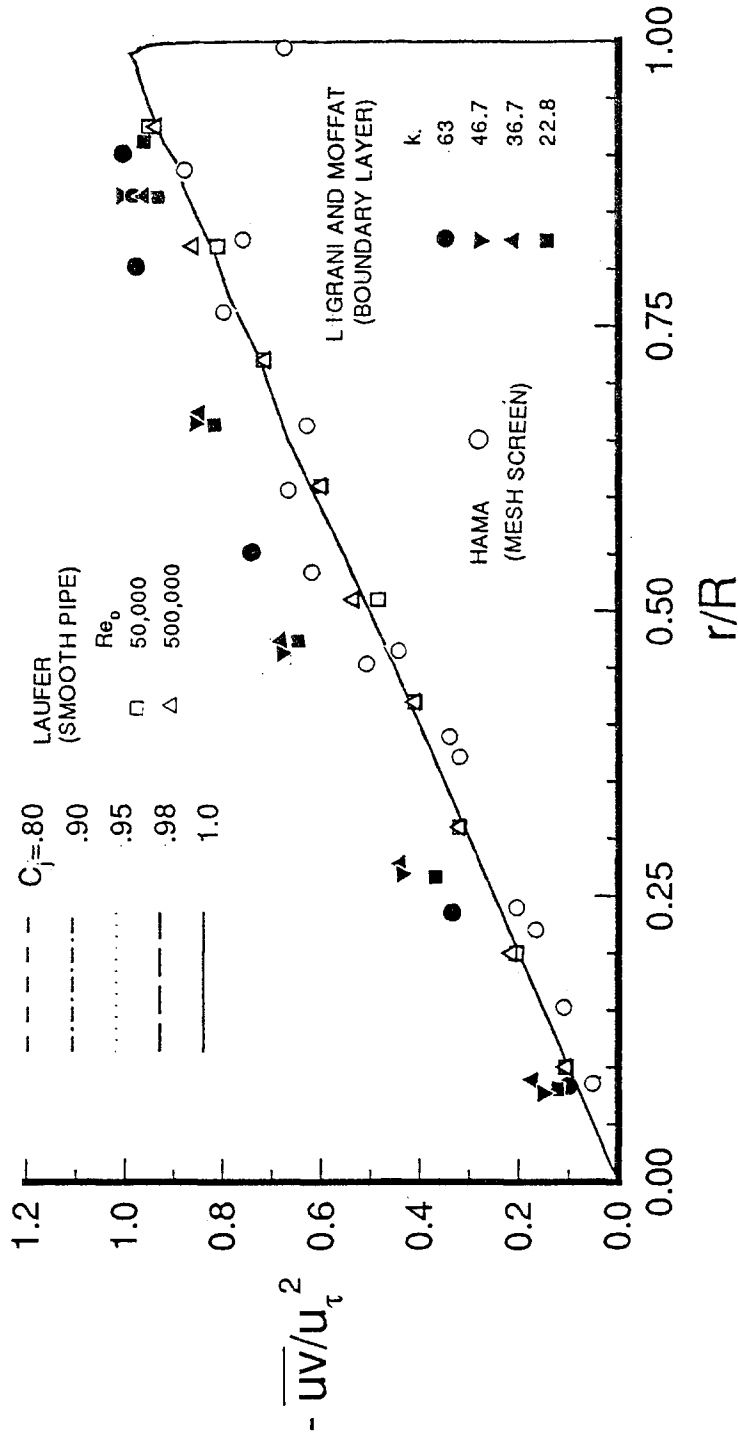


Figure 4.37 Variation of Reynolds shear stress with  $r/R$  for different  $C_j$  at  $x/D=80$  for  $Re_D=380,000$

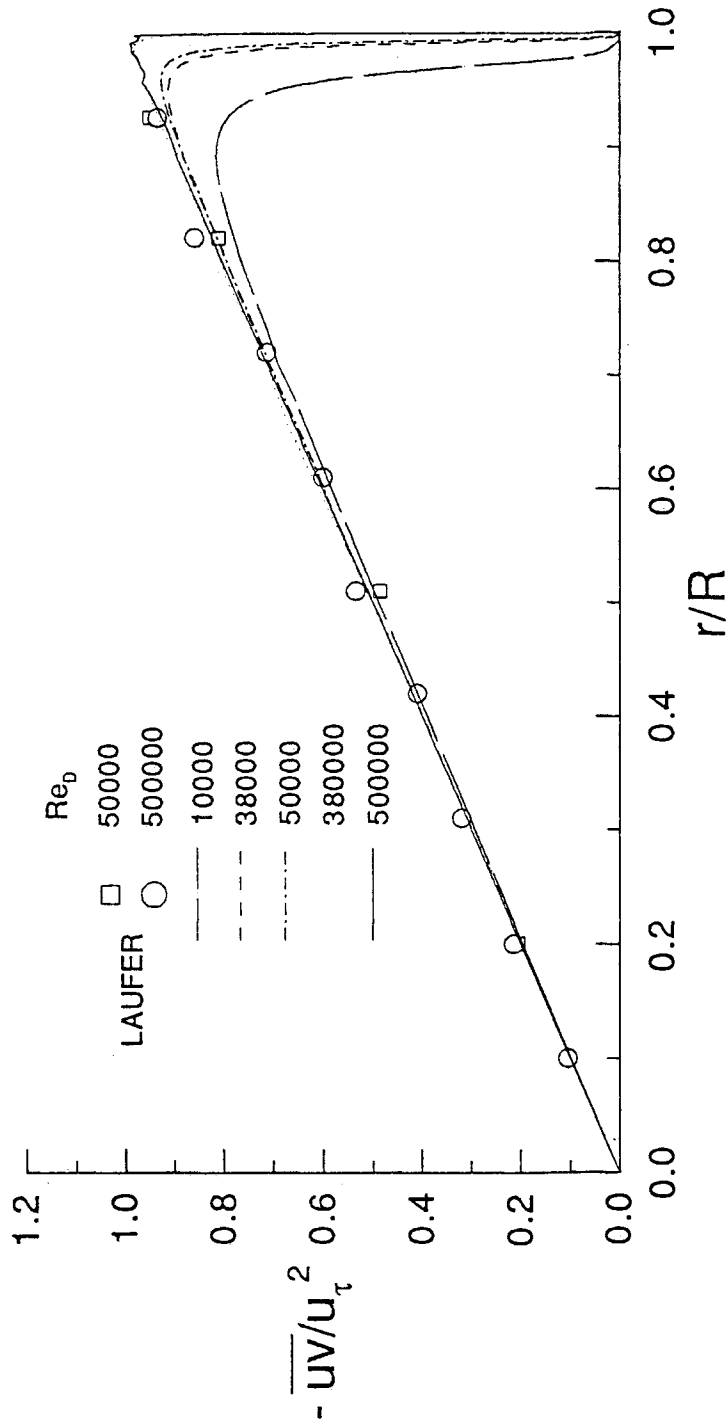


Figure 4.38 Variation of Reynolds shear stress with  $r/R$  for  $C_f=1.0$  at  $x/D=80$  for  $Re_D=10,000, 38,000, 50,000, 380,000$  and  $500,000$

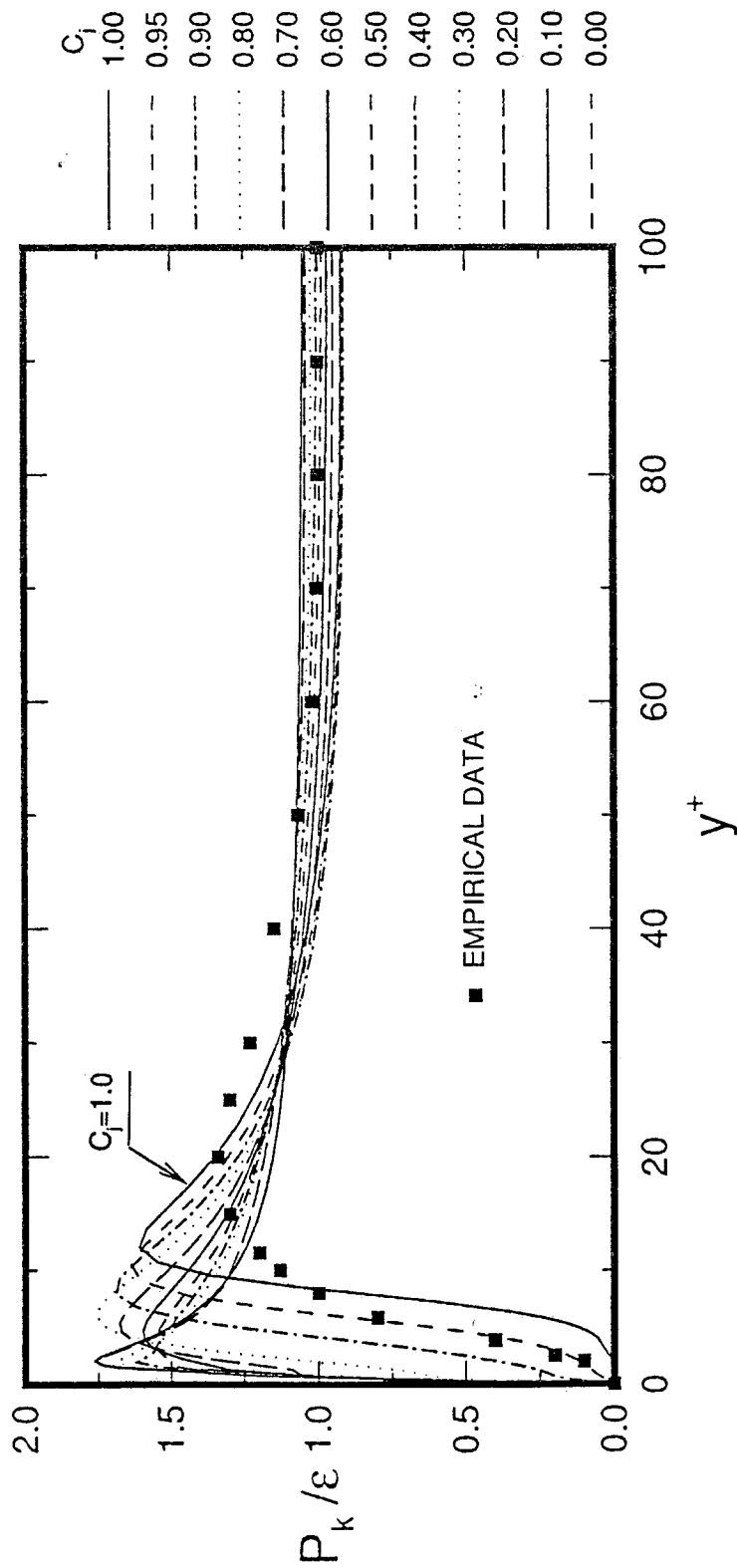


Figure 4.39 Near-wall variation of  $P_k/\epsilon$  for different  $C_j$  at  $x/D=80$  for  $Re_D=50,000$

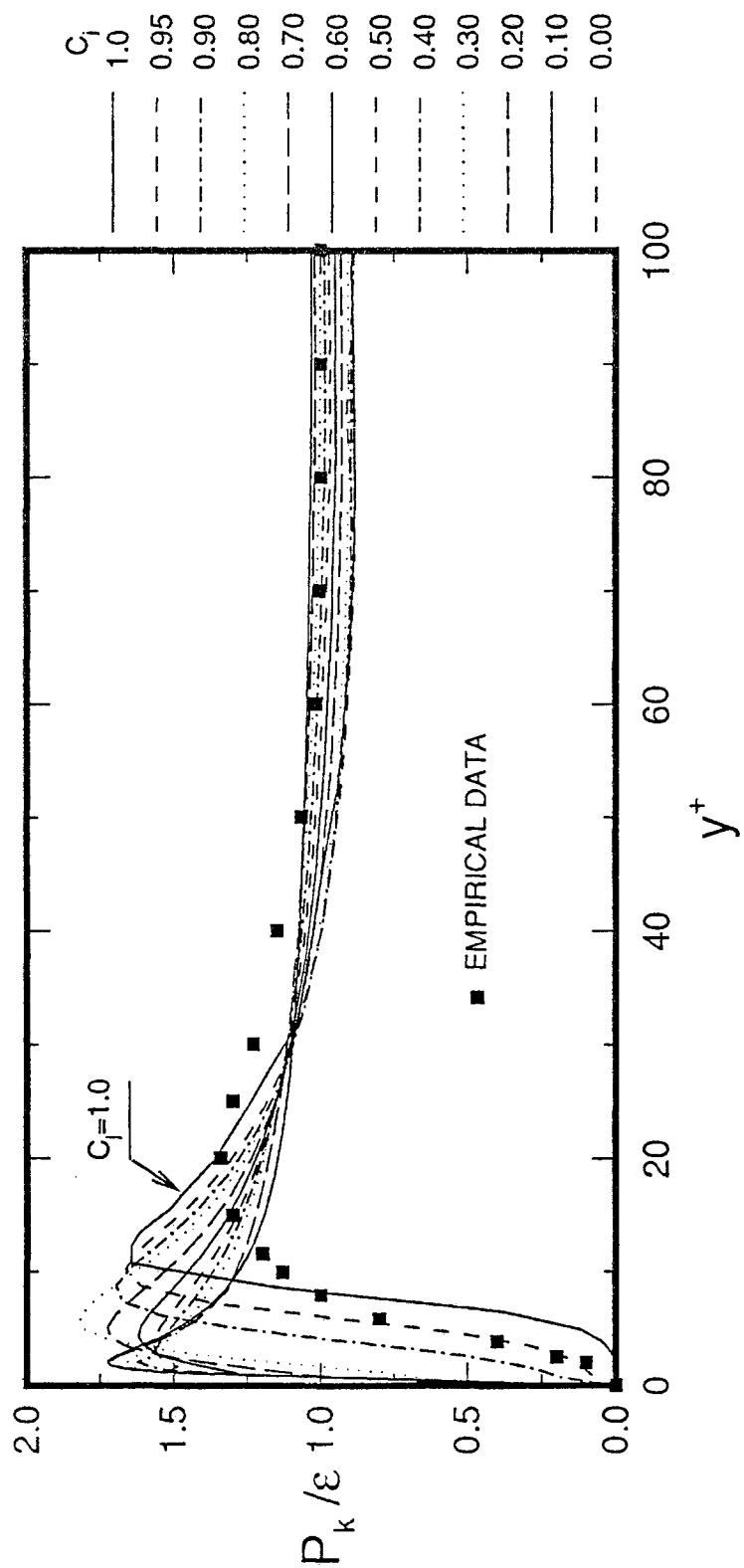


Figure 4.40 Near-wall variation of  $P_k/\epsilon$  for different  $C_j$  at  $x/D=80$  for

$Re_D=500,000$

Table 4.1 Comparison of roughness parameter  $C_j$  ( $k$ - $\epsilon$  turbulence model) and roughness Reynolds number  $k_*$  (van Driest's theory)

$k - \epsilon$ Turbulence Model			
$Re_D = 500,000$		$Re_D = 50,000$	
$C_j$	$k_*$	$C_j$	$k_*$
1.0	5	1.0	2
0.95	16	0.95	14
0.9	30	0.9	24
0.8	60	0.8	42
0.7	80	0.7	53
0.6	103	0.6	80
0.5	125	0.5	96
0.4	150	0.4	114
0.3	178	0.3	137
0.2	196	0.2	152
0.1	198	0.1	158
0.0	200	0.0	158

# Chapter 5

## Summary and Conclusions

In this chapter, the results of this dissertation are summarized and the main conclusions of the study are outlined.

### 1. SUMMARY

This dissertation is concerned with modelling of the turbulent flow near smooth and rough walls.

In Chapter 1, the merits and demerits of turbulence modelling are briefly introduced including near-wall turbulence modelling for the flow near smooth and rough walls.

In Chapter 2, starting from van Driest's theory for turbulent flow near a smooth wall a roughness parameter is introduced into the damping factor of van Driest's theory. The range of the new roughness parameter is from 1.0 to 0.0 corresponding to cases of turbulent flow over hydraulically smooth walls to that over fully rough walls, consistent with van Driest's theory. Comparisons of the two theories are carried out for the universal constant, mixing length, mean velocity and Reynolds shear stress.

In Chapter 3 the theory developed in Chapter 2 is verified by testing it in the case of developing turbulent flow in a pipe. The time-averaged Reynolds momentum equations are combined with the algebraic turbulence model (eddy viscosity) obtained in Chapter 2. Using a simultaneous solution method all flow properties are solved, line-by-line marching, from pipe inlet to exit. The effects of radial variations and near-wall variations of turbulence properties on the roughness parameter are demonstrated and compared with the results of van Driest's theory and available experimental data for the smooth wall. It is found that the new roughness parameter is inversely related to the roughness Reynolds number. Even though the algebraic turbulence model is poor at predicting the developing process of the mean velocity field, the numerical results in the fully developed region are in good agreement with experimental data.

In Chapter 4 the idea of the new damping factor is applied to a more flexible and popular higher order turbulence model. A low-Reynolds number  $k$ - $\epsilon$  two equation turbulence model of Lam and Bremhorst is modified to account for the effect of rough surfaces and tested in the case of developing turbulent flow in a pipe. Two computational parameters  $C_j$  and  $A_C$  are introduced into the damping factor of the damping function  $f_\mu$ . This basically eliminates the singularity problem in the original model of Lam and Bremhorst and accounts for the near-wall variations of the turbulent flow on smooth, transitionally rough and fully rough walls. By combining the new damping factor with the  $k$ - $\epsilon$  turbulence model the range of the application for the roughness on the wall is increased. In the near-wall region the experimental trend of a damping function  $f_\mu$  in the low-Reynolds number turbulence model is recovered by values of  $0.8 \leq C_j \leq 0.9$ . In the fully turbulent region overall results obtained show good agreement with experimental data and are favorably compared with numerical results of other turbulence models.



## 2. CONCLUSIONS

Based on the present results of the theoretical approach for turbulent flow near smooth and rough walls the following conclusions are obtained:

- 1) A new damping factor is suggested to predict turbulent flows near transitionally rough walls. A functional relationship between roughness Reynolds number and the new roughness parameter is obtained.
- 2) In the logarithmic law region the modified mean velocity profiles and Reynolds shear stress reproduce those of van Driest's formula.

Based on the present results of the computation of the algebraic turbulence model for a developing turbulent flow in a pipe the following conclusions are obtained:

- 1) A simultaneous solution technique was successfully employed for the Reynolds-averaged momentum equations combined with the algebraic turbulence model.
- 2) By introducing a new roughness parameter  $C_j$  into the damping factor of van Driest's model for a smooth wall a new algebraic turbulence model was obtained which predicts the turbulent flow near smooth, transitionally rough and fully rough walls. The correlation between the roughness Reynolds number  $k_*$  and computational parameter  $C_j$  was found to be an inverse relationship within a moderate range of wall roughness.
- 3) In the logarithmic region the overall results obtained showed good agreement with experimental data for flow near smooth walls. Very close to the wall the introduction of the new roughness function predicts higher values of turbulence properties compared with the experimental data from smooth walls. It is concluded that the new algebraic turbulence model has the ability to predict the near-wall mean velocity and Reynolds shear stress on the smooth, transitionally rough and fully rough walls.

Based on the present results of the computation using the modified low-Reynolds number  $k$ - $\epsilon$  two equation turbulence model the following conclusions are obtained:

- 1) A simultaneous solution technique was successfully employed for a set of fully elliptic Reynolds-averaged differential equations combined with a low-Reynolds number  $k$ - $\epsilon$  two equation turbulence model.
- 2) By introducing new computational parameter,  $C_j$  and  $A_C$  into a damping function  $f_\mu$  the prediction of the experimental curve of  $f_\mu$  is improved. It is found that the computational parameter  $C_j$  is inversely proportional to the roughness Reynolds number within moderate range of wall roughness.
- 3) In the fully turbulent region overall results obtained show good agreement with experimental data for smooth walls. Very close to the wall the introduction of the  $C_j$  predicts higher values of near-wall turbulence properties compared with the experimental data from smooth walls. This high level of turbulence properties is the characteristics of turbulence properties near rough walls. Due to the higher surface drag on the rough wall the mean velocity profiles on rough surface are less full than those obtained on a smooth wall.

The functional relationship between  $C_j$  and  $k_*$  obtained through the comparisons of the logarithmic mean velocity profiles calculated from theory, an algebraic turbulence model and a low-Reynolds number  $k$ - $\epsilon$  two equation model are shown in Figure 5.1 and Table 5.1. Over all it shows the linear relationship between  $C_j$  and  $k_*$ . It is concluded that the new damping function  $f_\mu$  has the ability to predict the near-wall turbulence properties on both the smooth and rough walls.

In the present analysis the new roughness parameter  $C_j$  is shown to be related only to the roughness Reynolds number  $k_*$ . But the number of parameters describing roughness is extraordinarily large owing to the great diversity of geometric forms. By adjusting  $C_j$  to the logarithmic mean velocity profile of any type of surface conditions the new model may be able to predict the turbulent flow near any roughened surfaces.

The limited comparisons to experimental data over rough walls carried out here are encouraging, but more detailed verifications must be performed before the utility and accuracy of the present approach is proven.

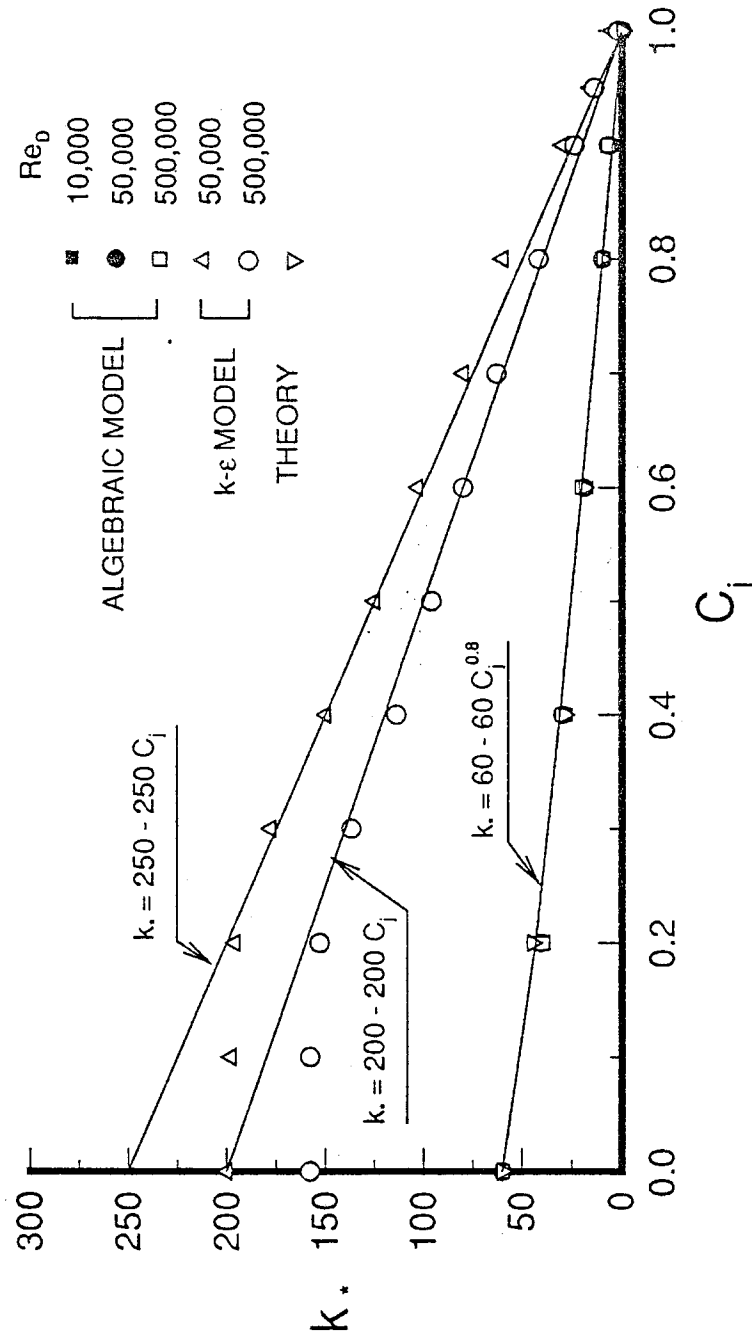


Figure 5.1 Functional relationship between roughness Reynolds number  $k^*$  (van Driest's theory) and present roughness parameter  $C_j$  for different turbulence models

# Bibliography

1. Boussinesq, J., "*Theorie de l'ecoulement Tourbillant*, Mem. Pre. Par. Div. Sav. (Acad. Sci., Paris, 1877), Vol. XXIII.
2. Prandtl, L., "Uber ein neues Formelsystem fur die ausgebildete Turbulenz," *Nachrichten Akademie der Wissenschaften*, Gottingen, Math.-Phys. Klasse, 1945, p. 6.
3. Kolmogorov, A. N., "Equations of Turbulent Motion of an Incompressible Fluid," *Izv. Akad. Nauk. SSR Seria Fizicheska Vi*, No. 1-2, 1942, pp. 56-58, also Mechanical Engineering Department Imperial College, London, England, Rept, ON/6, 1968.
4. Rodi, W., "Examples of Turbulence Models for Incompressible Flows," *AIAA Journal*, Vol. 20, No. 7, 1982, pp. 872-879.
5. Marvin, J. G., "Turbulence Modeling for Computational Aerodynamics," *AIAA Paper*, No. 82-0164, January 1992 also *AIAA Journal*, Vol. 21, No. 7, 1983, pp. 941-955.
6. Reichardt, H., "Vollstandige Darstellung der Turbulenten Geschwindigkeitsverteilung in glatten Leitungen," *Z. Angrew. Math. Mech.*, Vol. 31, 1951, pp. 208-

219.

7. Van Driest, E. R., "On Turbulent Flow Near a Wall," *Journal of the Aeronautical Sciences*, Vol. 23, No. 11, 1956, pp. 1007-1011, 1035.
8. Deissler, R. G., "Analysis of Turbulent Heat Transfer, Mass Transfer and Friction in Smooth Tubes at High Prandtl and Schmidt Numbers," *NACA TR 1210*, 1955.
9. Hanjalic, K. and Launder, B. E., "Contribution Towards a Reynolds-Stress Closure for Low-Reynolds-Number Turbulence," *Journal of Fluid Mechanics*, Vol. 74, 1976, pp. 593-610.
10. Hanjalic, K. and Launder, B. E., "A Reynolds Stress Model of Turbulence and its Application to Thin Shear Flows," *Journal of Fluid Mechanics*, Vol. 68, 1975, pp. 609-638.
11. Launder, B. E., Reece, G. J. and Rodi, W., "Progress in the Development of Reynolds-Stress Turbulence Model," *Journal of Fluid Mechanics*, Vol. 68, 1975, pp. 537-566.
12. Naot, D., Shavit, A. and Wolfstein, M., "Interactions Between Components of the Turbulent Velocity Correlations Tensor," *Israel Journal of Technology*, Vol. 8, 1970, p. 259.
13. So, R. M. C. and Yoo, G. J., "Low Reynolds Number Modeling of Turbulent Flows With and Without Wall Transpiration," *AIAA Journal*, Vol. 25, No. 12, 1987, pp. 1556-1564.
14. So, R. M. C., Lai, Y. G. and Zhang, H. S., "Second-Order Near-Wall Turbulence Closures:A Review," *AIAA Journal*, Vol. 29, No. 11, 1991, 1819-1834.
15. Harlow, F. H. and Welch, J. E., "Numerical Calculation of Time-Dependent Viscous Incompressible Flow of Fluid with a Free Surface," *Physics of Fluids*, Vol. 8, 1965, pp. 2182-2189.

16. Martinuzzi, R., "Comparative Study of Turbulence Models in Simulating Developing Turbulent Pipe Flow," M.S. Thesis, Dept. of Mechanical Engineering, Queen's University, Kingston, Ontario, Canada, 1985.
17. Martinuzzi, R. and Pollard, A., "Comparative Study of Turbulence Models in Predicting Turbulent Pipe Flow, Part 1: Algebraic Stress and  $k$ - $\epsilon$  Models," *AIAA Journal*, Vol. 27, No. 1, 1989, pp. 29-36.
18. Pollard, A. and Martinuzzi, R., "Comparative Study of Turbulence Models in Predicting Turbulent Pipe Flow, Part 2: Reynolds Stress and  $k$ - $\epsilon$  Models," *AIAA Journal*, Vol. 27, No. 12, 1989, pp. 1714-1721.
19. Launder, B. E. and Spalding, D. B., "The Numerical Computation of Turbulent Flows," *Computer Methods in Applied Mechanics and Engineering*, Vol. 3, 1974, pp. 269-289.
20. Patel, V. C., Rodi, W. and Scheuerer, G., "Turbulence Models for Near-Wall and Low-Reynolds Number Flows: A Review," *AIAA Journal*, Vol. 23, Sept. 1985, pp. 1308-1319.
21. Launder, B. E. and Sharma, B. I., "Application of the Energy Dissipation Model of Turbulence to the Calculation of Flow Near a Spinning Disc," *Letters in Heat and Mass Transfer*, Vol. 1, 1974, pp. 131-138.
22. Chien, K.-Y., "Predictions of Channel and Boundary-Layer Flows with a Low-Reynolds-Number Turbulence Model," *AIAA Journal*, Vol. 20, Jan. 1982, pp. 33-38.
23. Lam, C. K. G. and Bremhorst, K., "A Modified Form of  $k$ - $\epsilon$  Model for Predicting Wall Turbulence," *Journal of Fluids Engineering*, Vol. 103, 1981, pp. 456-460.
24. Wilcox, D. C. and Rubesin, W. M., "Progress in Turbulence Modeling for Complex Flow Fields Including Effects of Compressibility," NASA Tech. Paper 1517, 1980.

25. Fromm, K., "Stromungswiderstand in Rauhen Rohren," *ZAMM*, Vol. 3, 1923, pp. 339-358.
26. Hopf, L., "Die Messung der Hydraulischen Rauigkeit," *ZAMM*, Vol. 3, 1923, pp. 329-339.
27. Street, V. L., "Frictional Resistance in Artificially Roughened Pipes", *Proc. Amer. Soc. Civil Eng.*, Vol. 61, 1935, pp. 163-186.
28. Mobius, H., "Experimentelle Untersuchungen des Widerstandes und der Geschwindigkeits-Verteilung in Rohren mit regelmassig angeordneten Rauigkeiten bei turbulenter Stromung," *Phys. Z*, Vol. 41, 1940, pp. 202-225.
29. Fritsch, W., "Einfluss der Wandrauigkeit auf die turbulente Geschwindigkeitsverteilung in Rinnen," *ZAMM*, Vol. 8, 1928, pp. 199-216.
30. Nikuradse, J., "Stromungsgesetze in Rauhen Rohren," *Verein Deutscher Ingenieure-Forschungsheft*, No. 361, Series B, 4, 1933. (Also "Law of Flow in Rough Pipes," *NACA TM 1292*)
31. Schlichting, H., "Experimentelle Untersuchungen zum Rauigkeitsproblem," *Ing.-Arch. VII(1)*, pp. 1-34, 1936. (Also: *Experimental investigation of the problem of surface roughness, NACA TM 832*)
32. Bettermann, D., "Contribution a l'Etude de la Convection Force Turbulente le Long de Plaques Rugueuses," *International Journal of Heat and Mass Transfer*, Vol. 9, March 1966, pp. 153-164.
33. Dvorak, F. A., "Calculation of Turbulent Boundary Layers on Rough Surfaces in Pressure Gradient," *AIAA Journal*, Vol. 7, September 1969, pp. 1752-1759.
34. Simpson, R. L., "A Generalized Correlation of Roughness Density Effects on the Turbulent Boundary Layer," *AIAA Journal*, Vol. 11, February 1973, pp. 242-244.
35. Dirling, R. B., Jr., "A Method for Computing Roughwall Heat Transfer Rates on Re-Entry Nose Tips," *AIAA Paper 73-763*, July, 1973.



36. Dalle Donne, M. and Meyer, L., "Turbulent Convective Heat Transfer from Rough Surfaces with Two-Dimensional Rectangular Ribs," *International Journal of Heat and Mass Transfer*, Vol. 20, June 1977, pp. 583-620.
37. Coleman, H. W., Hodge, B. K. and Taylor, R. P., "A Re-Evaluation of Schlichting's Surface Roughness Experiment," *Transaction of the ASME Journal of Fluids Engineering*, Vol. 106, March 1984, pp. 60-65.
38. Sigal, A and Danberg, J. E., "New Correlation of Roughness Density Effect on the Turbulent Boundary Layer," *AIAA Journal*, Vol. 28, No. 3, 1989, pp. 554-556.
39. Koh, Y. M., "Turbulent Flow Near a Rough Wall," *Journal of Fluids Engineering*, Vol. 114, December 1992, pp. 537-542.
40. Healzer, J. M., Moffat, R. J. and Kays, W. M., "The Turbulent Boundary Layer on a Porous Rough Plate: Experimental Heat Transfer with Uniform Blowing," *AIAA Paper 74-680* and *ASME Paper 74-HT-14* Presented at the *AIAA/ASME 1974 Thermophysics and Heat Transfer Conference*, Boston, Mass., July 1974.
41. Cebeci, T. and Chang, K. C., "Calculation of Incompressible Rough-Wall Boundary-Layer Flows," *AIAA Journal*, Vol. 16, No. 7, 1978, pp. 730-735.
42. Ligrani, P. M., "The Thermal and Hydrodynamic Behavior of Thick, Rough-Wall, Turbulent Boundary Layers," *Ph. D Thesis*, the Department of Mechanical Engineering, Stanford University, Stanford, CA (also Report No. HMT-18)
43. Hodge, B. K. and Adams, J. C., "The Calculation of Compressible Turbulent and Relaminarization Boundary Layers Over Smooth and Rough Surfaces Using an Extended MixingLength Hypothesis," *AEDC-TR-77-96*, February 1978.
44. Lin, T. C. and Bywater, R. J., "Turbulence Models for High-Speed, Rough-Wall Boundary Layers," *AIAA Journal*, Vol. 20, March 1982, pp. 325-333.
45. Christoph, G. and Pletcher, R. H., "Prediction of Rough-Wall Skin Friction and Heat Transfer," *AIAA Journal*, Vol. 21, No. 4, April 1983, pp. 509-515.

46. Finson, M. L. and Wu, P. K. S., "Analysis of Rough Wall Turbulent Heating with Application to Blunted Flight Vehicles," *AIAA Paper 79-008*, 1979.
47. Finson, M. L. and Clarke, A. S., "The Effect of Surface Roughness Character on Turbulent Re-entry Heating," *AIAA Paper 80-1459*, 1980.
48. Finson, M. L., "A Model for Rough Wall Turbulent Heating and Skin Friction," *AIAA Paper 82-0199*, 1982.
49. Taylor, R. P., Coleman, H. W. and Hodge, B. K., "Prediction of Turbulent Rough-Wall Skin Friction Using a Discrete Element Approach," *Transaction of ASME Journal of Fluids Engineering*, Vol. 107, June 1985, pp. 251-257.
50. Taylor, R. P., Coleman, H. W. and Hodge, B. K., "Prediction of Heat Transfer in Turbulent Flow over Rough Surfaces," *Transaction of ASME Journal of Heat Transfer*, Vol. 111, May 1989, pp. 568-572.
51. Hosni, M. H., Coleman, H. W. and Taylor, R. P., "Measurements and Calculations of Rough-Wall Heat Transfer in the Turbulent Boundary Layer," *International Journal of Heat and Mass Transfer*, Vol. 34, No. 4/5, 1991, pp. 1067-1082.
52. Scaggs, W. F., Taylor, R. P. and Coleman, H. W., "Measurement and Prediction of Rough Wall Effects on Friction Factor - Uniform Roughness Results," *Transaction of ASME Journal of Fluid Engineering*, Vol. 110, December 1988, pp. 385-391.
53. Patankar, S. V. and Spalding, D. B., "A Calculation Procedure for Heat, Mass and Momentum Transfer in Three-Dimensional Parabolic Flows," *International Journal of Numerical Heat Transfer*, Vol. 5, 1972, pp. 1787-1806.
54. Patankar, S. V., "Numerical Heat Transfer and Fluid Flow," McGraw-Hill, 1980.
55. Latimer, B. R. and Pollard, A., "Comparison of Pressure-Velocity Coupling Solution Algorithms," *Numerical Heat Transfer*, Vol. 8, 1985, pp. 635-652.

56. Leonard, B. P., "A Stable and Accurate Convective Modelling Procedure Based on Quadratic Upstream Interpolation," *Computer Methods in Applied Mechanics and Engineering*, Vol. 25, 1982, pp. 293-313.
57. Pollard, A. and Siu, A. L.-W., "The Calculation of Some Laminar Flows Using Various Discretisation Schemes," *Computer Methods in Applied Mechanics and Engineering*, Vol. 35, 1982, pp. 293-311.
58. Van Doormal, J. P. and Raithby, G. D., "Enhancement of the SIMPLE Method for Predicting Incompressible Fluid Flows," *Numerical Heat Transfer*, Vol. 7, 1984, pp. 147-163.
59. Raithby, G. D. and Schneider, G. E., "Numerical Solution of Problems in Incompressible Fluid Flow, Treatment of the Velocity-Pressure Coupling," *Numerical Heat Transfer*, Vol. 2, 1979, pp. 417-440.
60. Jang, K. S., "Prandtl Number Effects on Laminar Mixed Convection Heat Transfer in a Lid-Driven Cavity," *Design Project for Engineering Degree*, Dept. of Mechanical Engineering, Polytechnic University, New York, also see *International Journal of Heat and Mass Transfer*, Vol. 35, No. 8, 1992, pp. 1881-1892.
61. Martinuzzi, R., "Comparative Study of Turbulence Models in Simulating Developing Turbulent Pipe Flow," *M.S. Thesis*, Dept. of Mechanical Engineering, Queen's University, Kingston, Ontario, Canada, 1985.
62. Martinuzzi, R. and Pollard, A., "Comparative Study of Turbulence Models in Predicting Turbulent Pipe Flow, Part 1: Algebraic Stress and  $k$ - $\epsilon$  Models," *AIAA Journal*, Vol. 27, No. 1, 1989, pp. 29-36.
63. Pollard, A. and Martinuzzi, R., "Comparative Study of Turbulence Models in Predicting Turbulent Pipe Flow, Part 2: Reynolds Stress and  $k$ - $\epsilon$  Models," *AIAA Journal*, Vol. 27, No. 12, 1989, pp. 1714-1721.

64. Jang, K. S. and Vradis, G., "Numerical Solutions for the Turbulent Planar Jet," *ME Report 91-09*, Dept. of Mechanical Engineering, Brooklyn, Polytechnic University, New York, 1991.
65. Benston, J. and Vradis, G., "A Two-Stage Pressure Correction Technique For the Incompressible Navier-Stokes Equations," *AIAA paper 87-0545*, 1987.
66. Vanka, S. P., "Block-Implicit Computation Techniques in Computational Fluids Dynamics," *AIAA Journal*, Vol. 22, 1984, pp. 1505-1513.
67. Rubin, S. G. and Reddy, D. R., "Analysis of Global Pressure Relaxation for Flows with Strong Interaction and Separation," *Computers and Fluids*, Vol. 11, No. 4, 1983, pp. 281-306.
68. Zedan, M. and Schneider, G. E., "A Coupled Strongly Implicit Procedure for Velocity and Pressure Computation in Fluid Flow Problems," *Numerical Heat Transfer*, Vol. 8, 1985, pp. 537-557.
69. Launder, B. E., Morse, A., Rodi, W., and Spalding, D. B., "Prediction of Free Shear Flows - A Comparison of the Performance of Six Turbulence Models," *NASA SP-321*, 1972, pp. 361-426.
70. Vanka, S. P., "Block-Implicit Computation of Viscous Internal Flows-Recent Results," *AIAA-87-0058 paper* at 25th AIAA Aerospace Science Meeting, Reno, Nevada, January, 12-15, 1987.
71. Chow, W. K. and Leung, W. M., "A Short Note on Achieving Convergent Results in Simulating Buliding Fire Using the k- $\epsilon$  Turbulence Model," *Numerical Heat Transfer*, Part A, Vol. 17, 1990, pp. 495-501.
72. Wagner, C. A., "Computations of A Horseshoe Vortex Around An End Wall Mounted Cylinder," Ph.D. Thesis, Conneticut University, 1989.
73. Jang, K. S. and Oyibo, G. A., "Numerical Simulation of Turbulent Flow In a Pipe," *POLY AE 92-26 Report*, Dept. of Aerospace Engineering, Polytechnic

- University, New York, January, 1993.
74. Jang, K. S. and Oyibo, G. A., "Numerical Simulation of Turbulent Flow In a Channel," *POLY AE 92-27 Report*, Dept. of Aerospace Engineering, Polytechnic University, New York, January, 1993.
  75. Jang, K. S. and Oyibo, G. A., "Simultaneous Solution Method In A Developing Turbulent Pipe Flow," *POLY AE 92-28 Report*, Dept. of Aerospace Engineering, Polytechnic University, New York, January, 1993.
  76. Lefebvre P. J. and White, F. M., "Detailed Measurements of Accelerating Flow Properties in Pipes," 4th Seminar in the Dept. of Aerospace Engineering, Farmingdale, Polytechnic University, December 3, 1992.
  77. Stokes, G. G., "On the Effect of the Internal Friction of Fluids on the Motion of Pendulums," *Cambr. Phil. Trans. IX*, Vol. 8, 1851, also *Math. and Phys. Papers*, Cambridge, III, 1901, pp. 1-141 also Schlichting, H., "*Boundary Layer Theory*," 7th ed. McGraw-Hill, 1979.
  78. Watson, J., "A Solution of the Navier-Stokes Equation Illustrating the Response of a Laminar Boundary Layer to a Given Change in the External Stream Velocity," *Quartly Journal of Mechanics and Applied Mathematics*, Vol. XI, Pt. 3, 1958, pp. 302-325.
  79. Schlichting, H., "*Boundary Layer Theory*," 7th ed., McGraw-Hill Book Company, New York, 1979.
  80. Prandtl, L., "Uber die ausgebildete Turbulenz," *ZAMM*, Vol. 5, 1925, pp. 136-139. and also in *Proc. 2nd Intern. Congr. Appl. Mech.*, Zurich 1962, pp. 62-75.
  81. Stroud, A. H. and Secrest, D., "Gaussian Quadrature Formulas", Prentice-Hall, Englewood, Cliffts, N.J., 1966.
  82. Kuo, S. S., "Numerical Methods and Computers," Reading, Mass.: Addison-Wesley Publishing Company, 1965.

83. Laufer, J., "The Structure of Turbulence in Fully Developed Pipe Flow," *NACA Rept. 1174*, 1954.
84. Ligrani, P. M. and Moffat, R. J., "Structure of Transitionally Rough and Fully Rough Turbulent Boundary Layers," *Journal of Fluid Mechanics*, Vol. 162, 1986, pp. 69-98.
85. Schubauer, G. B., "Turbulent Processes as Observed in Boundary Layer and Pipe," *Journal of Applied Physics*, Vol. 25, No. 2, 1954, pp. 188-196.
86. Welch, J. E., Harlow, F. H., Shannon, J. P. and Daly, B. J., "The MAC Method," *Los Alamos Scientific Lab. Rept. LA-3425*, 1966.
87. Pulliam, T. H., "Efficient Solution Methods for the Navier-Stokes Equations," *Lecture Notes for the Von Karman Institute for Fluid Dynamics Lecture Series: Numerical Techniques for Viscous Flow Computation In Turbomachinery Bladings*, Brussels, Belgium, Jan. 1986, pp. 20-24.
88. Isaacson, E. and Keller, B. H., "Analysis of Numerical Methods," Wiley, New York, 1966.
89. Nikuradse, J., "Gesetzma ß ig keit der turbulenten Stromung in glatten Rohren," *Verein Deutscher Ingenieure-Forschungsheft*, No. 356, 1932 or *NACA TM-1292*, 1965.
90. Townsend, A. A., *The Structure of Turbulent Shear Flow*, 2nd edn., Cambridge University Press, 1979, pp. 150-158.
91. Reynolds, O., "An Experimental Investigation of the Circumstances Which Determine Whether the Motion of Water shall be Direct or Sinuous, and of the Law of Resistance in Parallel Channels," *Phil. Trans. Roy. Sco.*, Vol. 174, 1883, pp.935-982.
92. Hama, F. R., "Boundary Layer Characteristics for Smooth and Rough Surfaces," *Transaction . Soc. Nav. Archit. Mar. Engrs.*, Vol. 62, 1954, pp. 333-358.

93. Grass, A. J., "Structure Feature of Turbulent Flow over Smooth and Rough Boundaries," *Journal of Fluid Mechanics*, Vol. 50, Part 2, 1971, pp. 233-255.
94. Perry, A. E. and Joubert, P. N., "Rough-Wall Boundary Layers in Adverse Pressure Gradients," *Journal of Fluid Mechanics*, Vol. 17, 1963, pp. 193-211
95. Liu, C. K., Kline, S. J. and Johnston, J. P., "An Experimental Study of Turbulent Boundary Layers on Rough Walls," *Report no. MD-15*, Thermosciences Division, Department of Mechanical Engineering, Stanford University, 1966.
96. Perry, A. E., Schofield, W. H. and Joubert, P. N., "Rough Wall Turbulent Boundary Layers," *Journal of Fluid Mechanics*, Vol. 37, 1969, pp. 383-413.
97. Antonia, R. A., and Luxton, R. E., "Energy Balance in a Turbulent Boundary Layer on a Rough Wall," *Physics Fluids*, Vol. 14, 1971, pp. 1027-1029.
98. Wood, D. H., and Antonia, R. A., "Measurements in a Turbulent Boundary over a D-type Surface Roughness," *Transaction of ASME E; Journal of Applied Mechanics*, Vol. 42, 1975, pp. 591.
99. Pimenta, M. M., Moffat, R. J. and Kays, W. M., "The Turbulent Boundary Layer: an experimental study of the transport of momentum and heat with the effect of roughness," *Report no. HMT-21*, Thermosciences Division, Department of Mechanical Engineering, Stanford University, 1975.
100. Coleman, H. W., Moffat, R. J. and Kays, W. M., "The Accelerated Fully Rough Turbulent Boundary Layer," *Journal of Fluid Mechanics*, Vol. 82, 1977, pp. 507-528.
101. Siuru, Jr. W. D. and Logan, Jr. E., "Response of a Turbulent Pipe Flow to a Change in Roughness," *Transaction of the ASME Journal of Fluids Engineering*, September 1977, pp. 548-555.
102. Barbin, A. J. and Jones, J. B., "Turbulent Flow in the Inlet Region of a Smooth Pipe," *ASME Journal of Basic Engineering*, Vol. 29, 1963, pp. 29-34.

103. Lawn, C. J., "Rate of Dissipation in Turbulent Pipe Flow," *Journal of Fluids Mechanics*, Vol. 48, 1971, pp. 477-505.
104. Richman, J. W. and Azad, R. S., "Developing Turbulent Flow in A Smooth Pipe," *Apl. Sci. Res.*, Vol. 28, 1973, pp. 419-441.
105. Hassid, S. and Poreh, M., "A Turbulent Energy Dissipation Model for Flows With Drag Reduction," *ASME Journal of Fluids Engineering*, Vol. 100, March 1978, pp. 107-112.
106. Gibson, M. M., Spalding, D. B. and Zinser, W., "Boundary Layer Calculations Using Hassid-Poreh One-Equation Energy Model," *Letters in Heat and Mass Transfer*, Vol. 5, 1978, pp. 73-80.
107. Wilcox, D. C., "*Private Communication*," December 29, 1992.
108. Miner, E. W., Swean, T. F., Handler, R. A. and Leighton, R. I., " Evaluation of Wall-Damping Models by Comparison with Direct Simulations of Turbulent Channel Flow." *Numerical Methods in Laminar and Turbulent Flow*, Vol. 6, Part 1, Taylor Gresho Sani and Hauser, 1989, pp. 273-284.
109. Handler, R. A., Hendricks, E. W. and Leighton, R. I., "Low Reynolds Number Calculations of Turbulent Channel Flow: A General Discussion," NRL Memorendum Report 6410, Naval Research Laboratory, Washington, D. C. 1989.



# Appendix

## Discretized Equations

The following finite difference equations are written on the nonuniform grid system for the equations(3.2)-(3.4).

Continuity Equation:

$$\frac{U_{i,j} - U_{i,j-1}}{dX_j} + \frac{1}{r_i} \left[ \frac{rv_{i+1}V_{i+1,j} - rv_iV_{i,j}}{rv_{i+1} - rv_i} \right] = 0 \quad (\text{A-1})$$

X-Momentum Equation:

$$\begin{aligned} & [U_{i,j}, 0.0] \frac{U_{i,j} - U_{i,j-1}}{dX_j} + [-U_{i,j}, 0.0] \frac{U_{i,j} - U_{i,j+1}}{dX_{j+1}} \\ & + [V_{av}, 0.0] \frac{u_{i,j} - u_{i-1,j}}{r_i - r_{i-1}} + [-V_{av}, 0.0] \frac{u_{i,j} - u_{i+1,j}}{r_{i+1} - r_i} \end{aligned}$$

$$\begin{aligned}
&= - \frac{P_{i,j+1} - P_{i,j}}{\frac{dX_{j+1} + dX_j}{2}} \\
&+ \frac{1}{\text{Re}_D} \frac{2}{dX_j + dX_{j+1}} \left[ (1+2v_{ti,j+1}) \frac{U_{i,j+1} - U_{i,j}}{dX_{j+1}} - (1+2v_{ti,j}) \frac{U_{i,j} - U_{i,j-1}}{dX_j} \right] \\
&+ \frac{1}{\text{Re}_D} \frac{1}{r_i} \frac{1}{rv_{i+1} - rv_i} \left[ (1+v_{tne})rv_{i+1} \left[ \frac{U_{i+1,j} - U_{i,j}}{r_{i+1} - r_i} - \frac{V_{i+1,j+1} - V_{i+1,j}}{\frac{dX_j + dX_{j+1}}{2}} \right] \right. \\
&\left. - \frac{1}{\text{Re}_D} \frac{1}{r_i} \frac{1}{rv_{i+1} - rv_i} \left[ (1+v_{tse})rv_i \left[ \frac{U_{i,j} - U_{i-1,j}}{r_i - r_{i-1}} + \frac{V_{i,j+1} - V_{i,j}}{\frac{dX_j + dX_{j+1}}{2}} \right] \right] \right]
\end{aligned}$$

$r$ -Momentum Equation:

$$\begin{aligned}
&[U_{av}, 0.0] \frac{V_{i,j} - V_{i,j-1}}{\frac{dX_j + dX_{j-1}}{2}} + [-U_{av}, 0.0] \frac{V_{i,j} - V_{i,j+1}}{\frac{dX_j + dX_{j+1}}{2}} \\
&+ [V_{i,j}, 0.0] \frac{V_{i,j} - V_{i-1,j}}{rv_i - rv_{i-1}} + [-V_{i,j}, 0.0] \frac{V_{i,j} - V_{i+1,j}}{rv_{i+1} - rv_i} \\
&= - \frac{P_{i,j} - P_{i-1,j}}{r_i - r_{i-1}}
\end{aligned}$$

$$\begin{aligned}
& + \frac{1}{\text{Re}_D} \frac{1}{dX_j} \left[ (1+v_{t,se}) \frac{V_{i,j+1} - V_{i,j}}{dX_j + dX_{j+1}} - (1+v_{t,sw}) \frac{V_{i,j} - V_{i,j-1}}{dX_j + dX_{j-1}} \right] \\
& + \frac{1}{\text{Re}_D} \frac{1}{dX_j} \left[ v_{t,se} \frac{U_{i,j} - U_{i-1,j}}{r_i - r_{i-1}} - v_{t,sw} \frac{U_{i,j-1} - U_{i-1,j-1}}{r_i - r_{i-1}} \right] \\
& + \frac{1}{\text{Re}_D} \frac{1}{rv_i} \frac{1}{r_i - r_{i-1}} \left[ (1+2v_{t,i,j})r_i \frac{V_{i+1,j} - V_{i,j}}{rv_{i+1} - rv_i} - (1+2v_{t,i-1,j})r_{i-1} \frac{V_{i,j} - V_{i-1,j}}{rv_i - rv_{i-1}} \right]
\end{aligned}$$

where the operator  $[A,B]$  is equivalent to  $AMAX1(A,B)$  in the computer language FORTRAN. The average values are calculated by the linear interpolation from the values in the neighbouring grid positions.

$$U_{av} = \frac{1}{2}(U_{i,j} + U_{i,j-1}) \quad (\text{A-4})$$

$$+ \frac{1}{2} \frac{(r_i - rv_i)}{(r_i - r_{i-1})} (U_{i-1,j} + U_{i-1,j-1} - U_{i,j} - U_{i,j-1})$$

$$V_{av} = \frac{1}{2}(V_{i,j} - V_{i+1,j}) \quad (\text{A-5})$$

$$+ \frac{1}{2} \frac{dX_j}{dX_j + dX_{j+1}} (V_{i,j+1} + V_{i+1,j+1} - V_{i,j} - V_{i+1,j})$$

And the average values for the turbulent viscosity are

$$v_{tan} = (v_{ti,j} - v_{ti+1,j}) \frac{(r_{i+1} - rv_{i+1})}{r_{i+1} - r_i} + v_{ti+1,j}$$

$$v_{tnp} = (v_{ti,j+1} - v_{ti+1,j+1}) \frac{r_{i+1} - rv_{i+1}}{r_{i+1} - r_i} + v_{ti+1,j+1}$$

$$v_{tnm} = (v_{ti,j-1} - v_{ti+1,j-1}) \frac{(r_{i+1} - rv_{i+1})}{r_{i+1} - r_i} + v_{ti+1,j-1}$$

$$v_{tne} = \frac{1}{2}(v_{tnp} - v_{tan}) \frac{2 dX_j}{dX_j + dX_{j+1}} + v_{tan}$$

$$v_{tnw} = \frac{1}{2}(v_{tan} - v_{tnm}) \frac{2 dX_{j-1}}{dX_j + dX_{j-1}} + v_{tnm} \quad (\text{A-6})$$

$$v_{tas} = (v_{ti-1,j} - v_{ti,j}) \frac{(r_i - rv_i)}{r_i - r_{i-1}} + v_{ti,j}$$

$$v_{tsp} = (v_{ti-1,j+1} - v_{ti,j+1}) \frac{r_i - rv_i}{r_i - r_{i-1}} + v_{ti,j+1}$$

$$v_{tsm} = (v_{ti-1,j-1} - v_{ti,j-1}) \frac{(r_i - rv_i)}{r_i - r_{i-1}} + v_{ti,j-1}$$

$$v_{tse} = \frac{1}{2}(v_{tsp} - v_{tas}) \frac{2 dX_j}{dX_j + dX_{j+1}} + v_{tas}$$

$$v_{tsw} = \frac{1}{2}(v_{tas} - v_{t sm}) \frac{2 dX_{j-1}}{dX_j + dX_{j-1}} + v_{t sm}$$